NASA Technical Paper 1290

Effects of Spanwise Blowing on the Surface Pressure Distributions and Vortex-Lift Characteristics of a Trapezoidal Wing-Strake Configuration

James F. Campbell and Gary E. Erickson

FEBRUARY 1979

NASA

NASA Technical Paper 1290

Effects of Spanwise Blowing on the Surface Pressure Distributions and Vortex-Lift Characteristics of a Trapezoidal Wing-Strake Configuration

James F. Campbell
Langley Research Center
Hampton, Virginia
and
Gary E. Erickson
Northrop Corporation
Hawthorne, California

National Aeronautics
and Space Administration

**Scientific and Technical
Information Office**

1979

SUMMARY

The present investigation was conducted to measure the effects of spanwise blowing on the surface pressures of a 44° swept trapezoidal wing-strake configuration. Wind-tunnel data were obtained at a free-stream Mach number of 0.26 for a range of model angle of attack, jet thrust coefficient, and nozzle chordwise location. Results of this study showed that spanwise blowing delayed the leading-edge vortex breakdown to larger span distances and increased the lifting pressures. Vortex lift was achieved at span stations immediately outboard of the strake-wing junction with no blowing, but spanwise blowing was necessary to achieve vortex lift at increased span distances. Blowing on the wing in the presence of the strake was not as effective as blowing on the wing alone. Spanwise blowing increased lift throughout the angle-of-attack range, improved the drag polars, and extended the linear pitching moment to higher values of lift. The leading-edge suction analogy can be used to estimate the effects of spanwise blowing on the aerodynamic characteristics.

INTRODUCTION

On thin, highly swept wings at moderate-to-high angles of attack, the flow is characterized by a separation-induced leading-edge vortex which provides large vortex-lift increments. This characteristic of slender wings designed for supersonic cruise vehicles has been understood for many years (refs. 1 to 5). However, for moderately swept wings of higher aspect ratios, which are generally of interest for fighter airplanes, vortex breakdown usually occurs at low angles of attack. (For example, see ref. 3.) Thus, this class of wing does not achieve the large vortex-lift increments that are desirable for maneuvering.

Two techniques for enhancing the wing leading-edge vortex and effectively delaying vortex breakdown to higher angles of attack are use of spanwise blowing and use of a highly swept wing strake. The spanwise-blowing concept consists of blowing a discrete jet spanwise over the wing upper surface and in a direction essentially parallel to the leading edge. Some of the early research on controlling separated flow regions by transverse blowing was reported in references 6 to 9. The photographs in figure 1 were taken from reference 9 and illustrate the leading-edge vortex that forms on a rectangular flat plate because of transverse blowing. The additional work reported in references 10 to 15 applied the concept to different types of lifting surfaces, such as swept wings, trailing-edge flaps, and rudders.

The highly swept strake, which is also used for generating vortex lift to improve high angle-of-attack maneuverability, is currently being utilized on several lightweight fighters. The strong vortex flows generated by the maneuver strakes on the General Dynamics YF-16 and Northrop YF-17 prototypes are shown in the photographs in figure 2. Experimental results from references 16 to 18 have indicated that the lift due to the addition of the strake is aug-

mented by the mutual interaction of the strake vortex and the wing flow field. To supplement this research, it is desirable to obtain detailed information concerning the simultaneous effects of both vortex-control techniques for wings of interest for fighter airplanes.

Accordingly, the present investigation was initiated to obtain surface pressure distributions on a wing-strake configuration having spanwise blowing from the fuselage. A trapezoidal-wing planform having a 44° leading-edge sweep was used for the study, which was conducted at a free-stream Mach number of 0.26. Data were acquired for a range of model angle of attack, jet thrust coefficient, and nozzle chordwise location. The blowing results obtained in these studies for the strake-off case are published in reference 19. The present paper analyzes the results obtained with the strake on and provides comparisons with appropriate aerodynamic theory that accounts for the wing leading-edge vortex.

SYMBOLS

Physical quantities in this paper are presented in the International System of Units (SI). Measurements and calculations were made in the U.S. Customary Units. All force and moment data are referred to the stability-axis system. The pitching-moment reference center is located at 25 percent of the center-line chord, defined by extending the leading and trailing edges to the model plane of symmetry (fig. 3).

b wing span

C_D wing drag coefficient, integrated section-drag values

C_L wing lift coefficient, integrated section-lift values

$C_{L,p}$ lift coefficient, potential flow

$C_{L,tot}$ $= C_{L,p} + C_{L,vle} + C_{L,vse}$

$C_{L,vle}$ lift coefficient, vortex flow at leading edge

$C_{L,vse}$ lift coefficient, vortex flow at side edge

C_m wing pitching-moment coefficient, $\dfrac{\text{Pitching moment}}{q_\infty S c_{r,t}}$

C_p pressure coefficient, $\dfrac{p - p_\infty}{q_\infty}$

ΔC_p $= C_{p,u} - C_{p,\ell}$

C_T	nozzle-thrust coefficient, $\frac{\text{Nozzle thrust}}{q_\infty S}$
c	local chord
c_{av}	average chord, S/b
c_d	section drag coefficient
c_l	section lift coefficient
Δc_l	$= c_{l,\text{jet on}} - c_{l,\text{jet off}}$
$c_{l,p}$	section lift coefficient, potential flow
$c_{l,v}$	section lift coefficient, vortex flow
$c_{l,tot}$	$= c_{l,p} + c_{l,v}$
c_r	root chord (chord at wing-fuselage juncture)
$c_{r,t}$	theoretical root chord (at fuselage center line)
d	nozzle diameter
h	height of nozzle center line above wing surface
M_∞	free-stream Mach number
p	static pressure
$p_{t,n}$	stagnation pressure in nozzle settling chambers
p_∞	free-stream static pressure
q_∞	free-stream dynamic pressure
S	wing reference area, 0.103 m^2
x	chordwise distance, measured from wing leading edge
x_n	chordwise distance of nozzle from leading edge of wing root chord (see fig. 3)
y	spanwise distance, measured from model plane of symmetry
z	vertical distance, measured from wing chord plane
α	angle of attack of model

Λ_{le} leading-edge sweep angle

Λ_n sweep angle of nozzle center line

Subscripts:

1,2 refers to nozzles 1 (left) and 2 (right), respectively

ℓ condition on lower surface of wing

max maximum

u condition on upper surface of wing

MODEL AND APPARATUS

The wind-tunnel model consisted of a wing-strake-fuselage combination with a discrete jet that was mounted in each side of the fuselage and oriented to blow air over the wing upper surface. A three-view drawing of the model is shown in figure 3, and photographs of the model installed in the wind tunnel are shown in figure 4.

The trapezoidal wing had a 44° leading-edge sweep angle and trailing-edge sweep angle of -5.7°. The aspect ratio, based on an area of 0.103 m^2, was 2.5 and the taper ratio was 0.2. The wing had no twist, camber, or dihedral and had an airfoil section (measured streamwise) which was a circular arc with sharp leading and trailing edges. The thickness ratio was 6 percent at the fuselage-wing junction (root chord) and varied linearly to 4 percent at the wing tip.

The wing was instrumented with 140 pressure orifices which were arranged in chordwise rows at six different span locations. (See fig. 3(b).) Pressures were measured on the lower surface of the left wing and on the upper surface of the right wing. The reader is referred to reference 19 for the coordinates of all the orifices as well as for information on the pressure-recording instrumentation.

The continuous-flow air system, which provided dry high-pressure air to the nozzles, is shown in the schematic diagram in figure 5. Each nozzle was connected to a cylindrical plenum, or settling, chamber to which air was supplied by a 0.953-cm-diameter stainless-steel supply line. The stagnation pressure in each settling chamber was recorded on a large-dial pressure gage. The size of the settling chambers necessitated the use of a fuselage fairing to cover them (shown in fig. 3(a)).

Details of the convergent nozzle geometry and location are shown in figure 6, where the subscripts 1 and 2 refer to nozzles 1 and 2, respectively. Each nozzle was made of 0.953-cm-diameter stainless-steel tubing, whose inner diameter converged from 0.775 cm to the diameter d_1 or d_2 of the circular exit shown in the figure. The exit diameters were slightly different for the two nozzles. The bottom of the tubing was shaped to allow the jet to be closer

to the wing surface. Both nozzles were calibrated prior to tunnel installation to obtain static nozzle thrust as a function of plenum total pressure, and the results are presented in reference 19.

TEST CONDITIONS AND PROCEDURE

The tests were conducted at a Mach number of 0.26 in the Langley high-speed 7- by 10-foot tunnel. The tunnel operating conditions included an average dynamic pressure of 4549 Pa with a temperature of 297 K. The Reynolds number was 5.2×10^5 per meter. The tests were performed without fixed transition on the model. An accelerometer, located in the nose of the fuselage, was used to record changes in the attitude of the model with respect to the horizontal. The test data were not corrected for tunnel blockage and flow angularity since these have been found to be negligible.

Pressure data were obtained for each configuration at angles of attack from 0° to 24° at 4° increments, with nozzle-thrust coefficients of 0.0 and 0.12. At the maximum α, C_T was varied from 0.0 to 0.18 at increments of 0.02. For all of the thrusting conditions, equal thrust was obtained for both nozzles by adjusting the plenum stagnation pressures to the values determined from the static calibration. (See ref. 19.) It was assumed that these static thrust levels would be essentially the same at the test condition of $M_\infty = 0.26$.

The test configurations consisted of nozzle chordwise locations x_n/c_r of 0.15, 0.23, and 0.32. The nozzle height above the wing surface h/d was 0.835, and the nozzle center-line sweep angle Λ_n was 44°, thus orienting the nozzle parallel to the wing leading edge.

PRESENTATION OF RESULTS

The results of the investigation are presented in the following figures:

DISCUSSION

The wing surface pressure measurements obtained during the wind-tunnel tests are presented in graphical form in figures 7 to 12. Upper and lower surface pressure coefficients are plotted against x/c, the nominal fraction of the local chord, for each of the span locations. The lower surface pressures are identified by a "+" inside the data symbol. The data were machine plotted and then faired with a cubic spline; this spline was integrated to obtain section forces and moments. The spanwise variations of the section properties were then fitted with a cubic spline and integrated to obtain the total forces and moments on the wing.

Detailed Effects of Spanwise Blowing

A large quantity of data were obtained in this investigation, all of which are presented herein. However, the model configuration with $x_n/c_r = 0.23$ will be used to discuss the detailed effects of spanwise blowing. The data trends that are discussed in the following sections for this configuration are typical of the trends obtained for the other nozzle chordwise locations investigated. The basic data for $x_n/c_r = 0.15$ and 0.32 are presented in figures 9 to 12 but are not discussed.

Chordwise distributions of C_p.- The effects of model angle of attack and nozzle-thrust coefficient on wing surface pressure distributions are presented in figures 7 and 8, respectively. In general, spanwise blowing results in significant effects on the wing upper surface pressures with little or no effect on the lower surface pressures. The blowing effects were more predominant at high angles of attack than at low angles of attack. At low angles of attack, such as 4.0° (fig. 7(b)), the high-velocity jet flow interacts with the wing flow field to induce effects on the wing surface pressures. These jet-induced effects are the same as those reported in reference 19 for the wing-alone condition; therefore, the reader is referred to reference 19 for a detailed discussion.

As angle of attack increases, the pressure distributions reflect an increasing lifting condition for the wing, as illustrated by the $\alpha = 20.8^\circ$ data in figure 7(f). For the blowing-off condition, large pressure peaks occur at the first station ($2y/b = 0.345$) outboard of the strake-wing intersection on the upper surface near the leading edge. As the distance from the strake-wing juncture increases, there is a decrease in the pressure peak and a rearward shift in the location. This trend is indicative of a wing leading-edge vortex which is well organized over a sizable portion of the wing, although its effect weakens as it expands toward the wing tip. In order to understand this trend better, pressure data from the current study with strake on are compared with strake-off data in figure 13. Similar results on a cambered wing-strake configuration are reported in reference 18.

For the blowing-on condition, the jet affects the pressures over most of the wing's upper surface except at the station inboard of the strake-wing juncture. For example, in figure 7(e), it is noted that the magnitude of the upper surface pressure peak is increased slightly by blowing, whereas some rearward locations on the wing experience pressure decreases. The largest effects of spanwise blowing occur at those conditions where, with no blowing, the wing leading-edge vortex breaks down and complete stall occurs. (See data for $2y/b = 0.866$, for example.) Figure 8 presents the pressure distributions for a range of C_T values for $\alpha \approx 24^\circ$. Although the pressure magnitudes change slightly, the distributions are similar for all the blowing rates, except for the highest C_T values for the inboard span station.

Chordwise distributions of ΔC_p.- Some of the effects of spanwise blowing on the pressure distributions that were discussed in the previous section are summarized in figures 14 and 15 for chordwise distributions of ΔC_p. Strake-

off data are presented to provide additional information for interpreting the strake-on results. For the wing-strake configuration, the effects of angle of attack on the pressure distribution at $2y/b = 0.501$ (fig. 14) are similar for blowing on or off. The data show that blowing on the wing in the presence of the strake is not as effective as blowing on the wing alone, which would be expected since both the strake and spanwise blowing attempt to control the wing vortex flow in the same manner.

Figure 15 illustrates the sensitivity of the blowing effects to span location for $\alpha \approx 21^{\circ}$. In general, the pressure distributions obtained without blowing are similar to those obtained on highly swept delta wings which have a natural leading-edge vortex (ref. 5). The same type of pressure distributions are obtained for the blowing-on case, but the lifting pressures are higher, particularly on the outboard portion of the wing ($2y/b = 0.707$, for example) where blowing delays the breakdown of the leading-edge vortex to larger span distances.

Section lift and drag characteristics.- The effects of spanwise blowing on the wing section lift characteristics are presented in figures 16 to 19. Generally, blowing increased the section lift (fig. 16) at all span stations outboard of the wing-strake juncture throughout the angle-of-attack range. The more pronounced effects occurred at the span locations outboard of $2y/b = 0.609$, which is consistent with the pressure results presented previously. These results occur because blowing enhances the vortex, delaying vortex breakdown to higher α and to span stations farther out on the wing.

Theoretical predictions of the wing section lift characteristics were calculated by using the leading-edge suction analogy. This theory accounts for the effect of the leading-edge vortex on the wing aerodynamic characteristics, but it does not model the interaction effects between the wing and jet. The basic assumptions which are used in reference 1 to apply the suction analogy to a wing with a fully developed leading-edge vortex flow are assumed to apply here on a sectional basis. A similar approach was taken in reference 19 for the wing-alone case. The potential and vortex-lift coefficients for a wing section with zero leading-edge suction are given by equations (1) and (2) in reference 19. The section thrust, suction, and lift-curve slope used in these equations were determined at different span locations by the lifting-surface theory of reference 20. For the wing station aft of the strake, only the potential wing section lift was calculated in order to be able to compare with the pressure data located on the wing.

Theoretical estimates for section lift with no vortex lift $c_{l,p}$ and with full vortex lift $c_{l,p} + c_{l,v}$ are presented in figure 16. For the case with $C_T = 0$, the section lift is estimated reasonably well at the low angles of attack, below 4°, by the potential lift estimate, which implies that the wing has little or no leading-edge vortex flow at low angles of attack. At higher angles of attack, with or without blowing, the vortex has formed and the full vortex-lift theory (dashed line) provides reasonable estimates of c_l up to the angle of attack where the vortex breaks down. The data at $2y/b = 0.866$ illustrate the effect of vortex breakdown on c_l for blowing on and off. At some span stations, the jet induces higher values of c_l than those predicted by the vortex-lift theory. For example, at $2y/b = 0.501$, the increase in c_l

due to blowing at $\alpha = 0^{o}$ is due to a jet-induced camber effect, which was observed in the studies reported in references 10 and 19.

A comparison is shown in figure 17 between experimental and theoretical section lift with various amounts of blowing for $\alpha \approx 24^{o}$. These results give an indication of the amount of spanwise blowing required to achieve the full vortex-lift level at the various span locations. The potential and full vortex-lift levels are represented by the solid and dashed lines, respectively.

With blowing off ($C_T = 0$) in figure 17(a), the strake-induced effects are large enough to achieve full vortex lift at $2y/b = 0.501$ and 0.609. With $C_T = 0.02$, the section lift at $2y/b = 0.501$ and 0.609 increases but appears relatively insensitive to further increases in C_T. At $2y/b = 0.707$, it is necessary to increase the blowing to $C_T \approx 0.17$ in order to achieve full vortex lift. At the two outermost stations, the full vortex-lift level was not attained with the C_T values considered in the current tests.

Another way of looking at the effectiveness of spanwise blowing is shown in figure 17(b), which presents the variation of section lift along the span for a range of blowing rates. The dashed line, which represents the theoretical estimate, is truncated at the strake-wing intersection located at $2y/b = 0.345$. The shape of the experimental c_l distribution curves is similar to the theoretical curve, although shifted inboard somewhat. The highest blowing rate yielded the largest section-lift values. Apparently, extremely large values of C_T would be required to achieve full vortex lift at the outboard stations.

The lift augmentation ratio $\Delta c_l/C_T$, where $\Delta c_l \equiv c_{l,\text{jet on}} - c_{l,\text{jet off}}$, is shown in figure 18 for the range of C_T values. As might be expected from some of the previous results, the data for the smallest blowing rate yield the largest augmentation ratios. The variation of augmentation ratio with C_T is not consistent at all span stations, but a decrease in $\Delta c_l/C_T$ is, in general, noted for increasing C_T. The maximum augmented lift for a given C_T occurs at $2y/b = 0.707$ for all values of C_T.

The effects of spanwise blowing on span loading are shown in figure 19 for the same data presented in figure 17(b). Blowing increased the span load outboard of the strake-wing junction, with the highest load occurring at $2y/b = 0.501$ for the largest value of C_T.

Figure 20 shows the effect of spanwise blowing on section drag characteristics for various span locations. Blowing improves the drag polars over most of the span, the most noticeable effect being at $2y/b = 0.707$ and 0.866. Estimates for the lift-dependent drag were obtained by taking the section normal force to be the resultant section force, which would be the case with zero leading-edge suction. For the situation with no vortex lift, this leads to the equation

$$c_d = c_{l,p} \tan \alpha \tag{1}$$

and for full vortex lift, to the equation

$$c_d = c_{l,tot} \tan \alpha \tag{2}$$

The $c_{l,p}$ and $c_{l,tot}$ values used in these equations are plotted in figure 16. Since the predicted values of c_d are functions of $c_{l,p}$, $c_{l,tot}$, and α, the limitations of the suction analogy that were observed for the lift results in figure 16 apply to this discussion of induced drag. The results in figure 20 show that the vortex-lift theory reasonably estimates the drag polars up to the condition where vortex breakdown occurs. In these data, vortex breakdown is indicated by a dramatic reduction in c_l. (See $2y/b = 0.866$, for example.) At some span stations, the drag is lower than the theoretical prediction, which is consistent with the jet-induced lift effects discussed in figure 16.

Wing aerodynamic characteristics.- The wing-section aerodynamic data were integrated spanwise from $2y/b = 0.259$ to 1.0 to obtain the wing aerodynamic coefficients presented in figure 21. In general, spanwise blowing on the wing results in an increase in lift at a given α, an increase in $C_{L,max}$, and improved drag polars. There also appears to be a small jet-camber effect at $\alpha = 0^o$ (refs. 10 and 19) resulting in a slight increase in C_L. Pitching moment remained linear to the higher lifts generated by blowing.

Theoretical estimates for lift were obtained by spanwise integration of the $c_{l,p}$ and $c_{l,v}$ values presented in figure 16. The $C_{L,tot}$ values presented in figure 21 include the additional lift increment due to the tip vortex as suggested by reference 20. The lift results were used to obtain estimates for lift-dependent drag. The estimates for pitching moment were obtained by using the method described in reference 20. The theory for full vortex lift for the wing (with strake on) predicts reasonably well the data obtained for the blowing-off and blowing-on cases, although the theory more closely estimates the blowing-on data ($C_T = 0.12$). As with the section characteristics, deviations from the theory occur due to vortex breakdown and jet-induced effects.

Effects of Nozzle Chordwise Location

The discussion thus far has been devoted to just one of the test configurations, where $x_n/c_r = 0.23$. The effects of blowing on the aerodynamic characteristics for all three nozzle positions are presented in figures 22 to 26.

The effect of nozzle chordwise location x_n/c_r on the wing surface pressures is illustrated in figures 22 and 23. Chordwise distributions of ΔC_p at $2y/b = 0.501$ are shown for $C_T = 0.06$ and 0.12 at an angle of attack of 24^o in figure 22 and are illustrated for $\alpha = 12.4^o$ and 20.8^o at $C_T = 0.12$ in figure 23. Moving the nozzle position rearward from $x_n/c_r = 0.15$ reduces the lifting pressures near the leading and trailing edges for all three angles of attack and increases the pressures over the midportion of the wing section at the high angles of attack.

The effect of spanwise blowing on the longitudinal aerodynamic characteristics for the configuration with $x_n/c_r = 0.15$ and 0.32 is presented in figures 24 and 25, respectively. Comparisons of these data with the theoretical predictions are similar to those observed for the $x_n/c_r = 0.23$ configuration in figure 21. The effect of nozzle position on the aerodynamic characteristics is summarized in figure 26. Increasing x_n/c_r from 0.15 generally decreases

C_L, increases C_D, and has little effect on C_m over most of the angle-of-attack range.

CONCLUSIONS

The present investigation was conducted to measure the effects of spanwise blowing on the pressure distributions of a 44° swept trapezoidal wing-strake configuration. Wind-tunnel data were obtained at a free-stream Mach number of 0.26 for a range of model angle of attack, jet thrust coefficient, and nozzle chordwise location. Results of this study lead to the following conclusions:

1. The pressure distributions obtained on this wing-strake configuration with blowing off are similar to those obtained on a highly swept wing which has a well-established leading-edge vortex. Spanwise blowing delays the vortex breakdown to larger span distances and, hence, increases the lifting pressures.

2. Vortex lift was achieved at span stations immediately outboard of the strake-wing junction with no blowing, but increased levels of spanwise blowing are necessary to achieve vortex lift at increased span distances.

3. Blowing on the wing in the presence of the strake is not as effective as blowing on the wing alone.

4. Moving nozzle position rearward decreased lift, increased drag, and had little effect on pitching moment over the angle-of-attack range.

5. Spanwise blowing increases, in general, total lift throughout the angle-of-attack range, thus increasing the maximum lift coefficient. In addition, blowing improves the drag polar and extends the linear pitching moment to higher lifts.

6. The leading-edge suction analogy provided reasonable estimates of lift, induced drag, and pitching moment resulting from spanwise blowing up to wing stall and where jet-induced effects were negligible.

Langley Research Center
National Aeronautics and Space Administration
Hampton, VA 23665
December 11, 1978

REFERENCES

1. Polhamus, Edward C.: A Concept of the Vortex Lift of Sharp-Edge Delta Wings Based on a Leading-Edge-Suction Analogy. NASA TN D-3767, 1966.

2. Polhamus, Edward C.: Application of the Leading-Edge-Suction Analogy of Vortex Lift to the Drag Due to Lift of Sharp-Edge Delta Wings. NASA TN D-4739, 1968.

3. Wentz, William H., Jr.; and Kohlman, David L.: Wind Tunnel Investigations of Vortex Breakdown on Slender Sharp-Edged Wings. Rep. FRL 68-013 (Grant NGR-17-002-043), Univ. of Kansas Center for Research, Inc., Nov. 27, 1969. (Available as NASA CR-98737.)

4. Polhamus, Edward C.: Predictions of Vortex-Lift Characteristics by a Leading-Edge Suction Analogy. J. Aircr., vol. 8, no. 4, Apr. 1971, pp. 193-199.

5. Hummel, D.: Study of the Flow Around Sharp-Edged Slender Delta Wings With Large Angles of Attack. NASA TT F-15,107, 1973.

6. Werlé, H.: Partage et Rencontre d'Écoulements Fluides. Étude Effectuée à la Cuve à Huile et au Tunnel Hydrodynamique à Visualisation de l'O.N.E.R.A. La Rech. Aeron., no. 79, Nov.-Dec. 1960, pp. 9-26.

7. Cornish, J. J., III: High Lift Applications of Spanwise Blowing. ICAS Paper No. 70-09, Sept. 1970.

8. Werlé, H.; and Gallon, M.: Flow Control by Cross Jet. NASA TT F-14,548, 1972.

9. Werlé, Henri: Sur l'Écoulement au Bord d'Attaque d'un Profil Portant. La Rech. Aérospatiale, no. 4, July-Aug. 1973, pp. 197-218.

10. Dixon, C. J.: Lift Augmentation by Lateral Blowing Over a Lifting Surface. AIAA Paper No. 69-193, Feb. 1969.

11. Dixon, C. J.: Lift and Control Augmentation by Spanwise Blowing Over Trailing Edge Flaps and Control Surfaces. AIAA Paper No. 72-781, Aug. 1972.

12. Bradley, R. G.; and Wray, W. O.: A Conceptual Study of Leading-Edge-Vortex Enhancement by Blowing. J. Aircr., vol. 11, no. 1, Jan. 1974, pp. 33-38.

13. Dixon, C. J.; Theisen, J. G.; and Scruggs, R. M.: Theoretical and Experimental Investigations of Vortex Lift Control by Spanwise Blowing. Volume I - Experimental Research. LG73ER-0169, Lockheed Aircraft Corp., Sept. 15, 1973.

14. Bradley, R. G.; Wray, W. O.; and Smith, C. W.: An Experimental Investigation of Leading-Edge Vortex Augmentation by Blowing. NASA CR-132415, 1974.

15. Erickson, Gary E.; and Campbell, James F.: Augmentation of Maneuver Performance by Spanwise Blowing. NASA TM X-73998, 1977.

16. Henderson, William P.; and Huffman, Jarrett K.: Effect of Wing Design on the Longitudinal Aerodynamic Characteristics of a Wing-Body Model at Subsonic Speeds. NASA TN D-7099, 1972.

17. Ray, Edward J.; McKinney, Linwood W.; and Carmichael, Julian G.: Maneuver and Buffet Characteristics of Fighter Aircraft. NASA TN D-7131, 1973.

18. Henderson, William P.: Pressure Distributions on a Cambered Wing-Body Configuration at Subsonic Mach Numbers. NASA TN D-7946, 1975.

19. Campbell, James F.: Effects of Spanwise Blowing on the Pressure Field and Vortex-Lift Characteristics of a 44° Swept Trapezoidal Wing. NASA TN D-7907, 1975.

20. Lamar, John E.; and Gloss, Blair B.: Subsonic Aerodynamic Characteristics of Interacting Lifting Surfaces With Separated Flow Around Sharp Edges Predicted by a Vortex-Lattice Method. NASA TN D-7921, 1975.

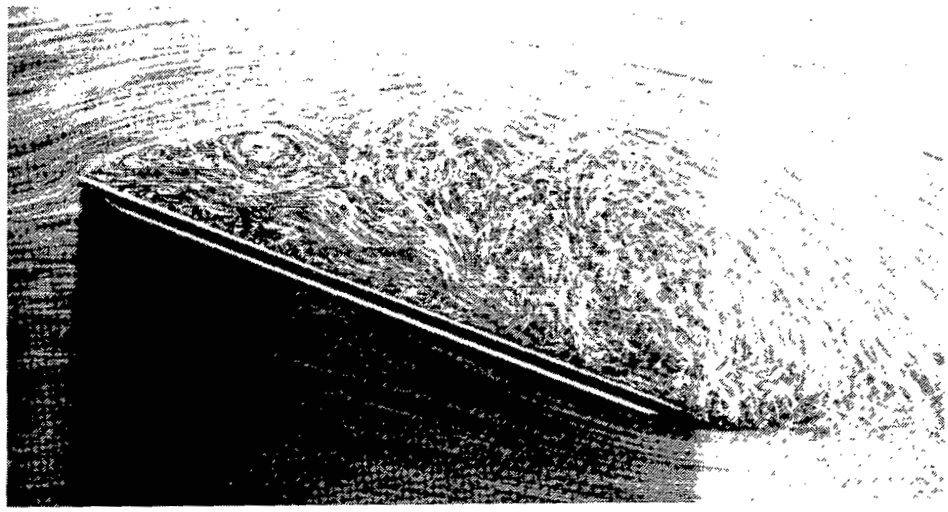

(a) Without transverse blowing.

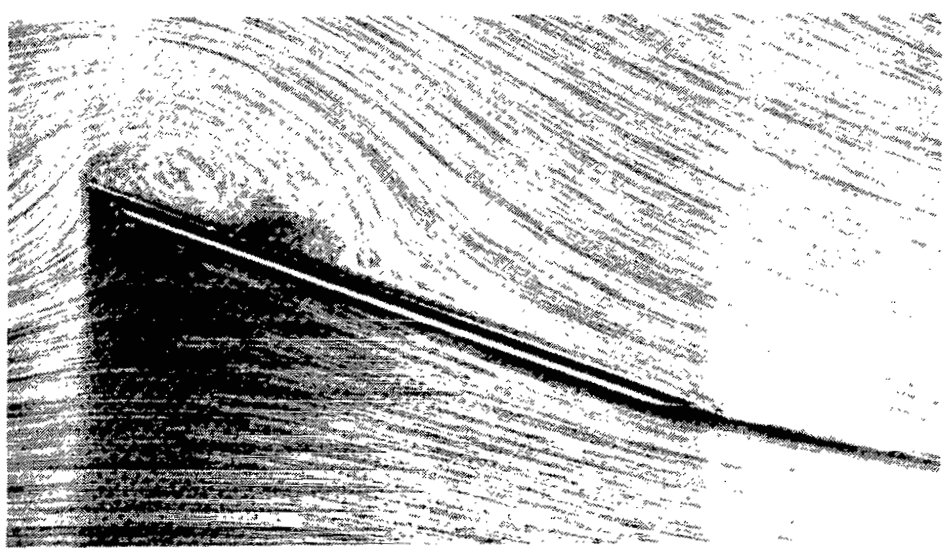

(b) With transverse blowing.

L-75-146

Figure 1.- Photographs of spanwise blowing on a rectangular flat plate (from ref. 9).

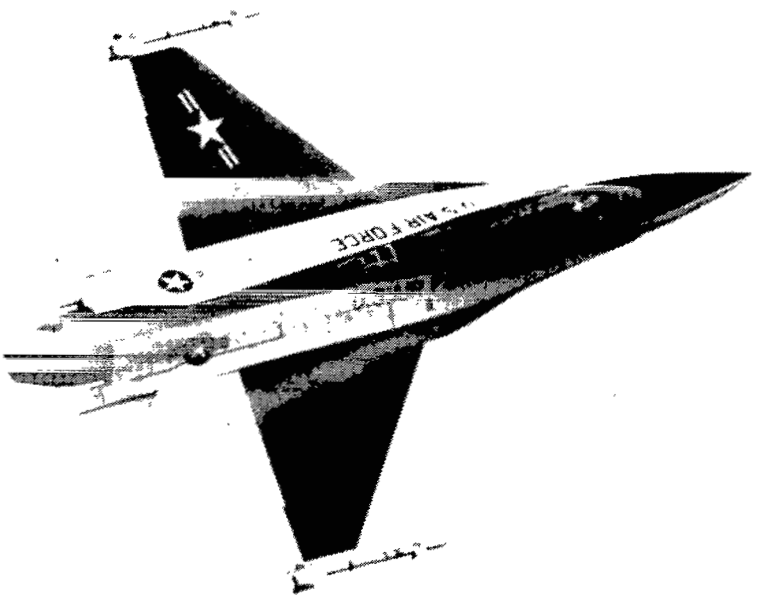

L-78-165

(a) General Dynamics YF-16 lightweight fighter, from Aviation Week and Space Technology, June 16, 1975, p. 23. (Copyright Aviation Week and Space Technology, reprinted with permission.)

Figure 2.- Photographs of vortex flow generated by highly swept maneuver strakes.

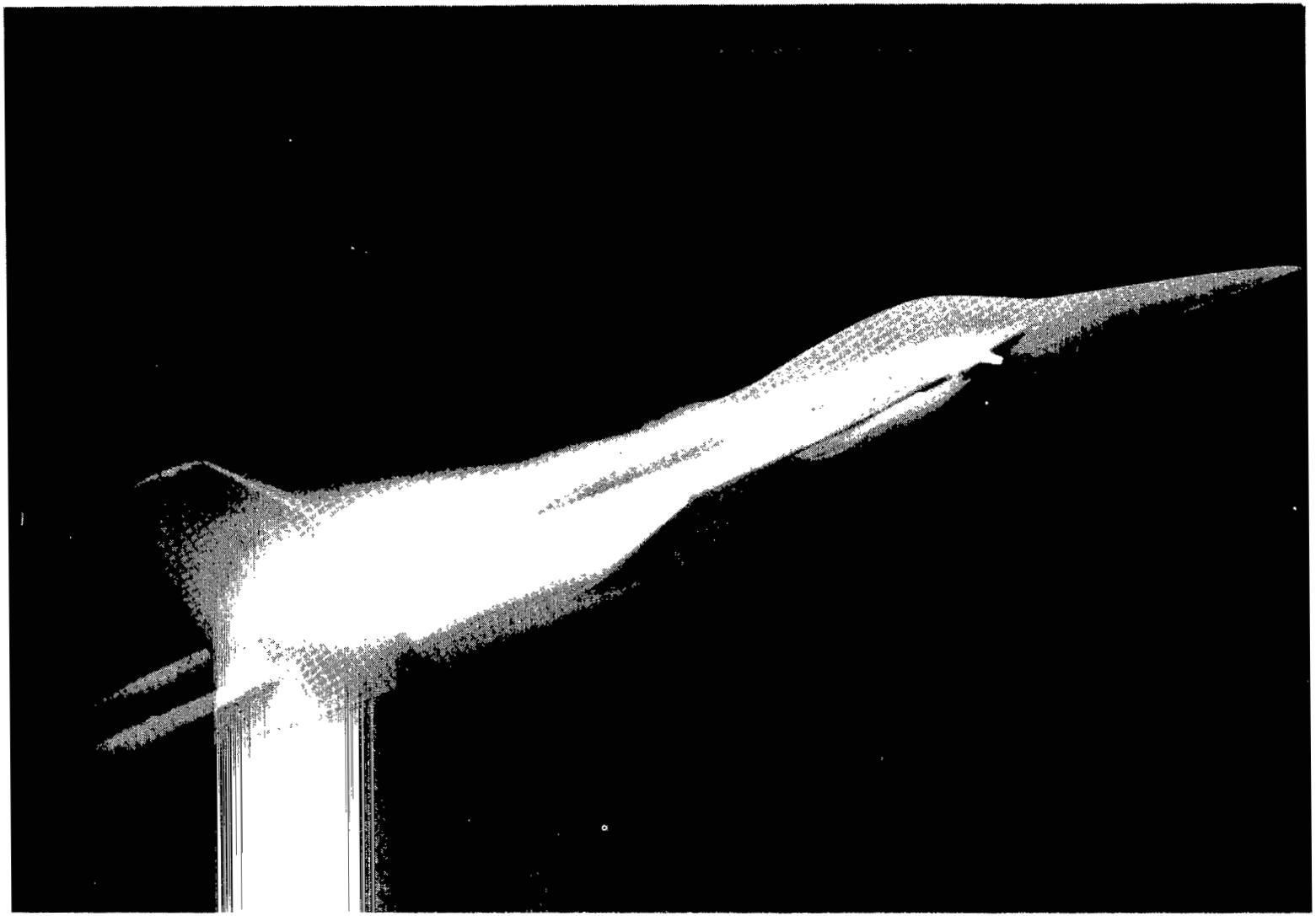

L-78-166

(b) Northrop YF-17 water-tunnel model.

Figure 2.- Concluded.

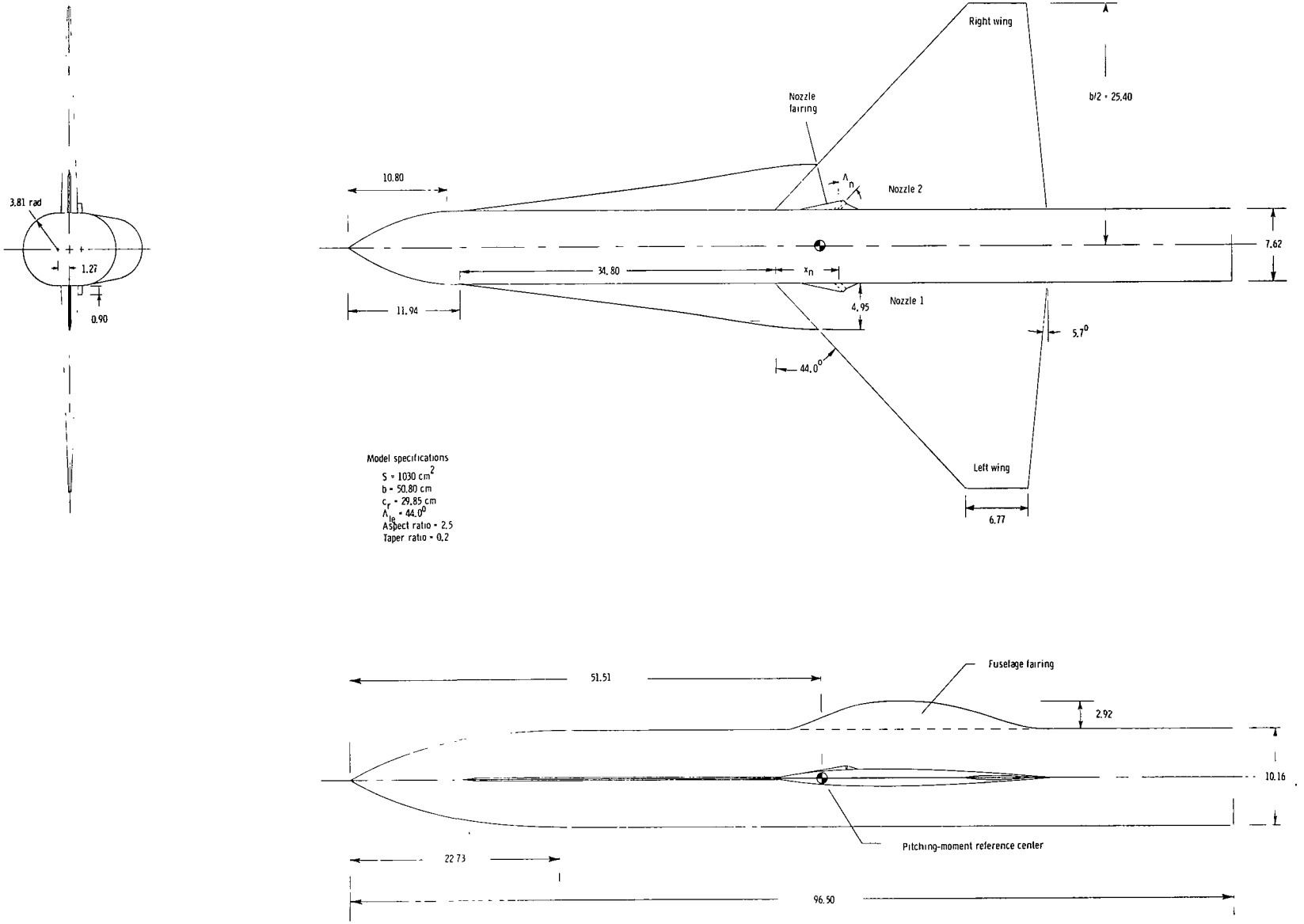

(a) Three-view drawing.

Figure 3.- Details of wind-tunnel model. All dimensions are in centimeters.

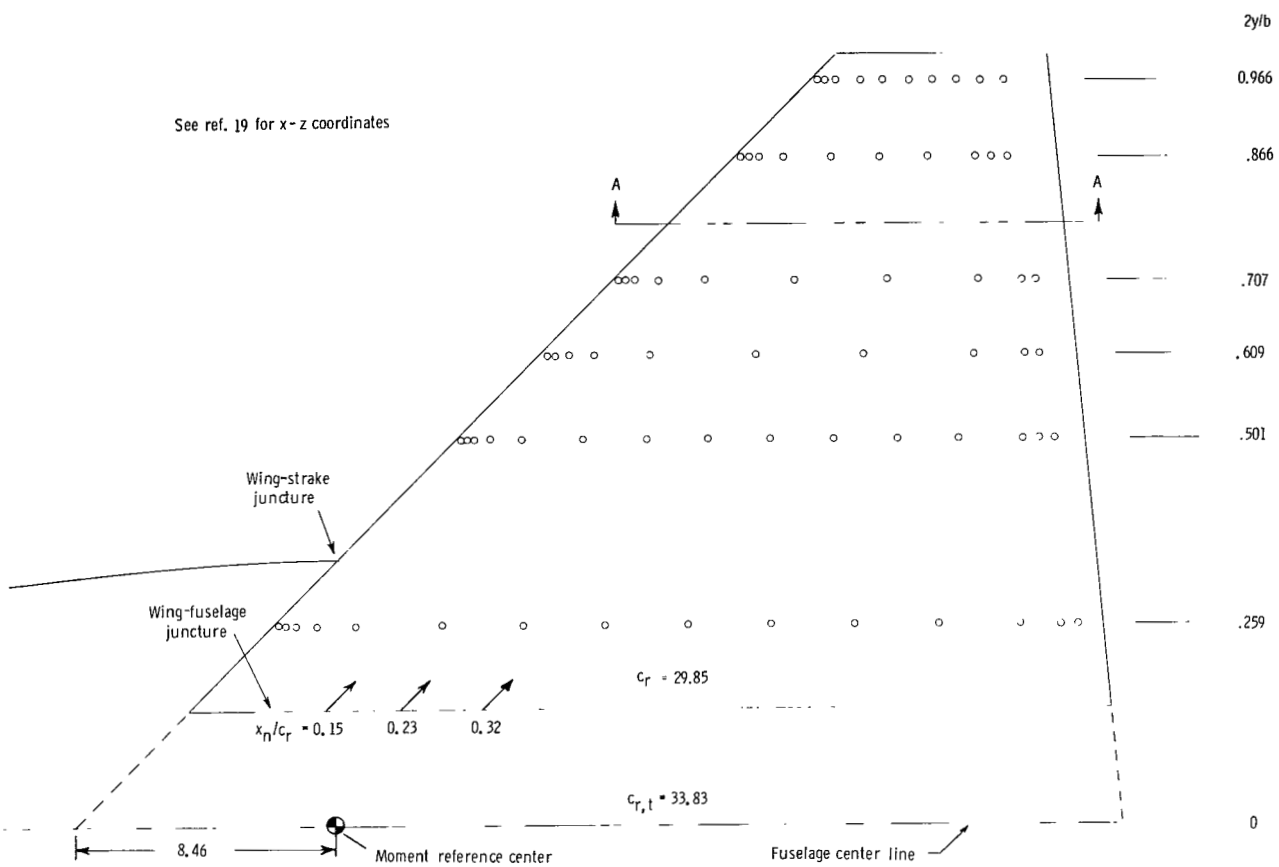

Section A-A (typical)

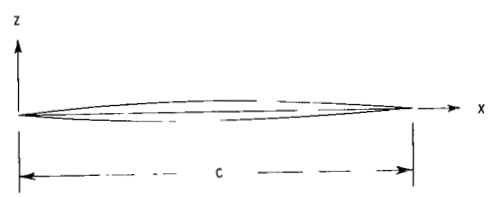

(b) Location of pressure orifices on upper surface of right wing and lower surface of left wing.

Figure 3.- Concluded.

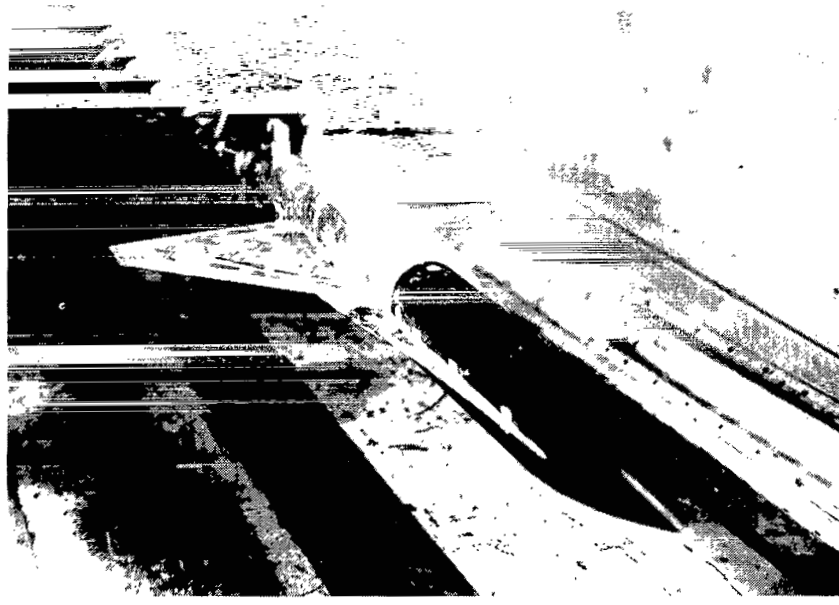

L-73-5688

Front view

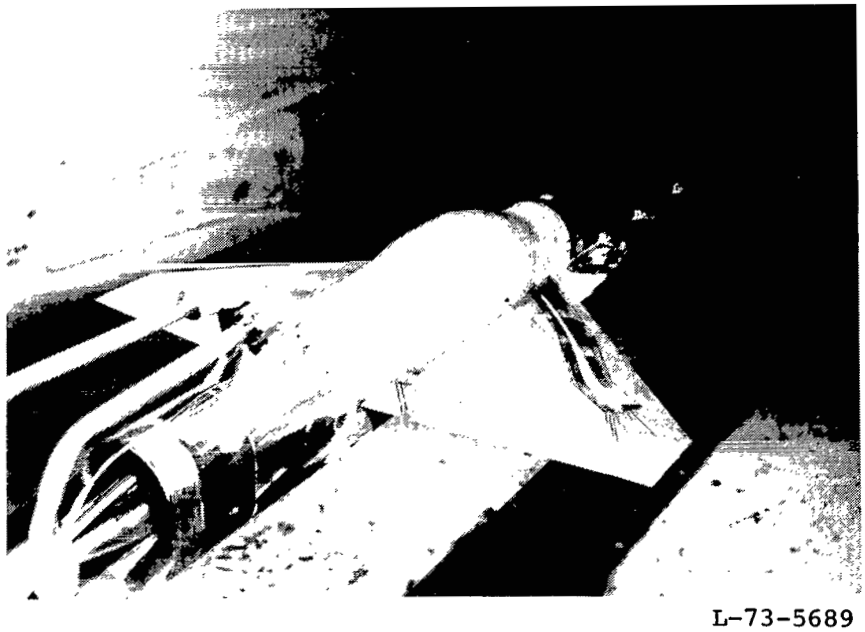

L-73-5689

Rear view

Figure 4.- Photographs of model mounted in the test section of the Langley high-speed 7- by 10-foot tunnel.

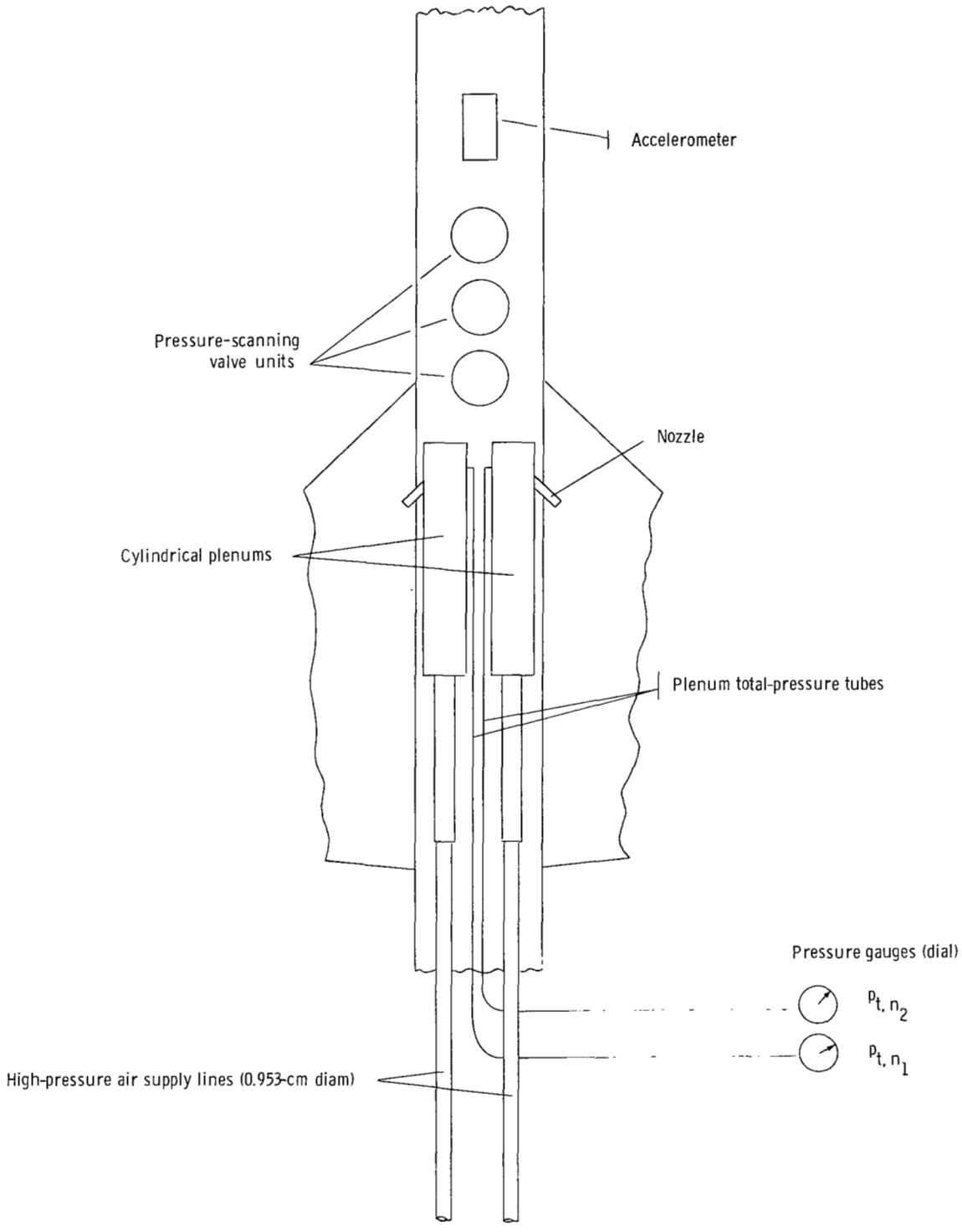

Figure 5.- Schematic diagram of air supply and measurement devices.

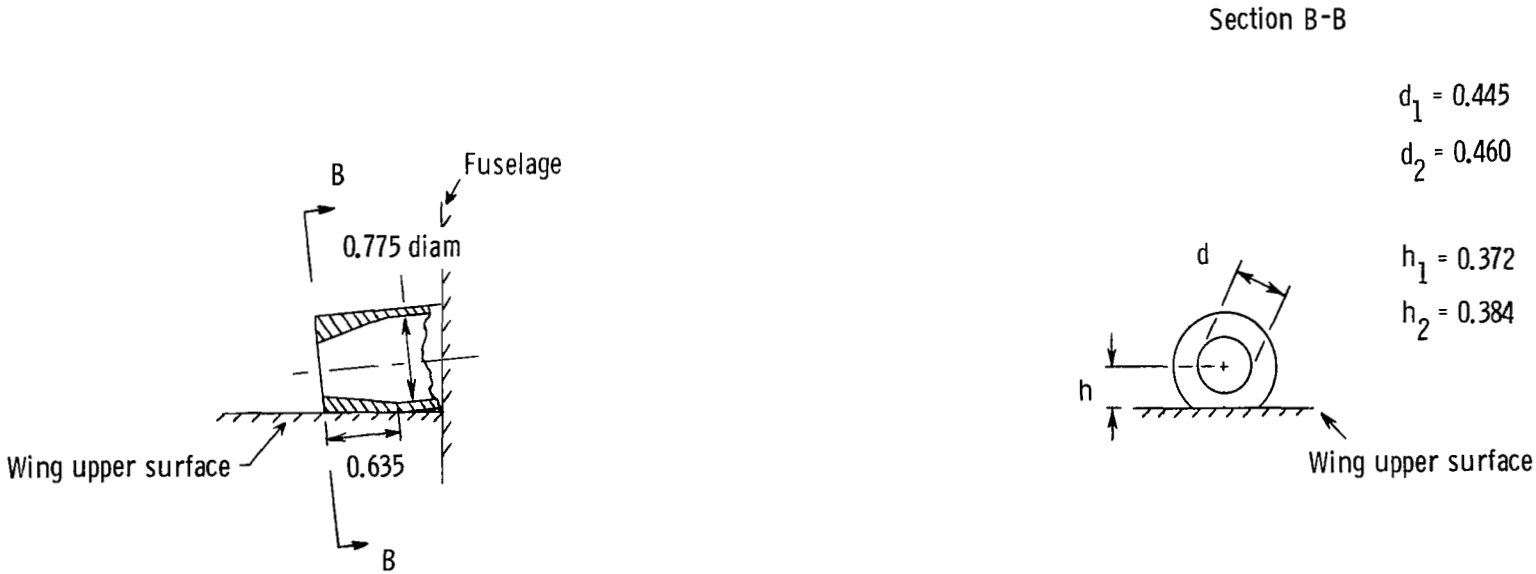

Figure 6.- Nozzle geometry and vertical location. h/d = 0.835 for all test conditions. All dimensions are in centimeters.

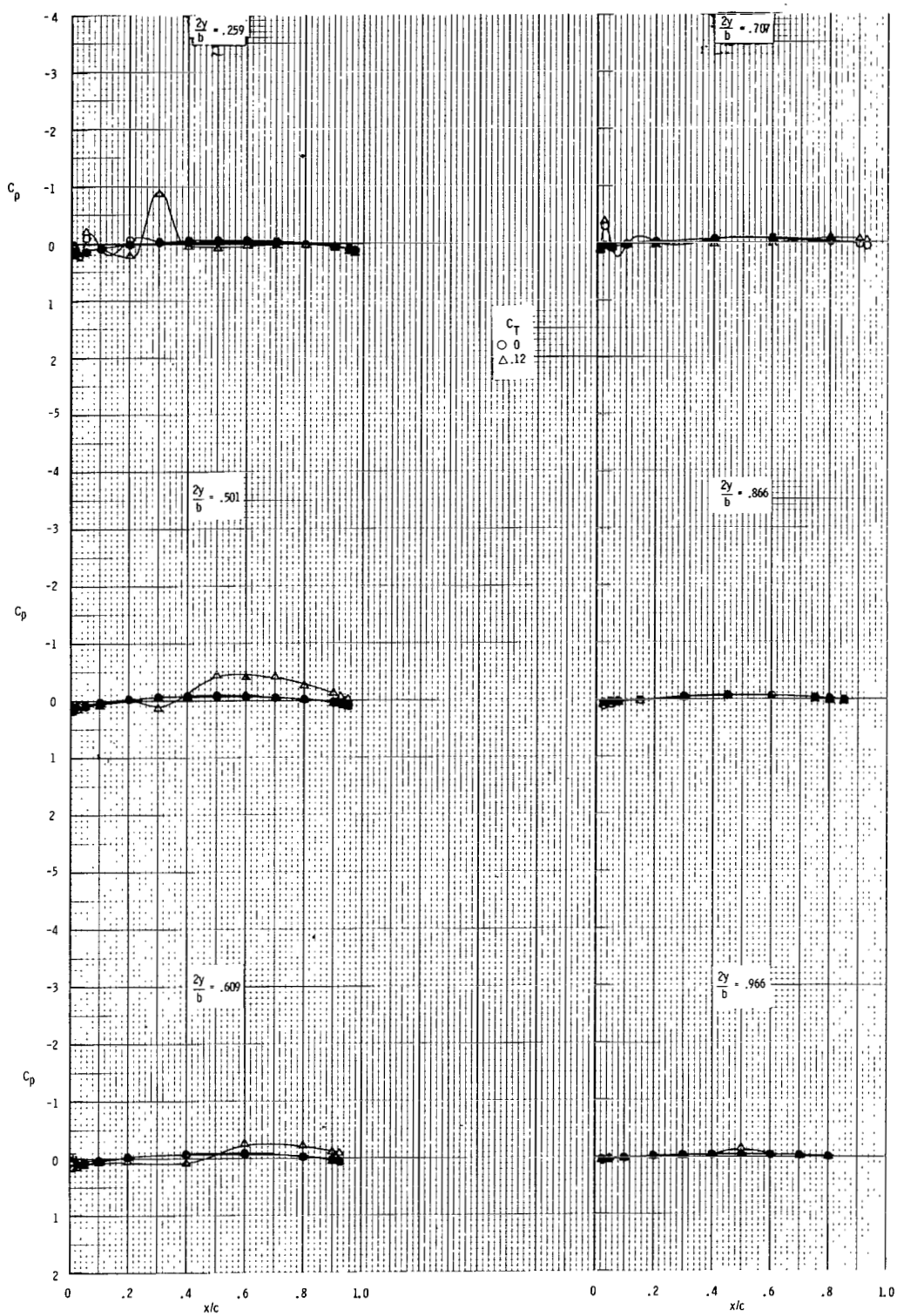

(a) $\alpha = 0^{o}$.

Figure 7.- Effect of spanwise blowing on chordwise distributions of C_p for a range of α with strake on. $x_n/c_r = 0.23$.

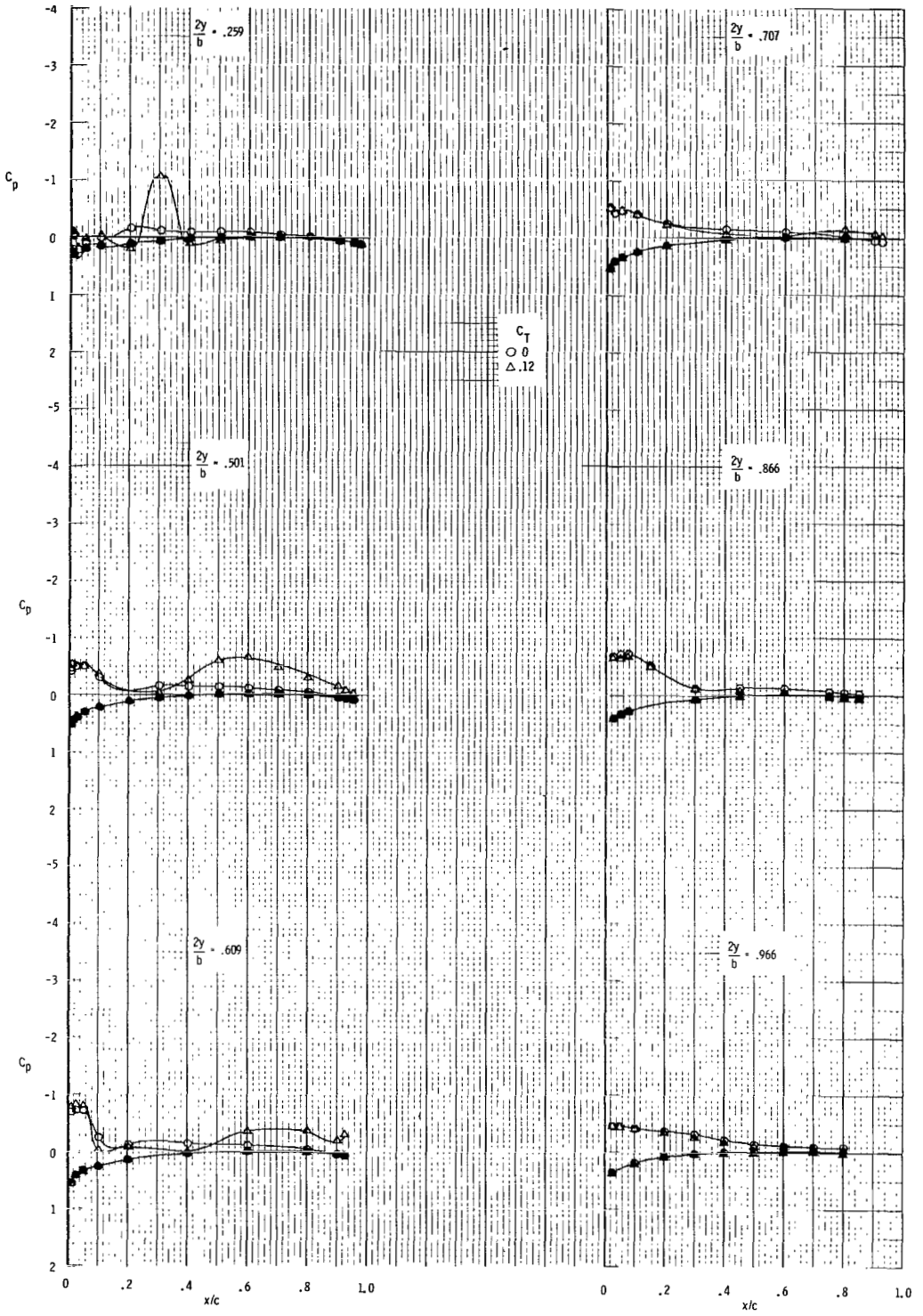

(b) $\alpha = 4.0^{\circ}$.

Figure 7.- Continued.

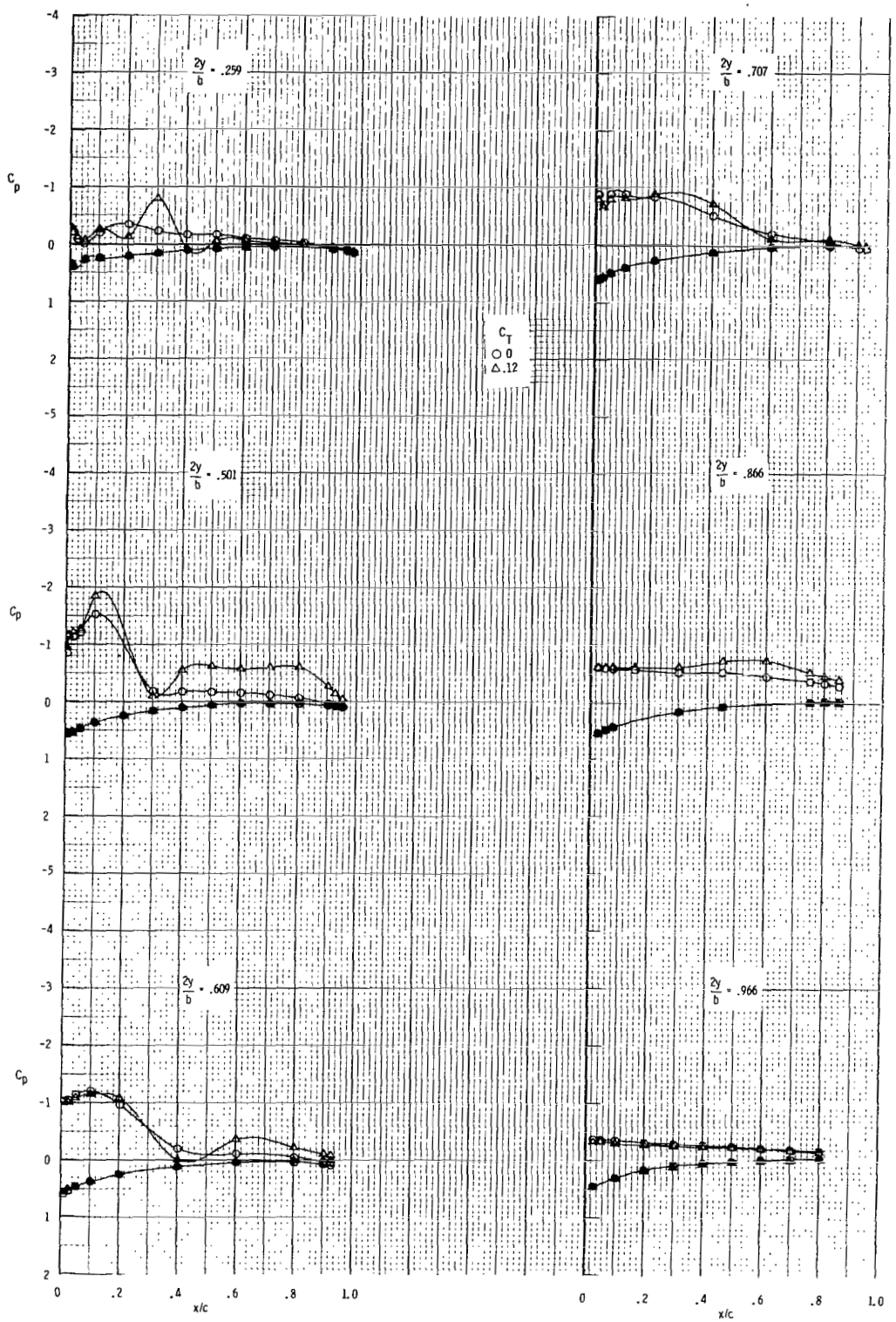

(c) $\alpha = 8.1^{\circ}$.

Figure 7.- Continued.

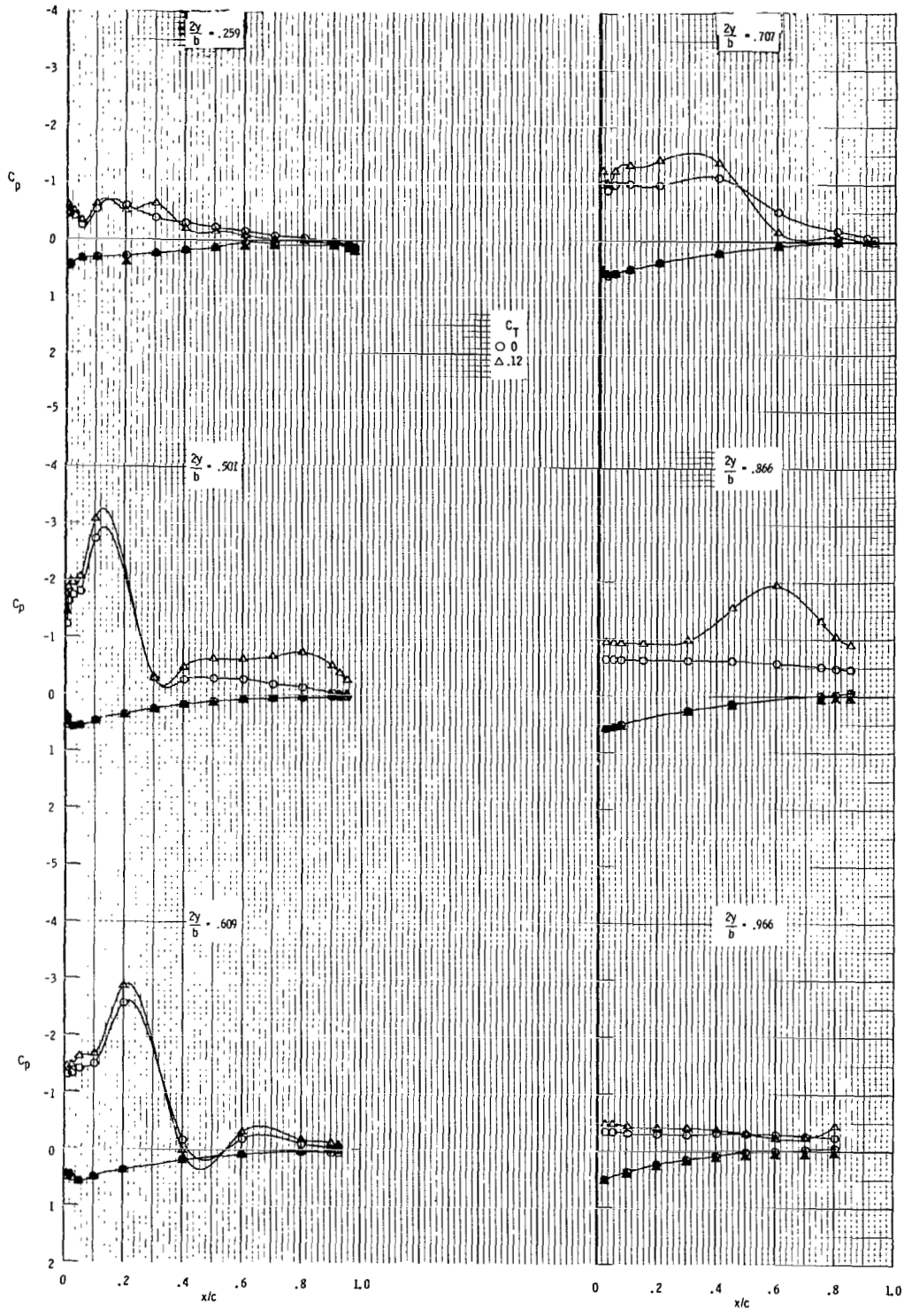

(d) $\alpha = 12.4^{\circ}$.

Figure 7.- Continued.

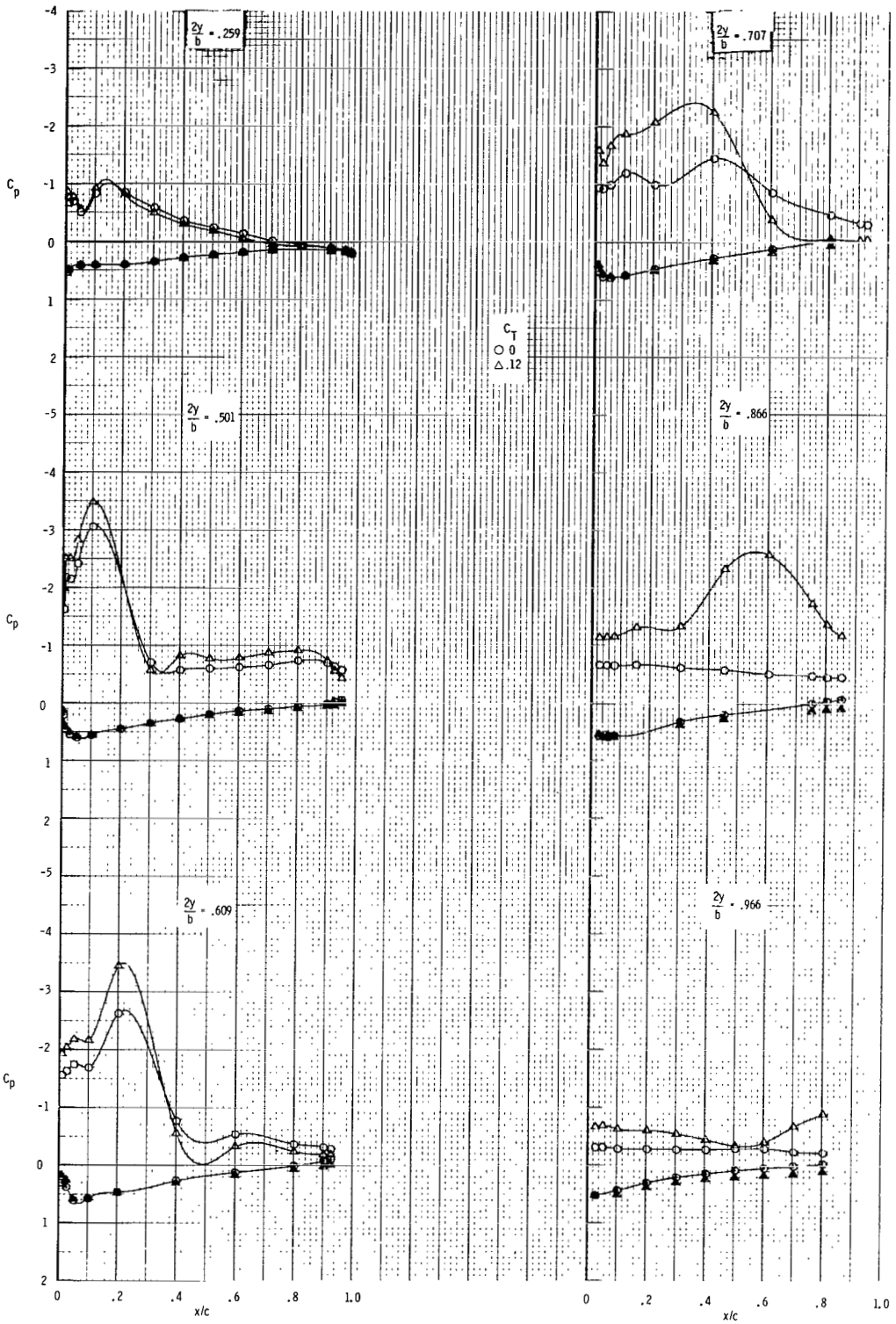

(e) $\alpha = 16.3^{\circ}$.

Figure 7.- Continued.

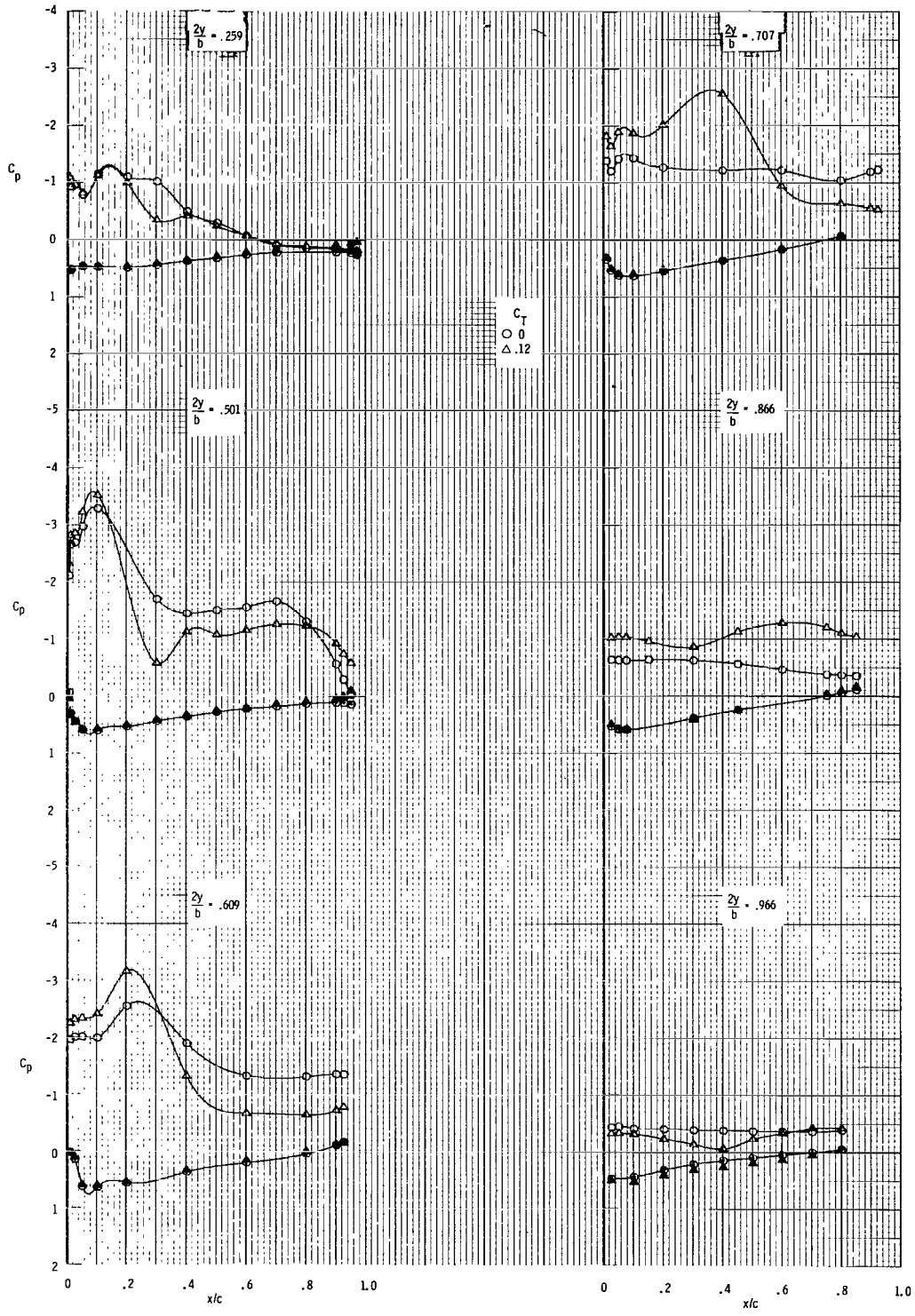

(f) $\alpha = 20.8^{\circ}$.

Figure 7.- Continued.

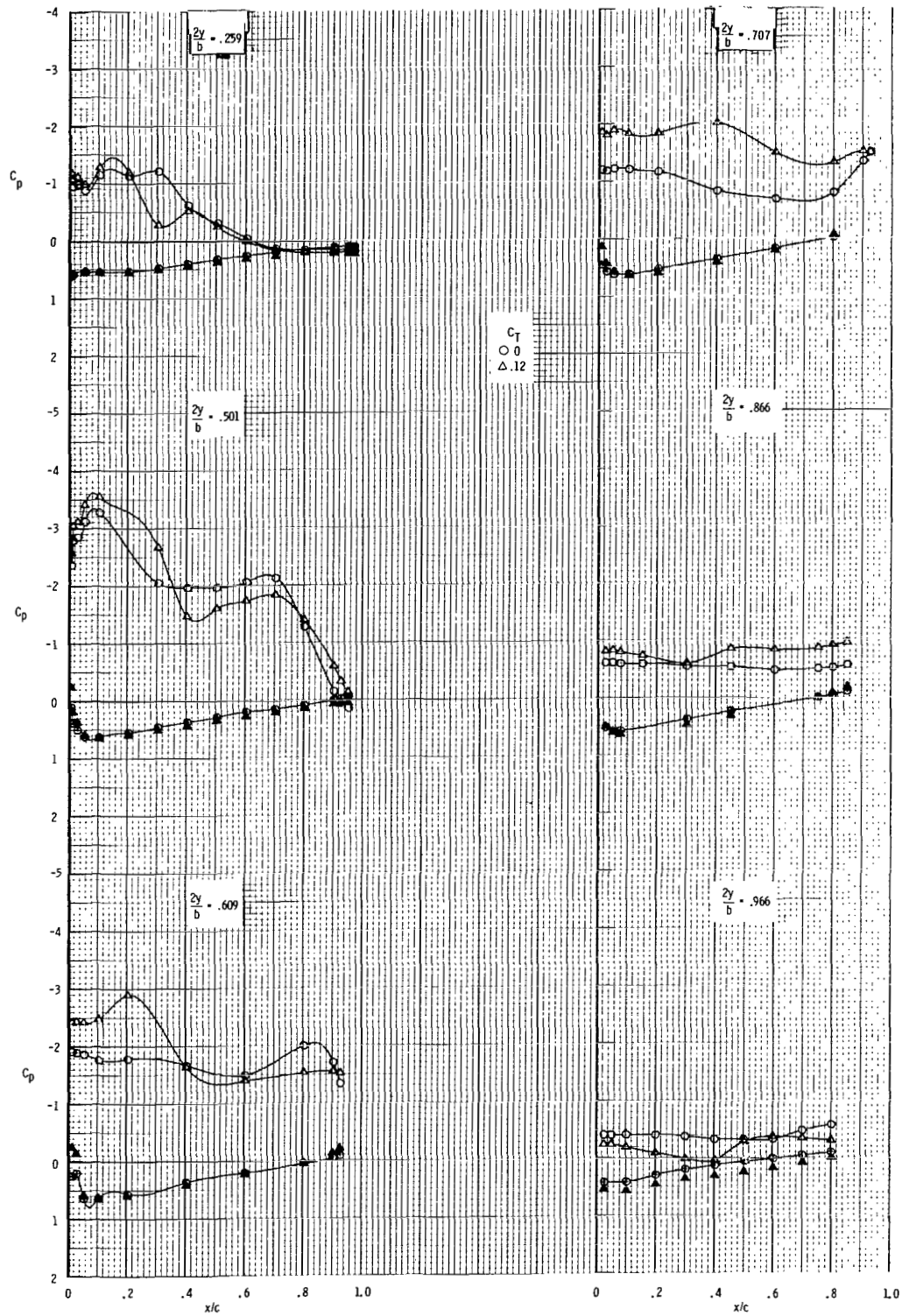

(g) $\alpha = 23.9^{\circ}$.

Figure 7.- Concluded.

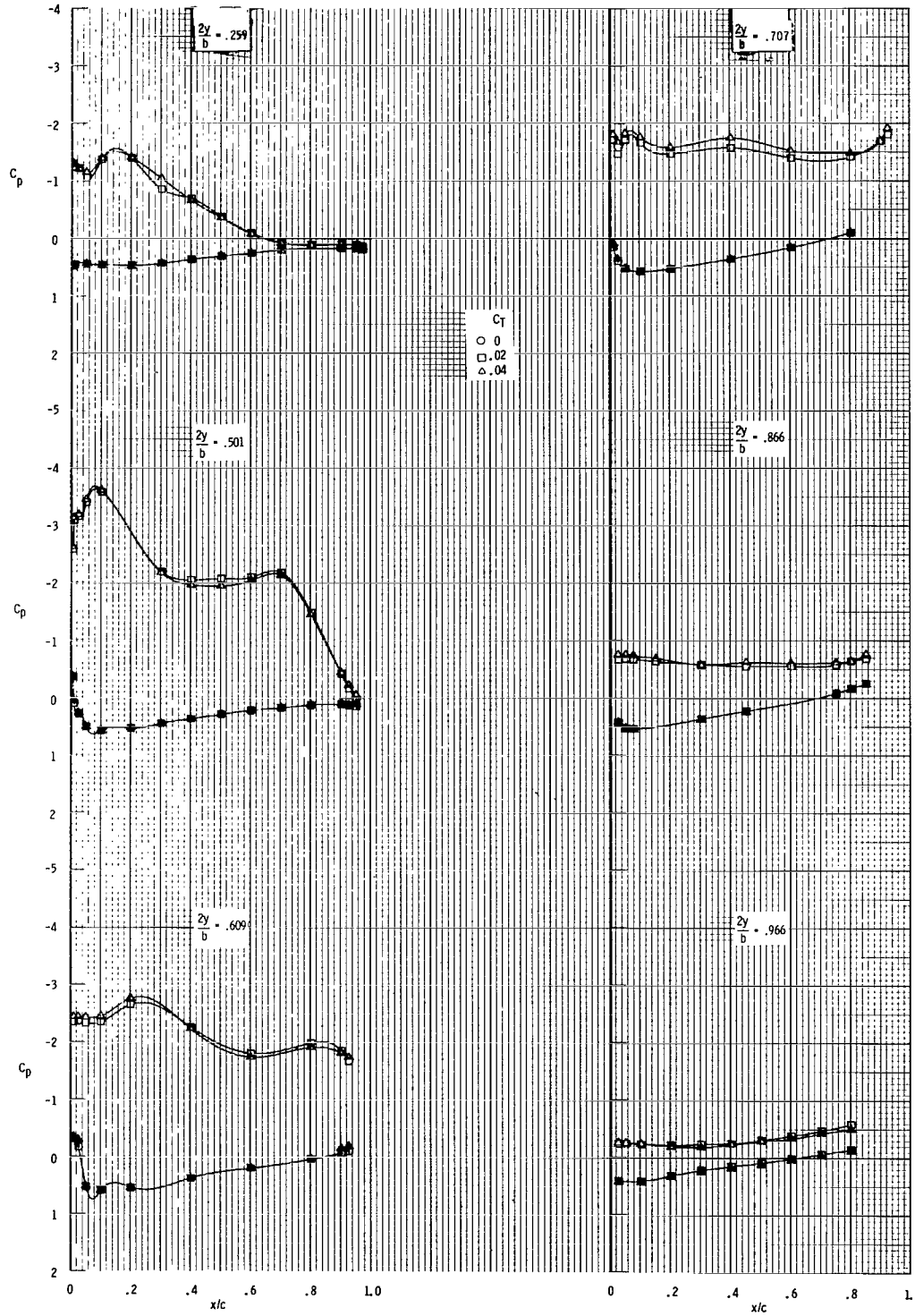

(a) C_T = 0, 0.02, and 0.04.

Figure 8.- Effect of C_T on chordwise distributions of C_p for $\alpha \approx 24^o$ with strake on. x_n/c_r = 0.23.

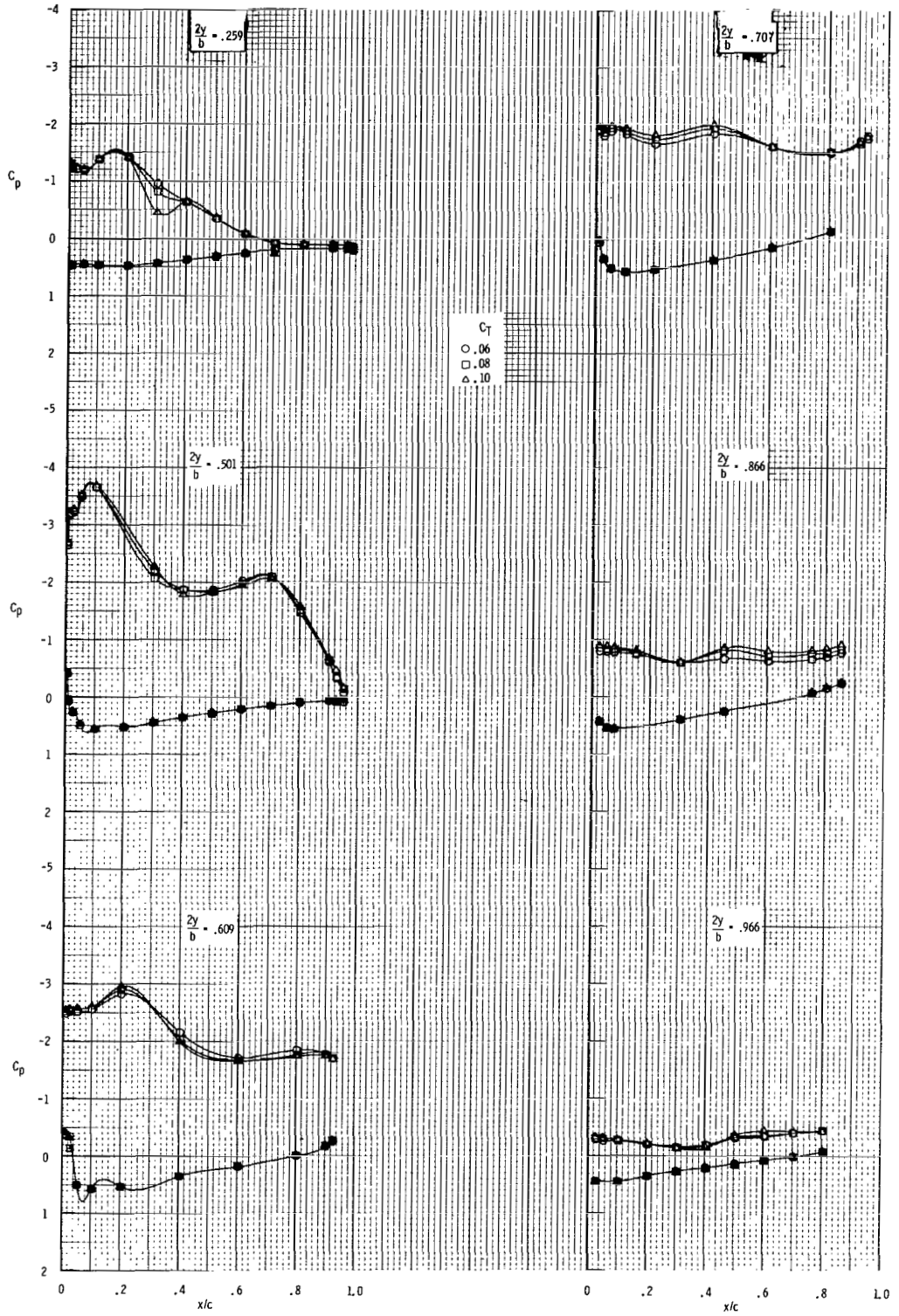

(b) C_T = 0.06, 0.08, and 0.10.

Figure 8.- Continued.

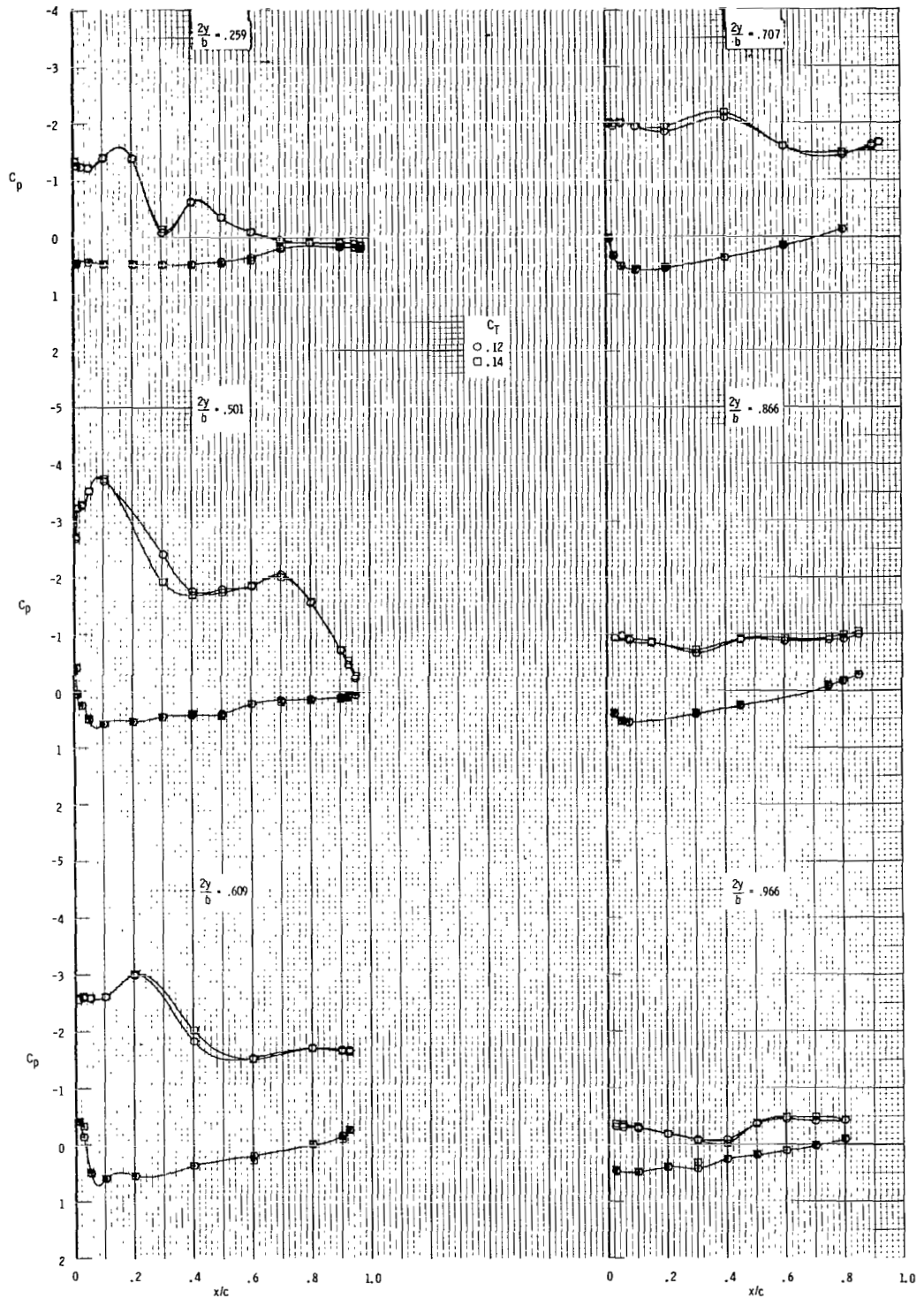

(c) C_T = 0.12 and 0.14.

Figure 8.- Continued.

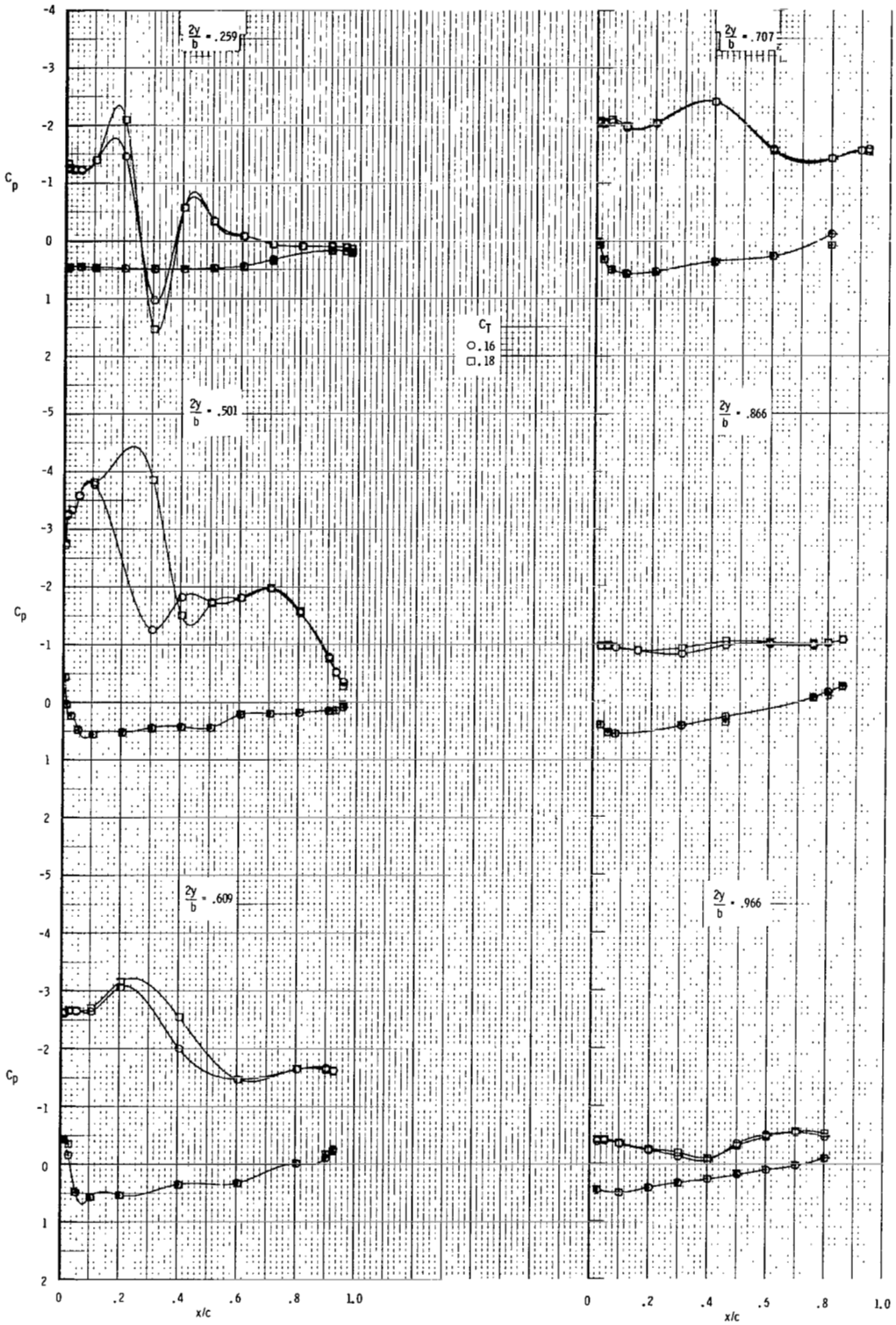

(d) C_T = 0.16 and 0.18.

Figure 8.- Concluded.

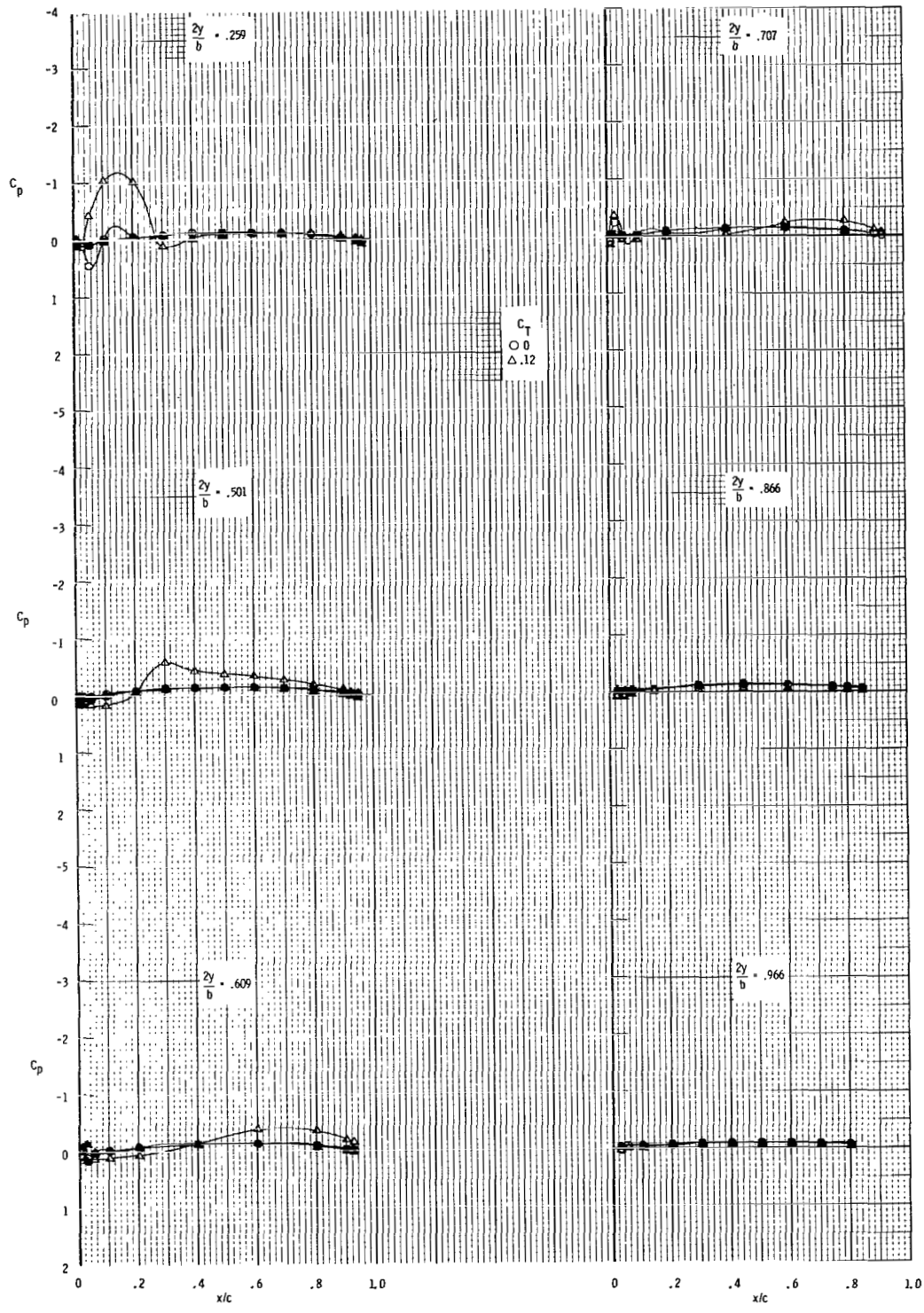

(a) $\alpha = 0^{o}$.

Figure 9.- Effect of spanwise blowing on chordwise distributions of C_p for a range of α with strake on. $x_n/c_r = 0.15$.

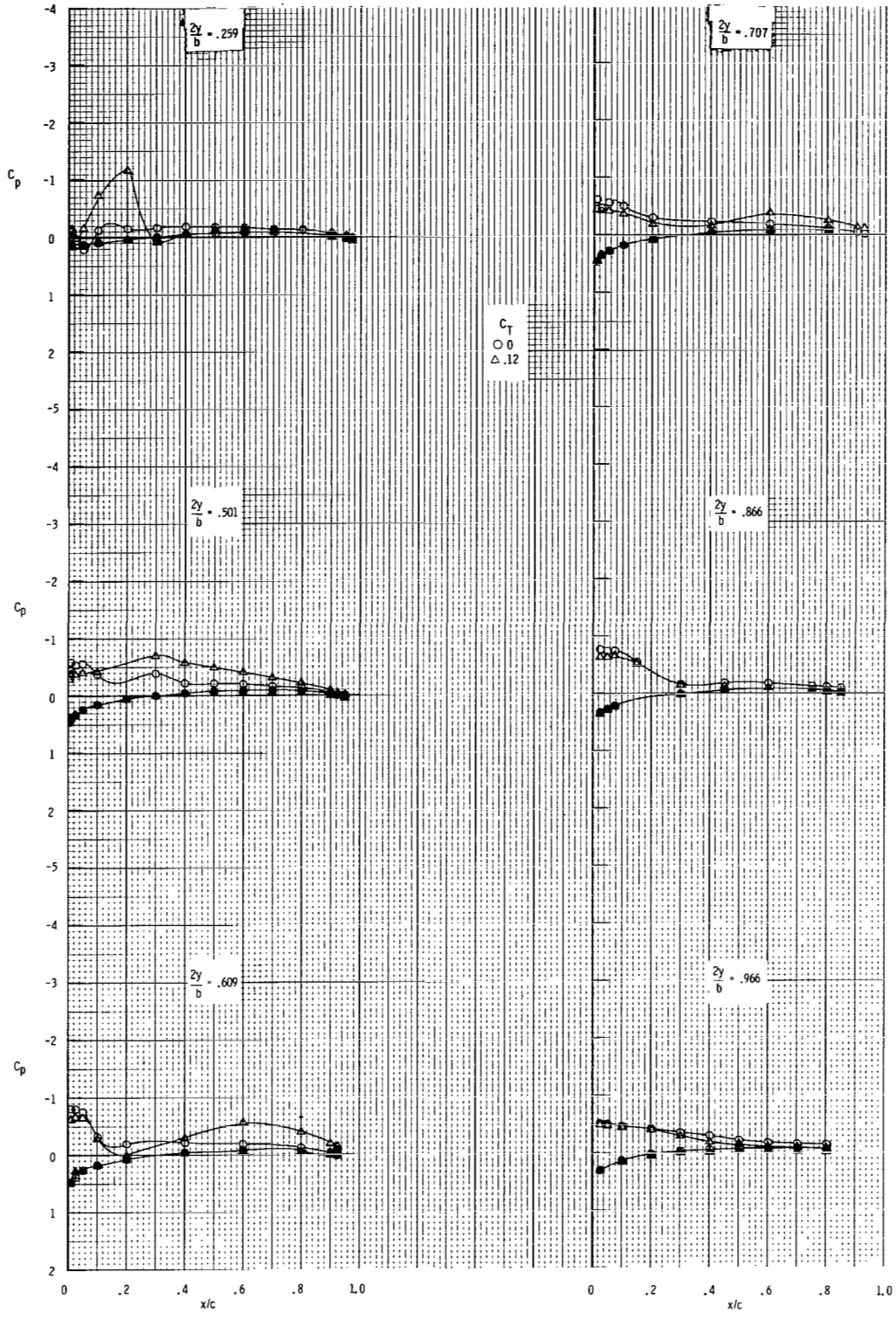

(b) $\alpha = 4.0^{\circ}$.

Figure 9.- Continued.

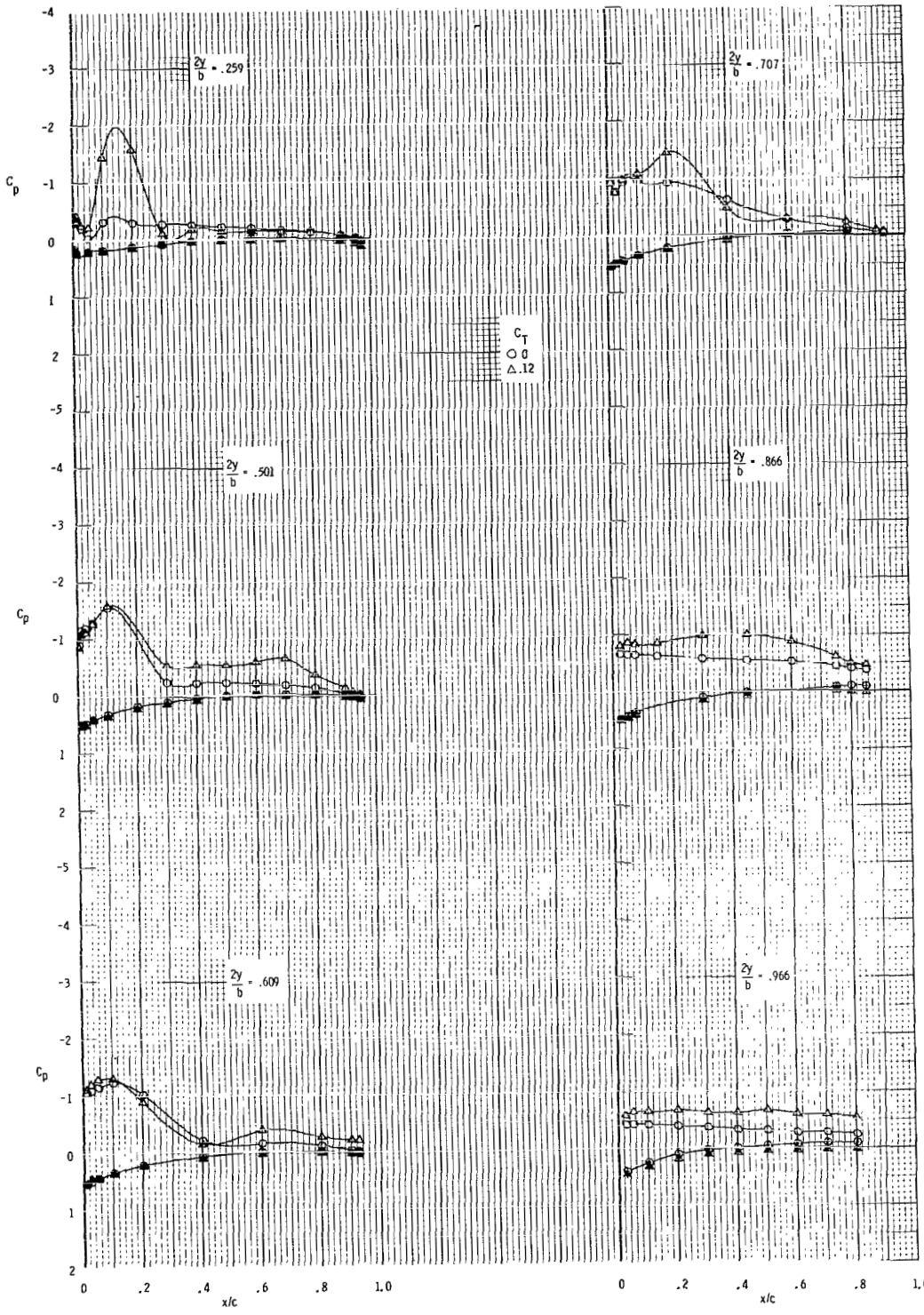

(c) $\alpha = 8.1^{\circ}$.

Figure 9.- Continued.

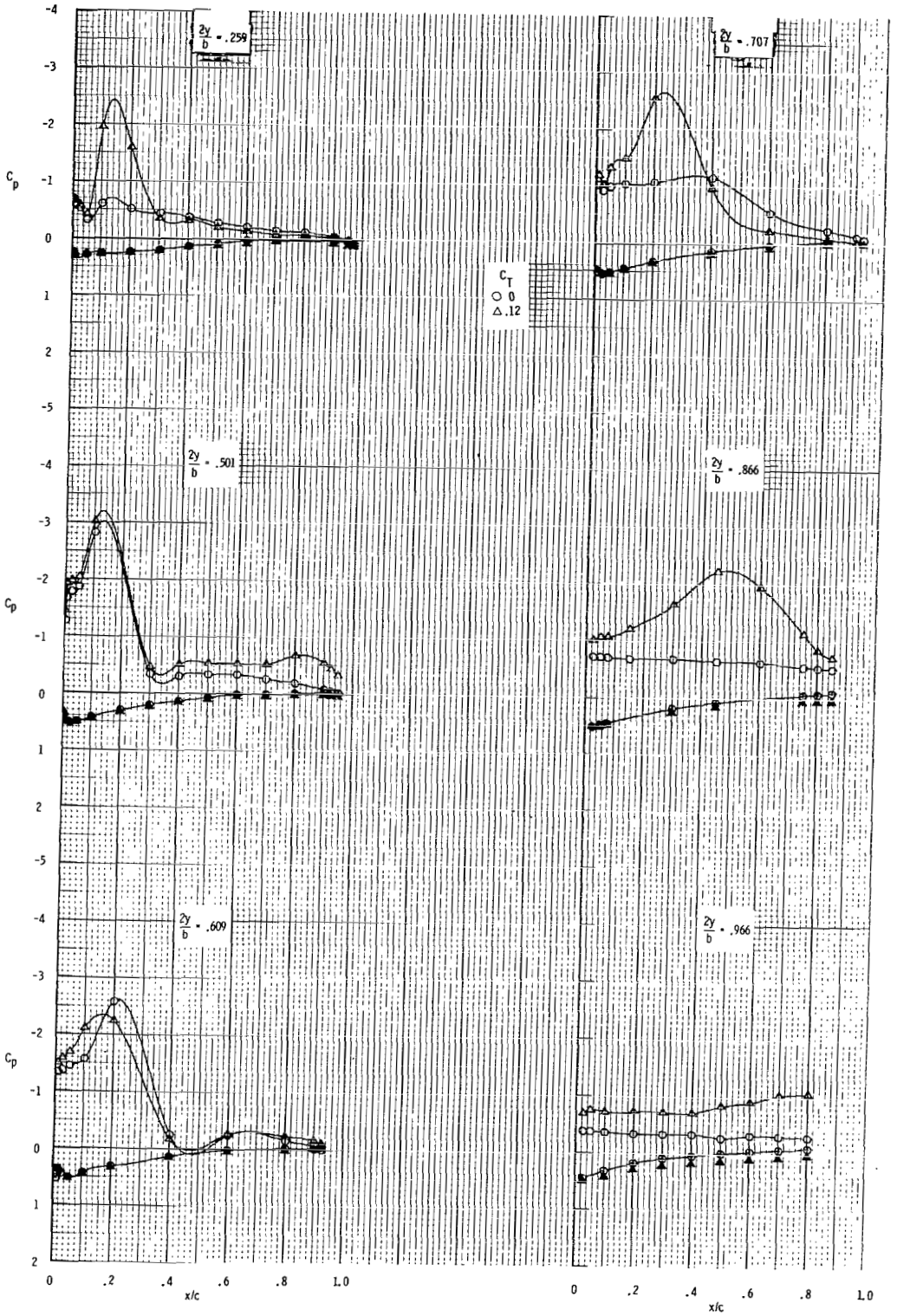

(d) $\alpha = 12.4^{\circ}$.

Figure 9.- Continued.

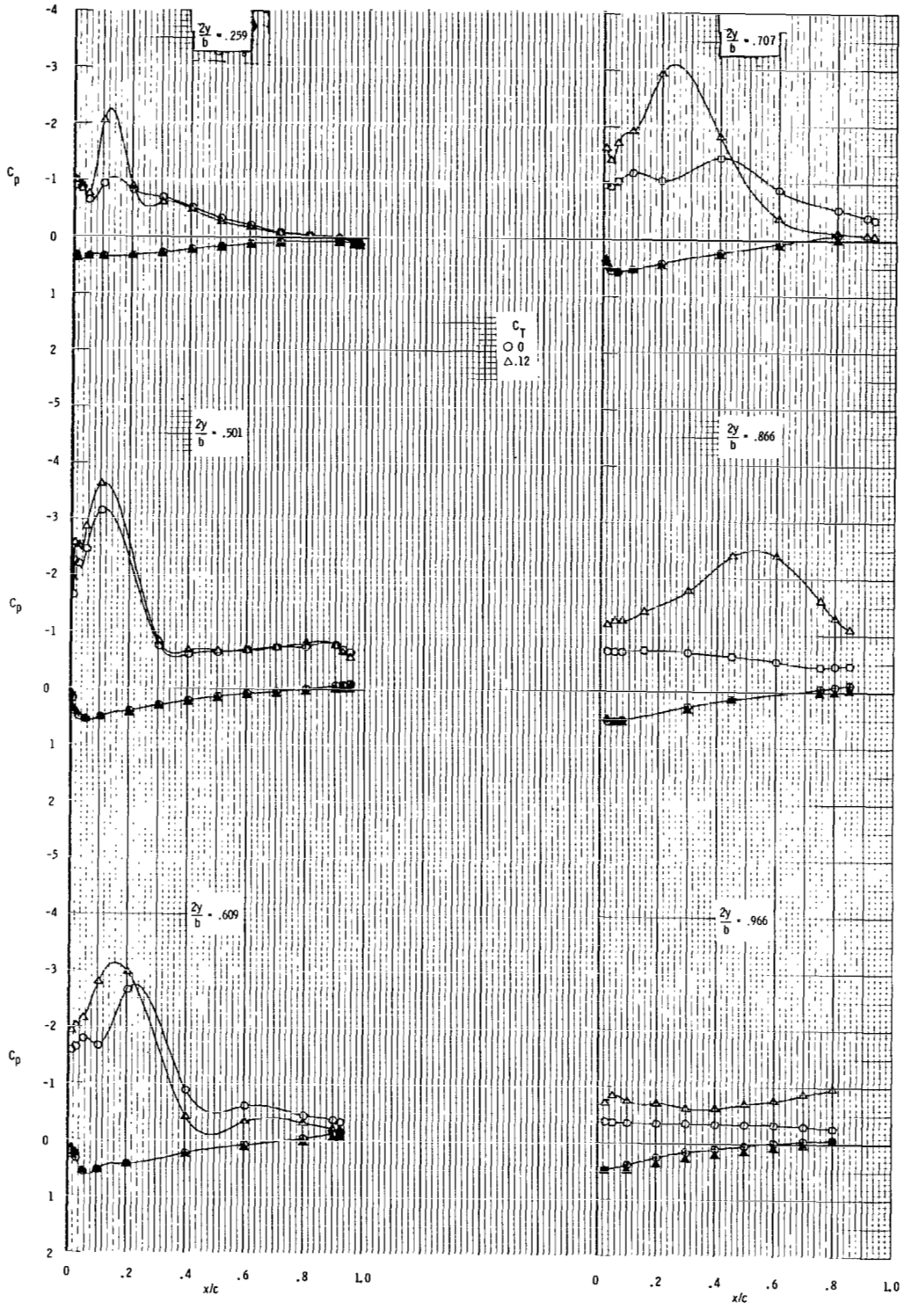

(e) $\alpha = 16.6^{o}$.

Figure 9.- Continued.

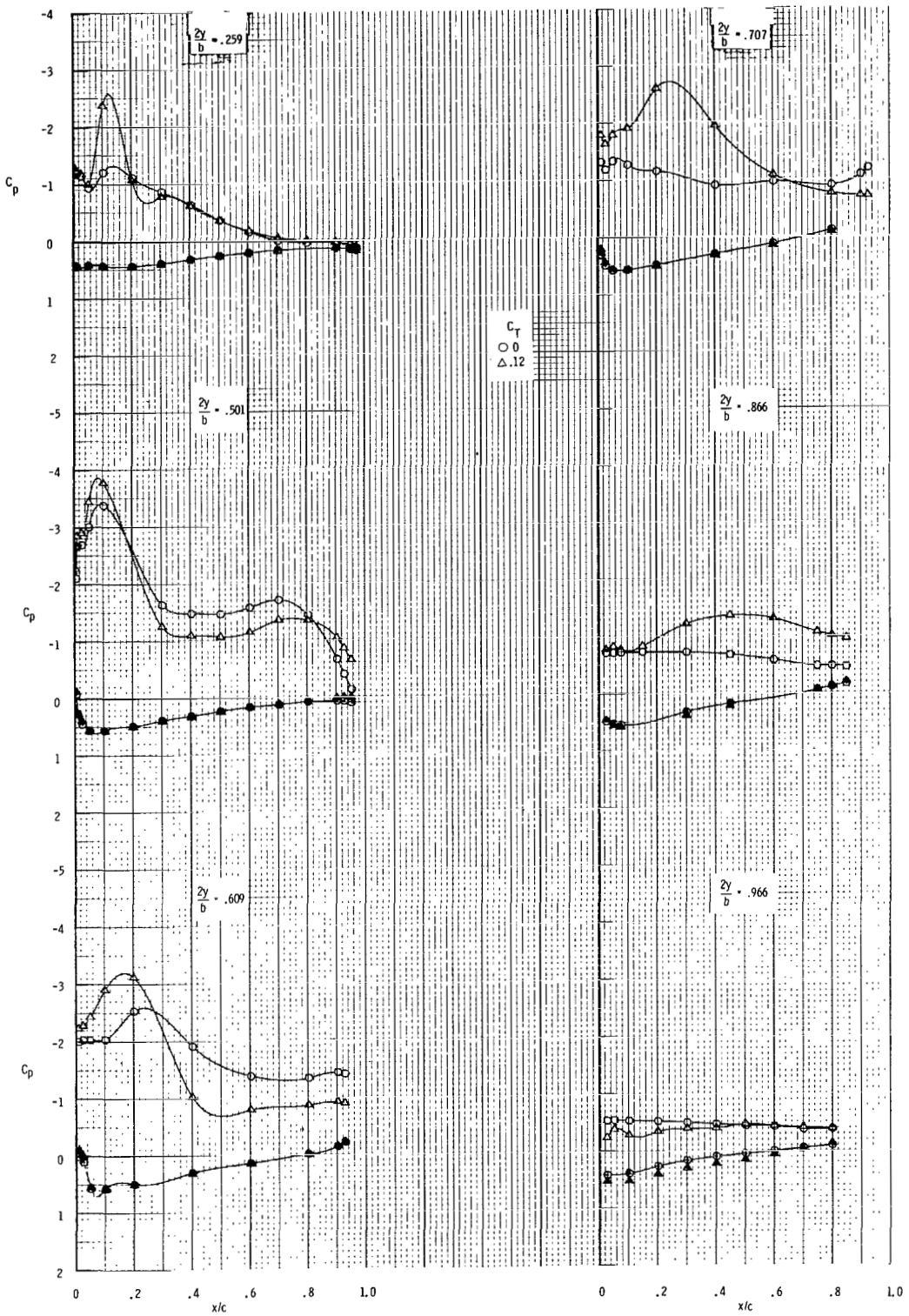

(f) $\alpha = 20.7^{\circ}$.

Figure 9.- Continued.

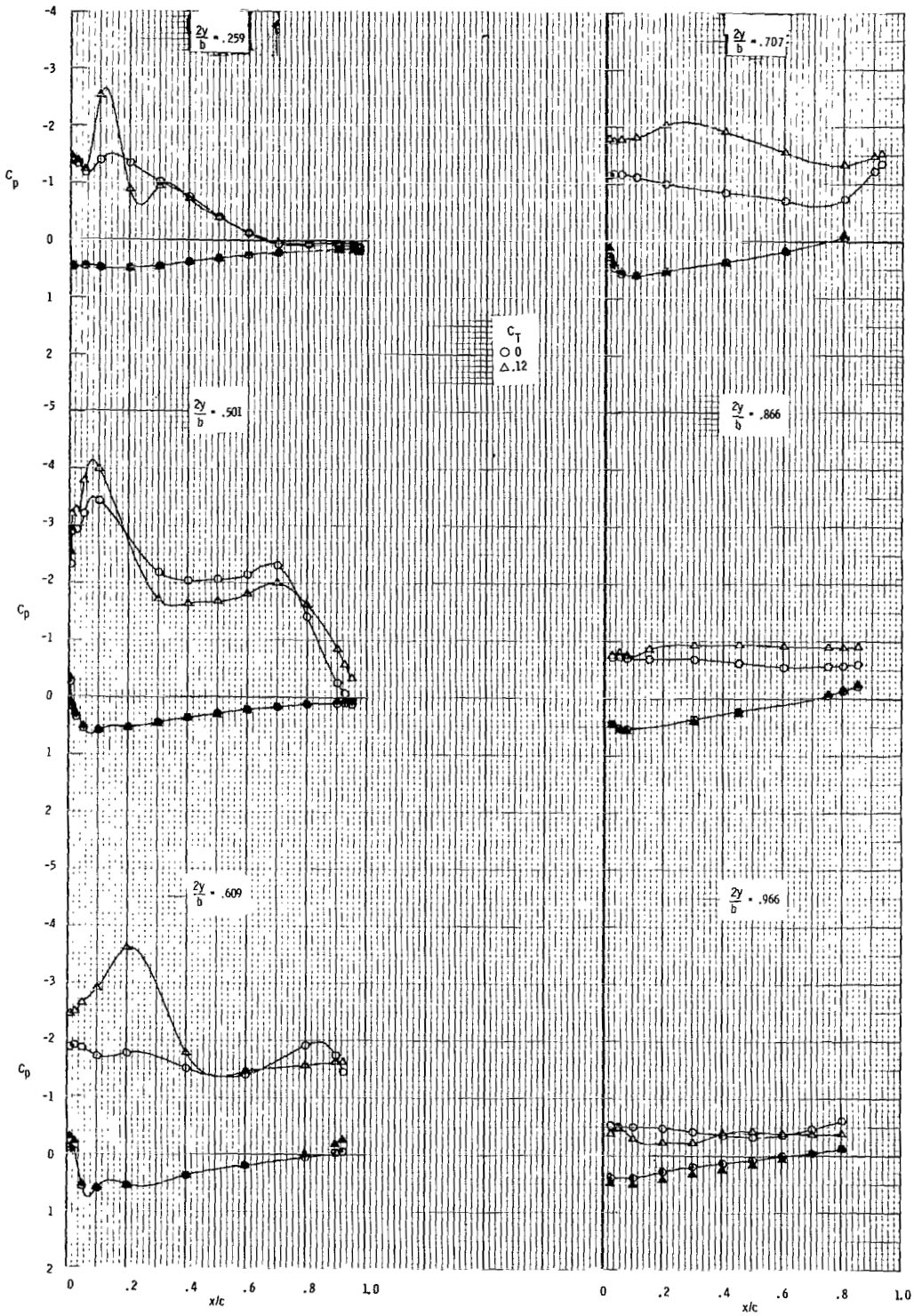

(g) $\alpha = 23.9^{\circ}$.

Figure 9.- Concluded.

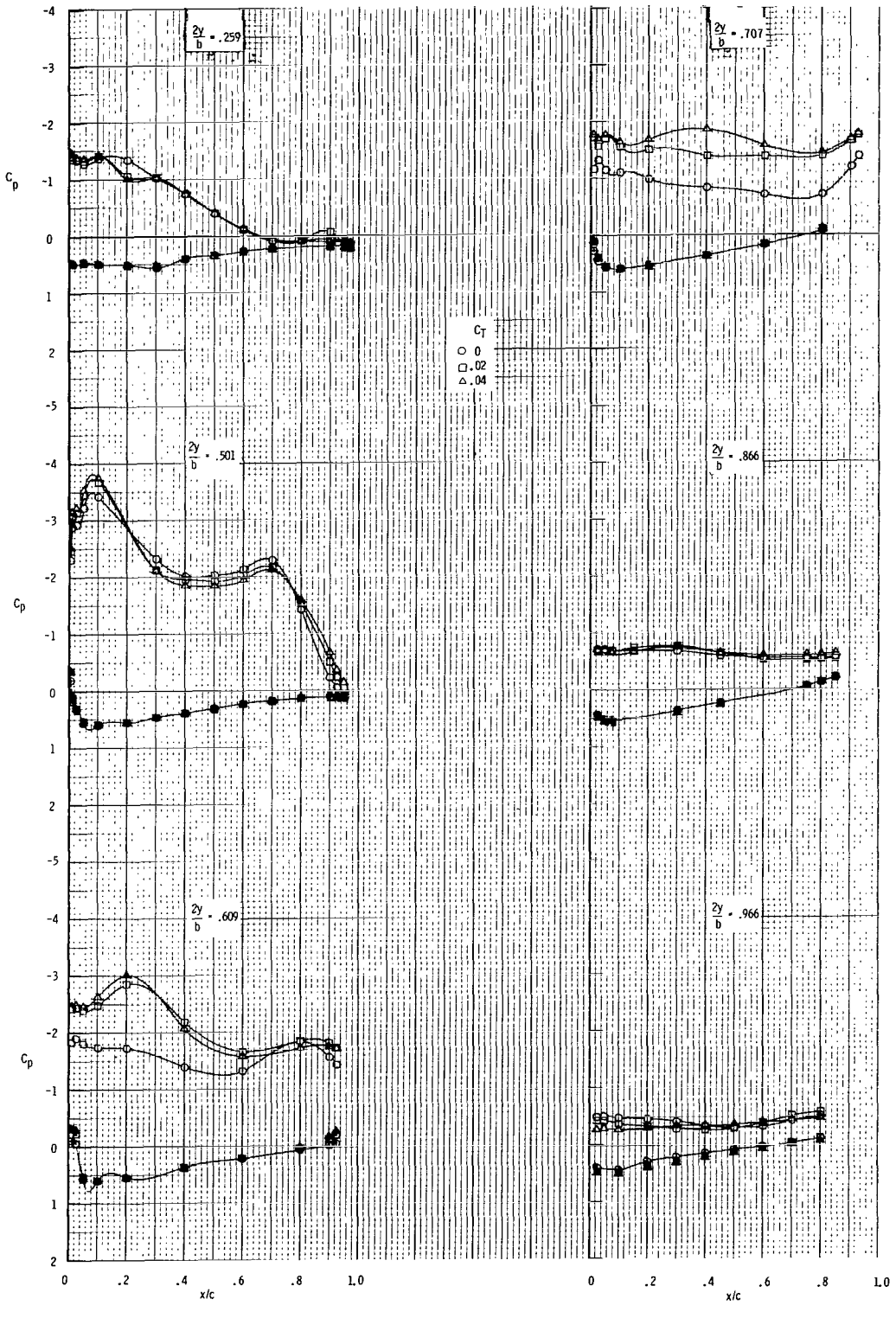

(a) C_T = 0, 0.02, and 0.04.

Figure 10.- Effect of C_T on chordwise distributions of C_p for $\alpha \approx 24^o$ with strake on. x_n/c_r = 0.15.

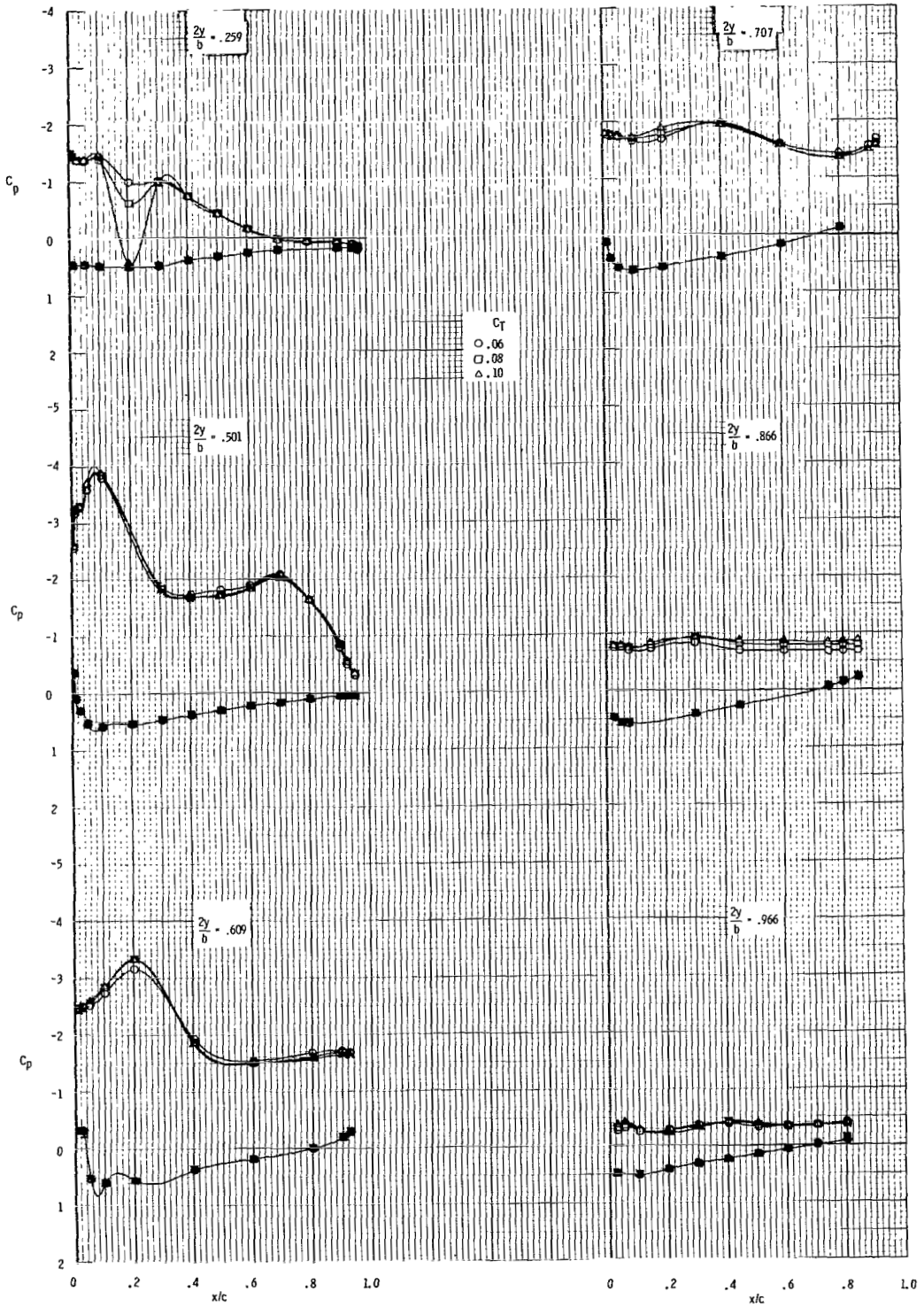

(b) C_T = 0.06, 0.08, and 0.10.

Figure 10.- Continued.

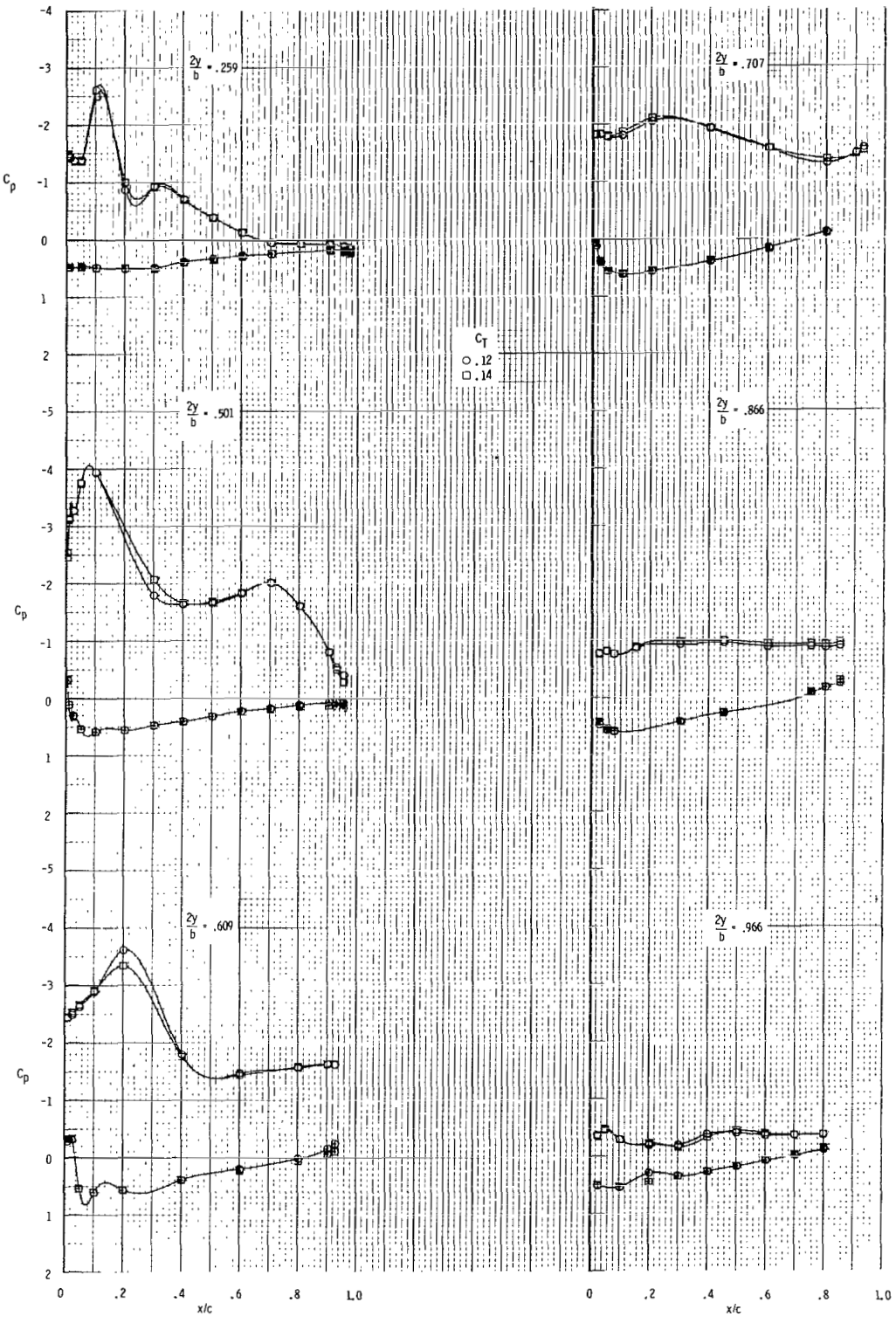

(c) C_T = 0.12 and 0.14.

Figure 10.- Continued.

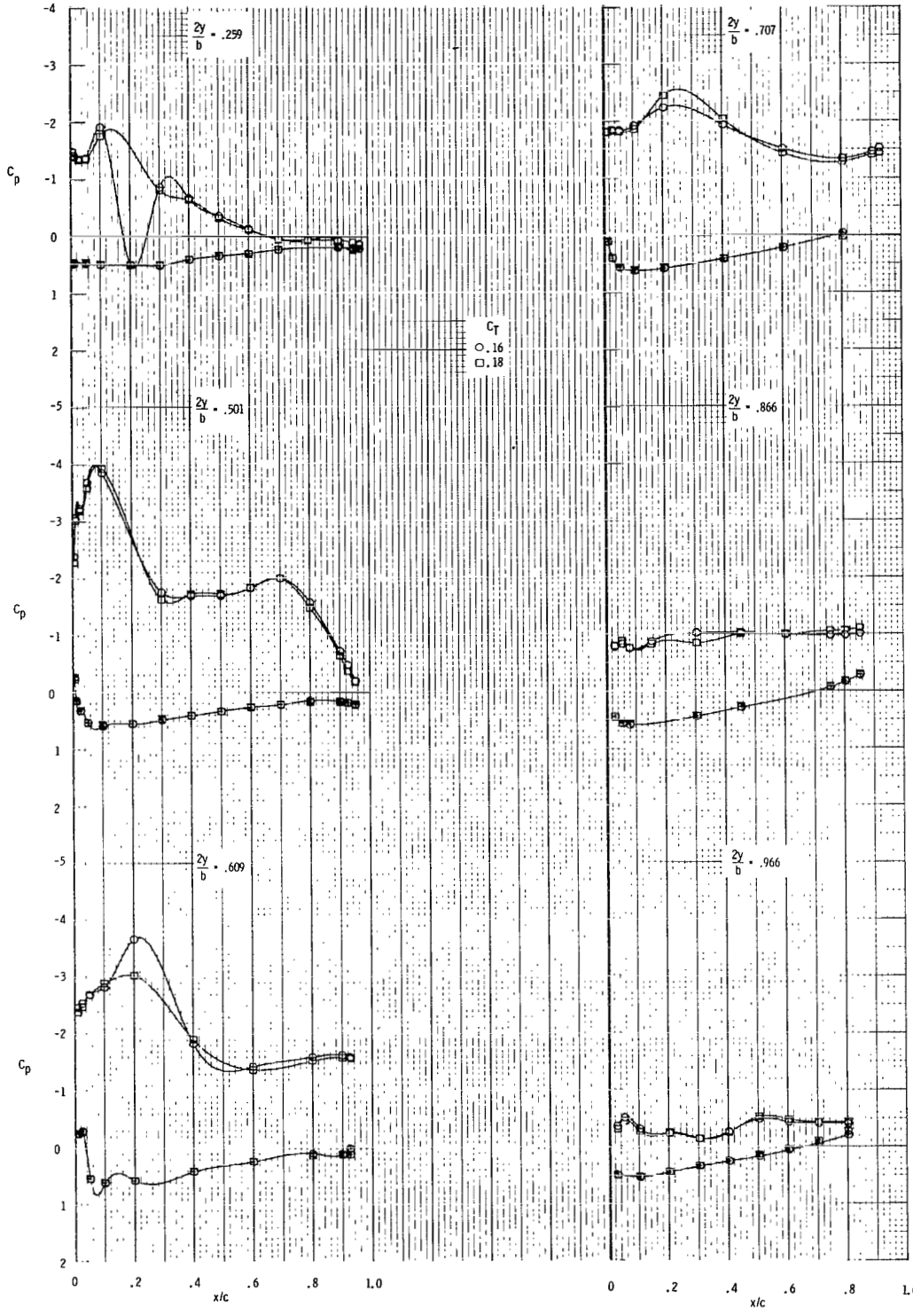

(d) C_T = 0.16 and 0.18.

Figure 10.- Concluded.

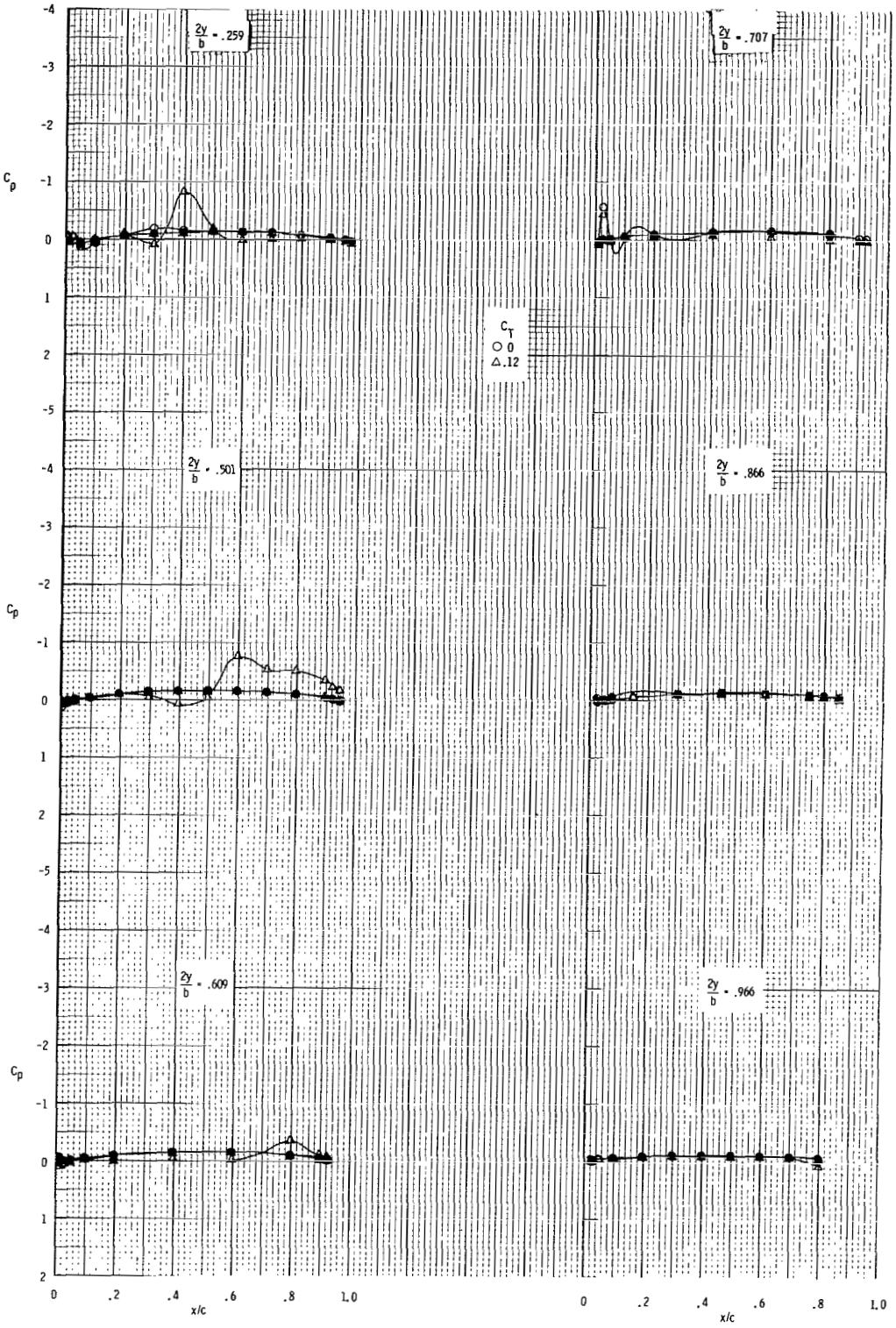

(a) $\alpha = 0^{o}$.

Figure 11.- Effect of spanwise blowing on chordwise distributions of C_p for a range of α with strake on. $x_n/c_r = 0.32$.

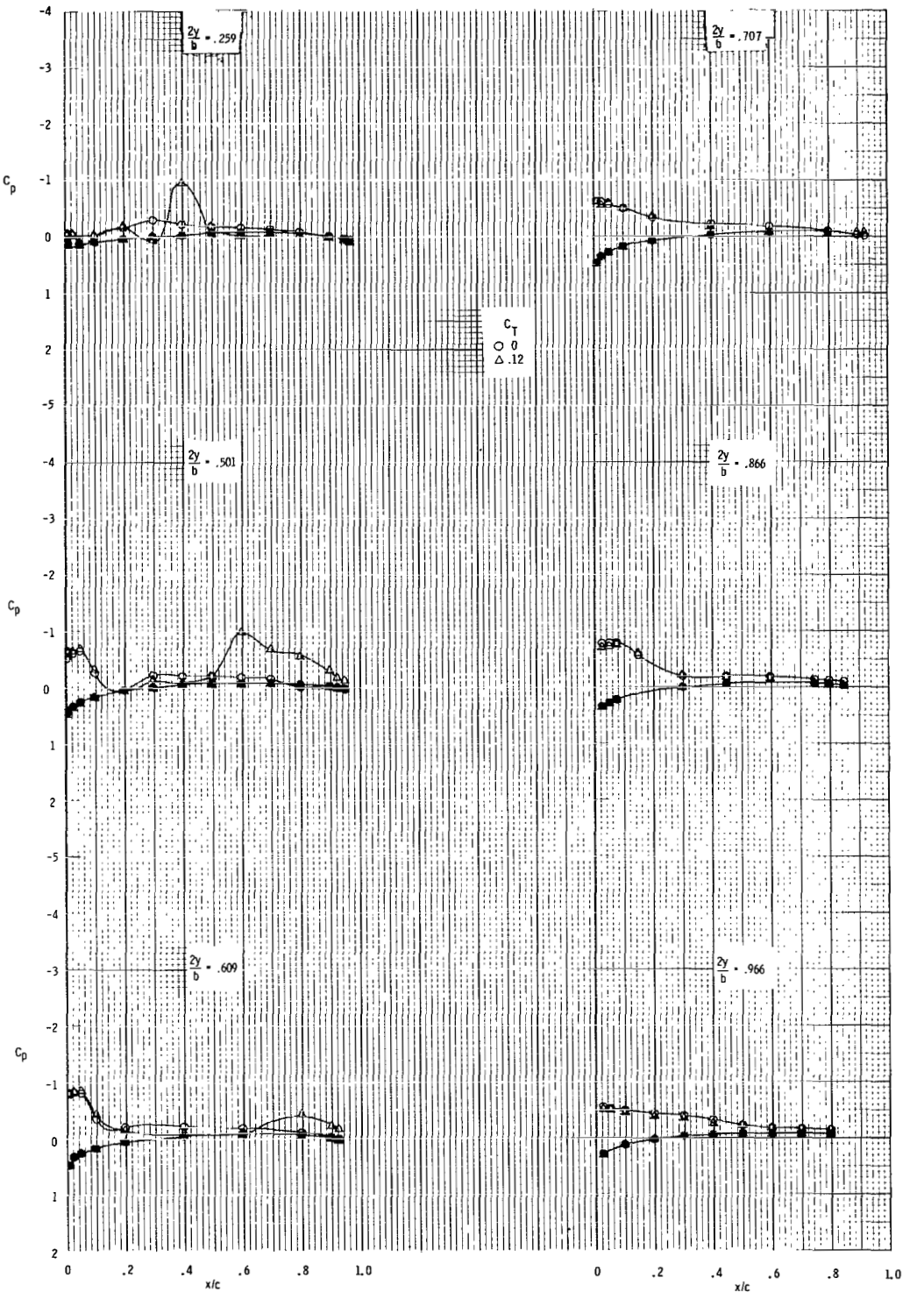

(b) $\alpha = 4.0^{\circ}$.

Figure 11.- Continued.

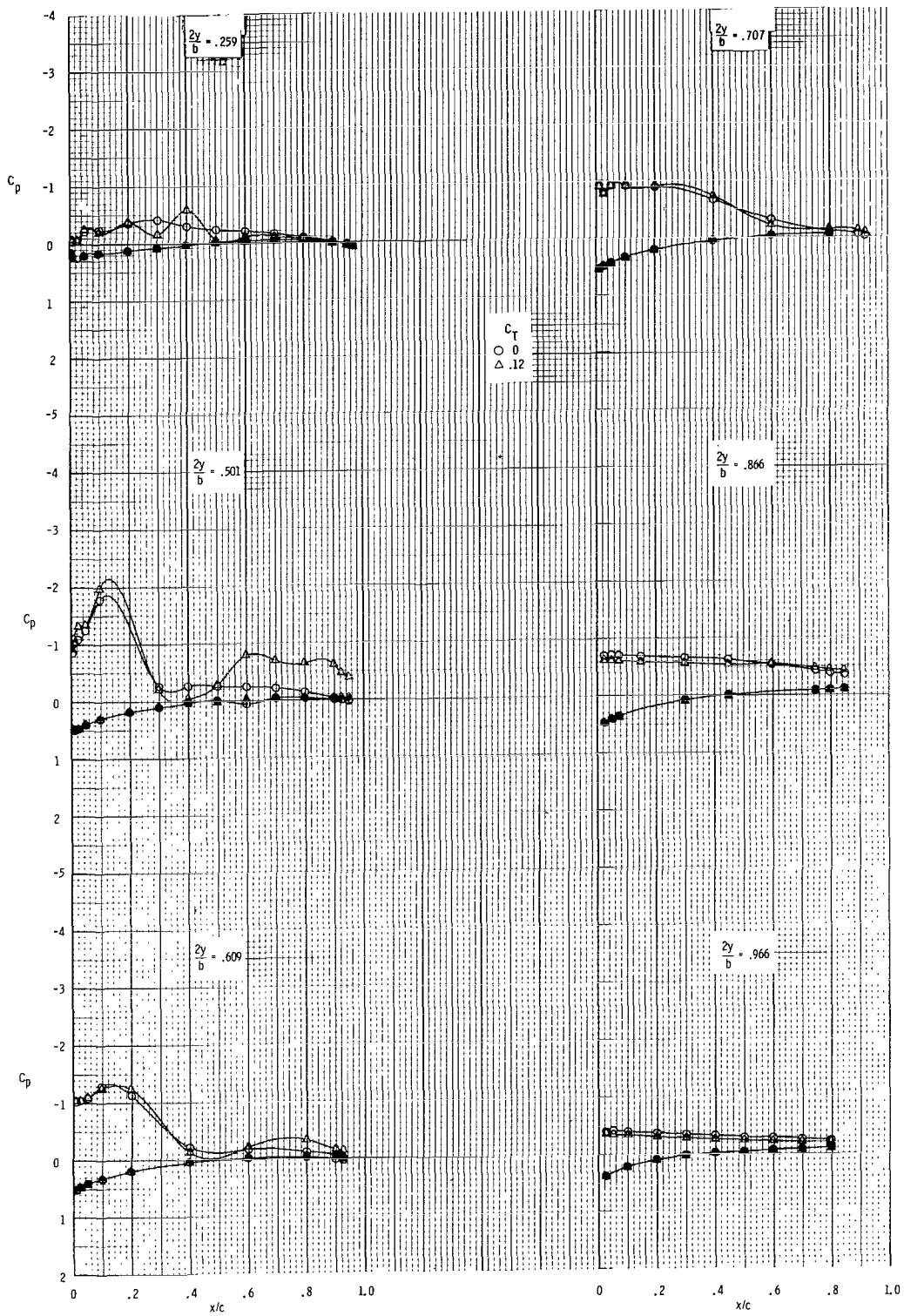

(c) $\alpha = 8.1^{\circ}$.

Figure 11.- Continued.

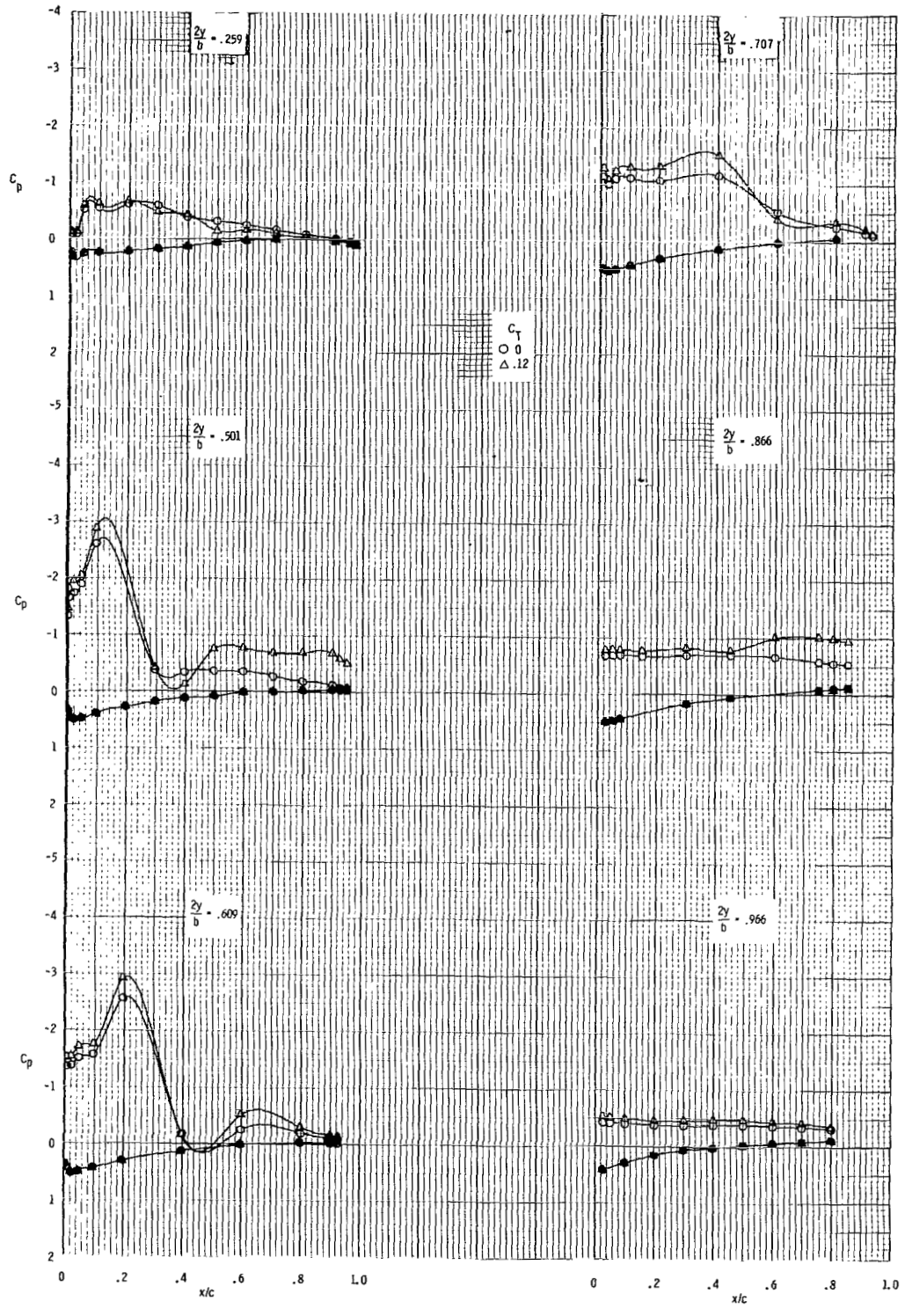

(d) $\alpha = 12.4^{\circ}$.

Figure 11.- Continued.

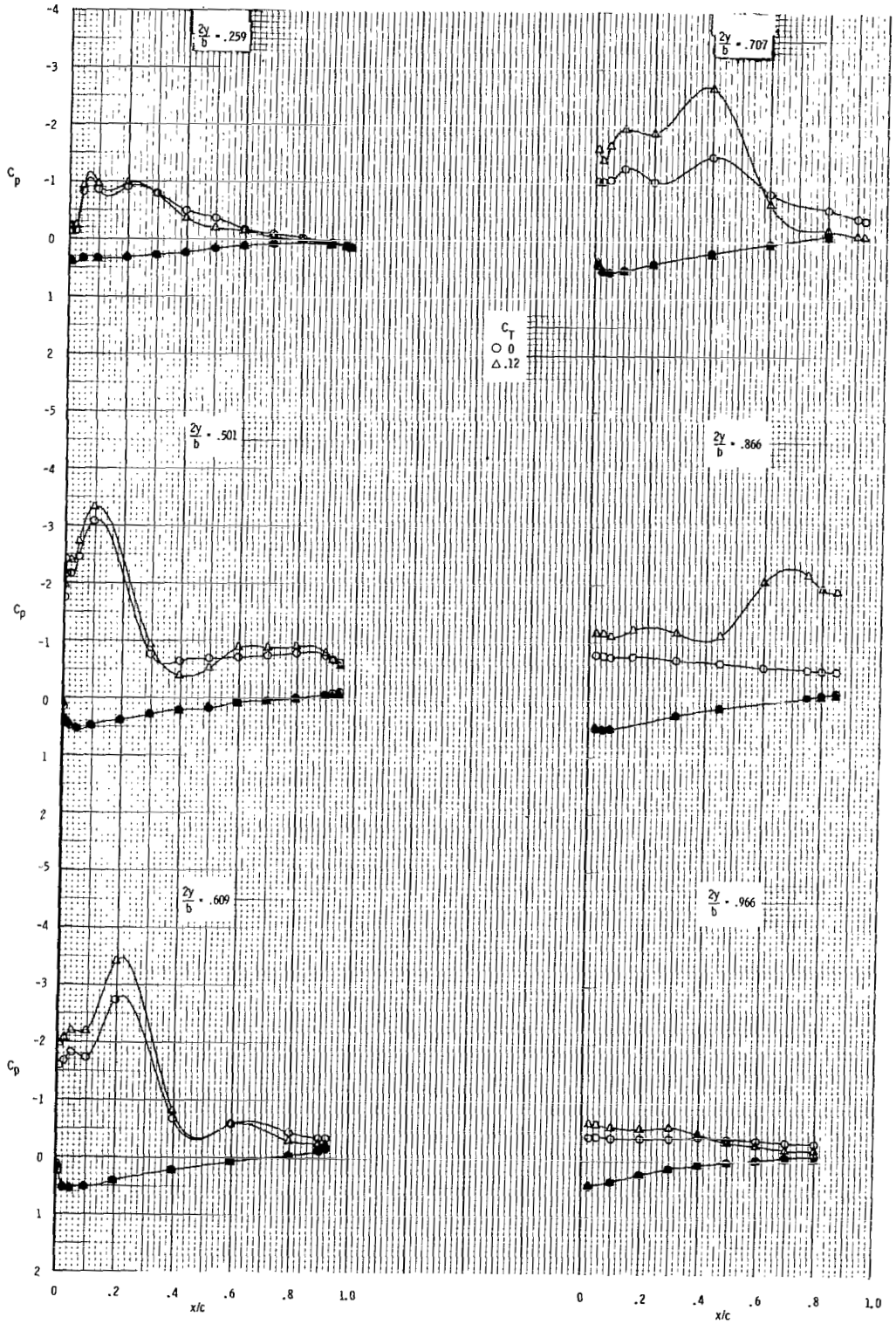

(e) $\alpha = 16.7^{\circ}$.

Figure 11.- Continued.

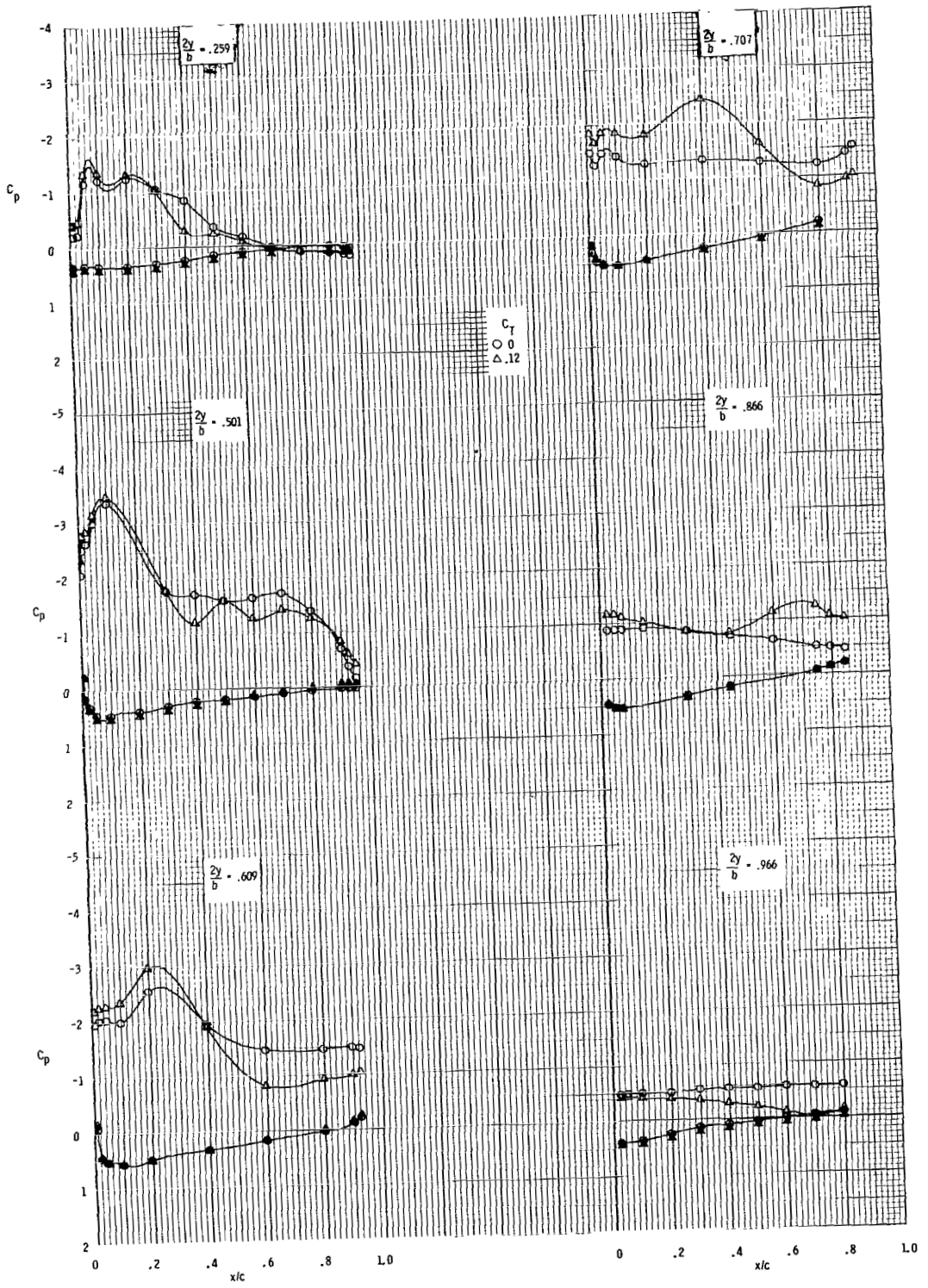

(f) $\alpha = 20.8^{\circ}$.

Figure 11.- Continued.

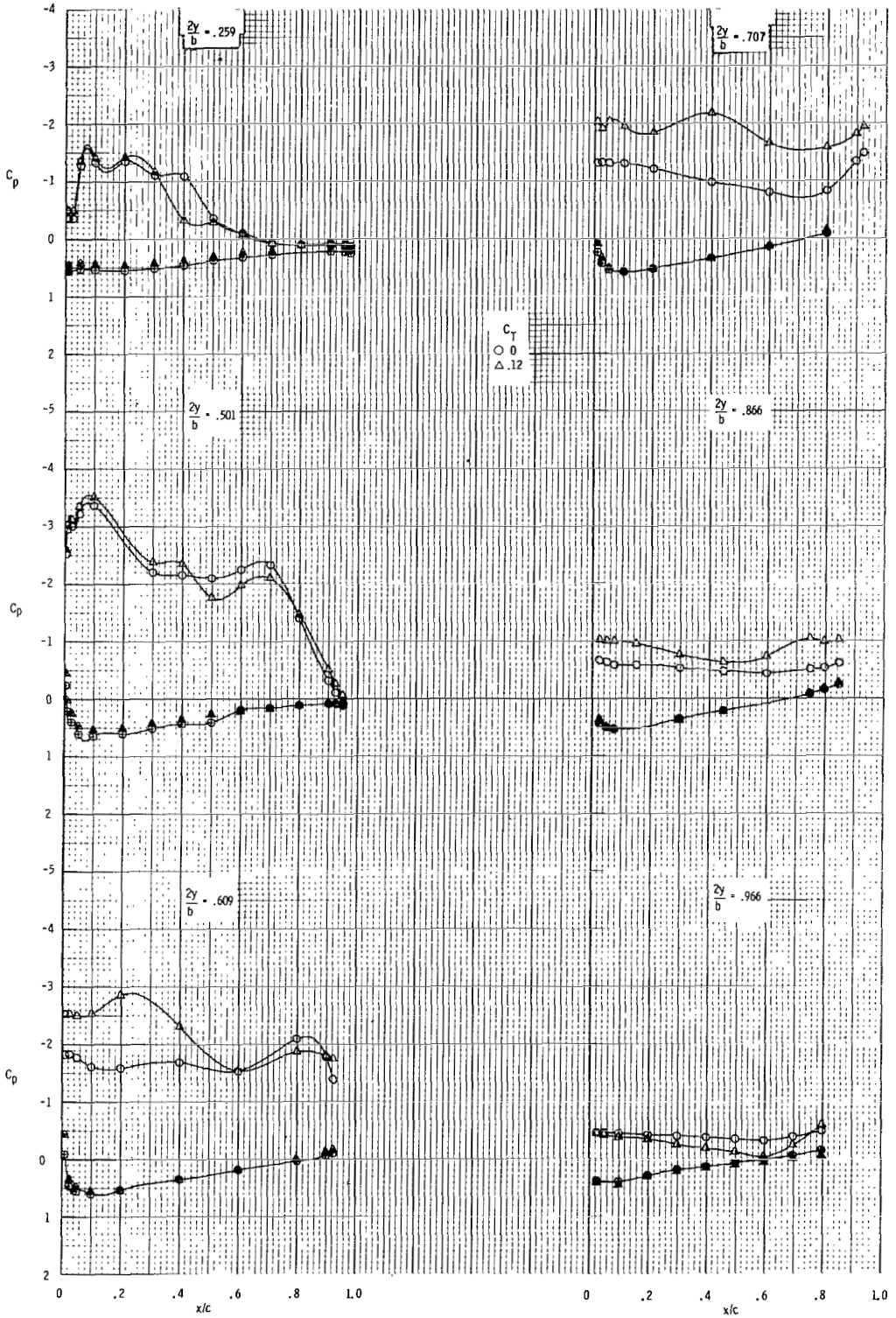

(g) $\alpha = 24.1^{\circ}$.

Figure 11.- Concluded.

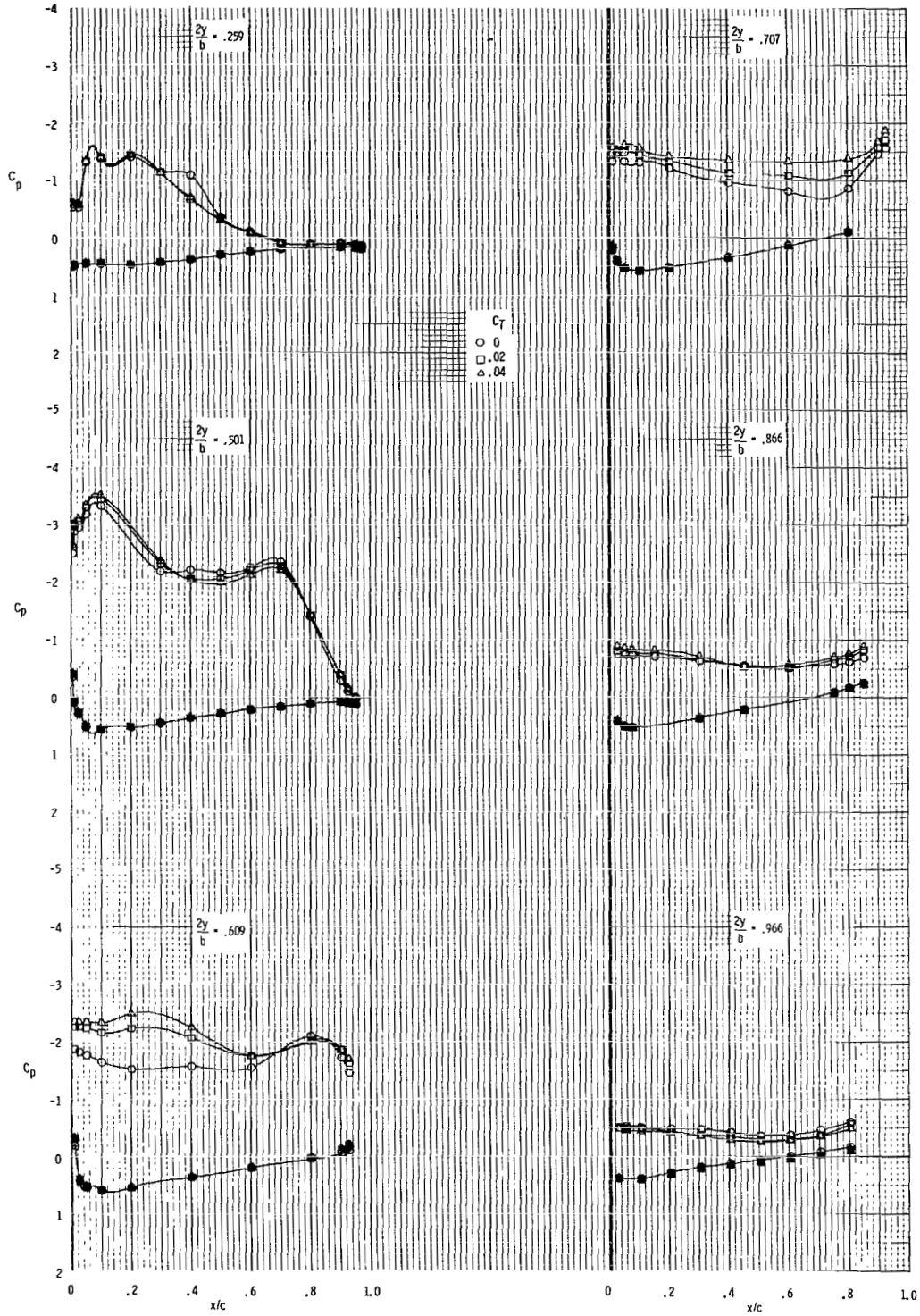

(a) C_T = 0, 0.02, and 0.04.

Figure 12.- Effect of C_T on chordwise distributions of C_p for $\alpha \approx 24^o$ with strake on. x_n/c_r = 0.32.

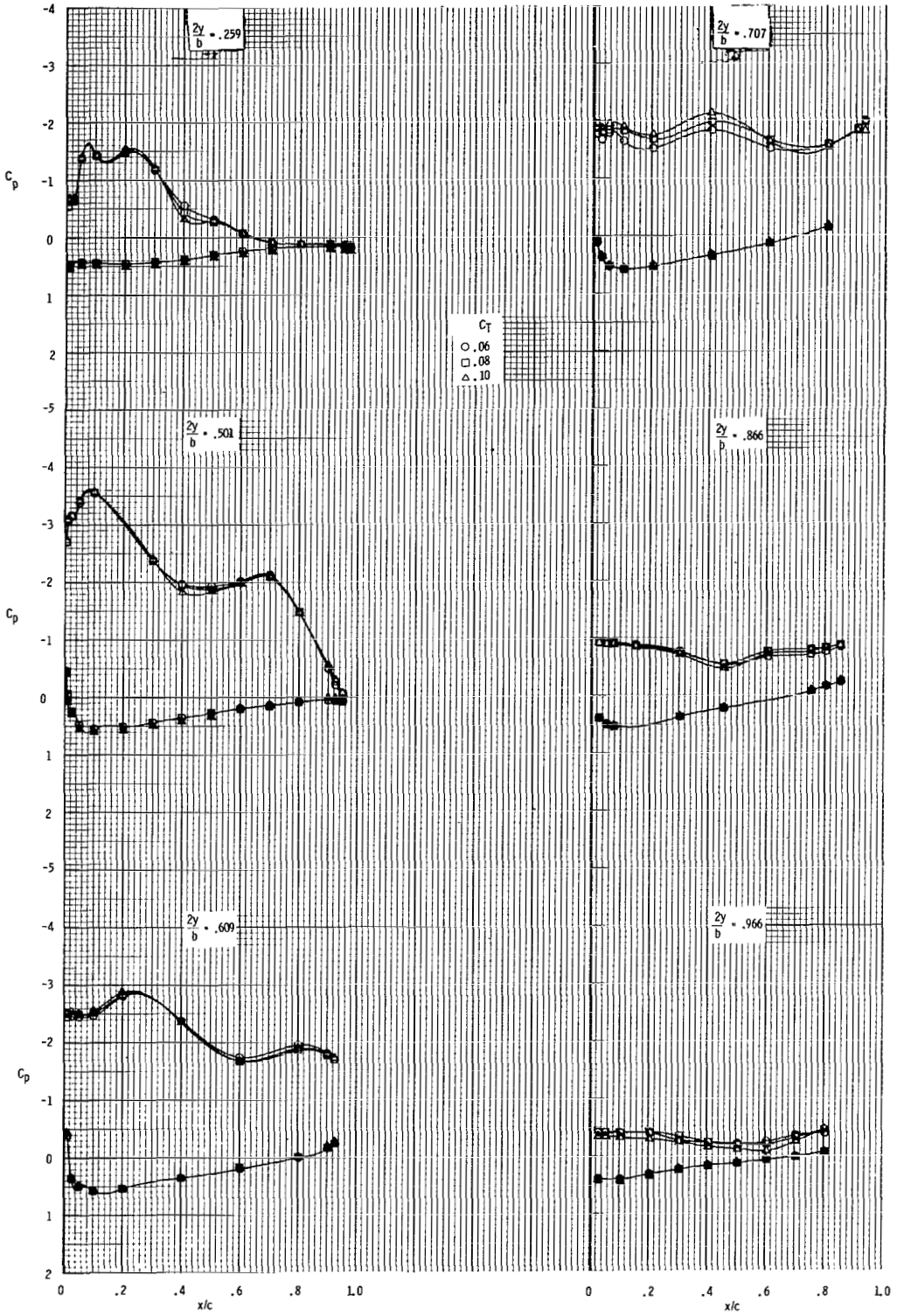

(b) C_T = 0.06, 0.08, and 0.10.

Figure 12.- Continued.

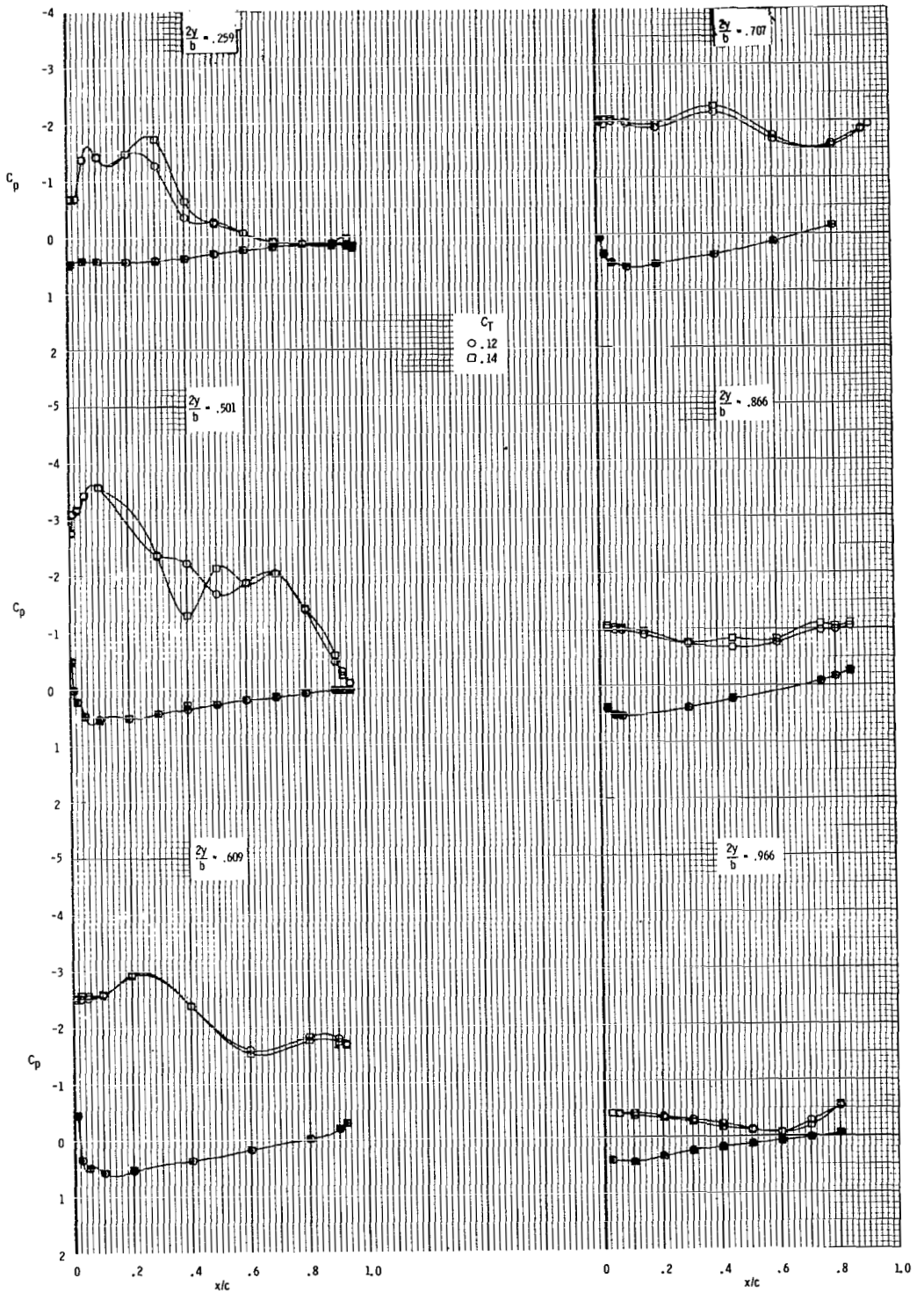

(c) C_T = 0.12 and 0.14.

Figure 12.- Continued.

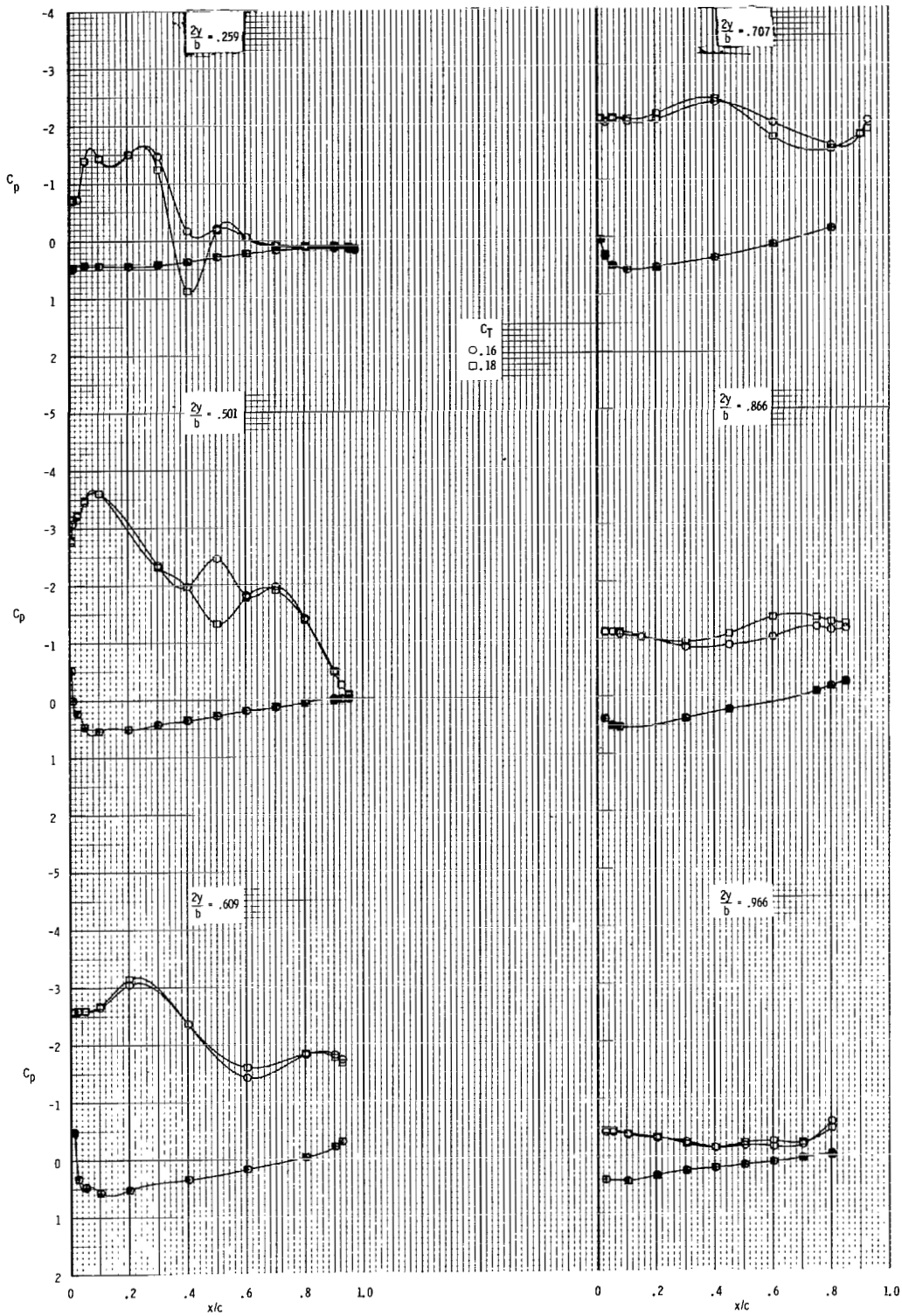

(d) C_T = 0.16 and 0.18.

Figure 12.- Concluded.

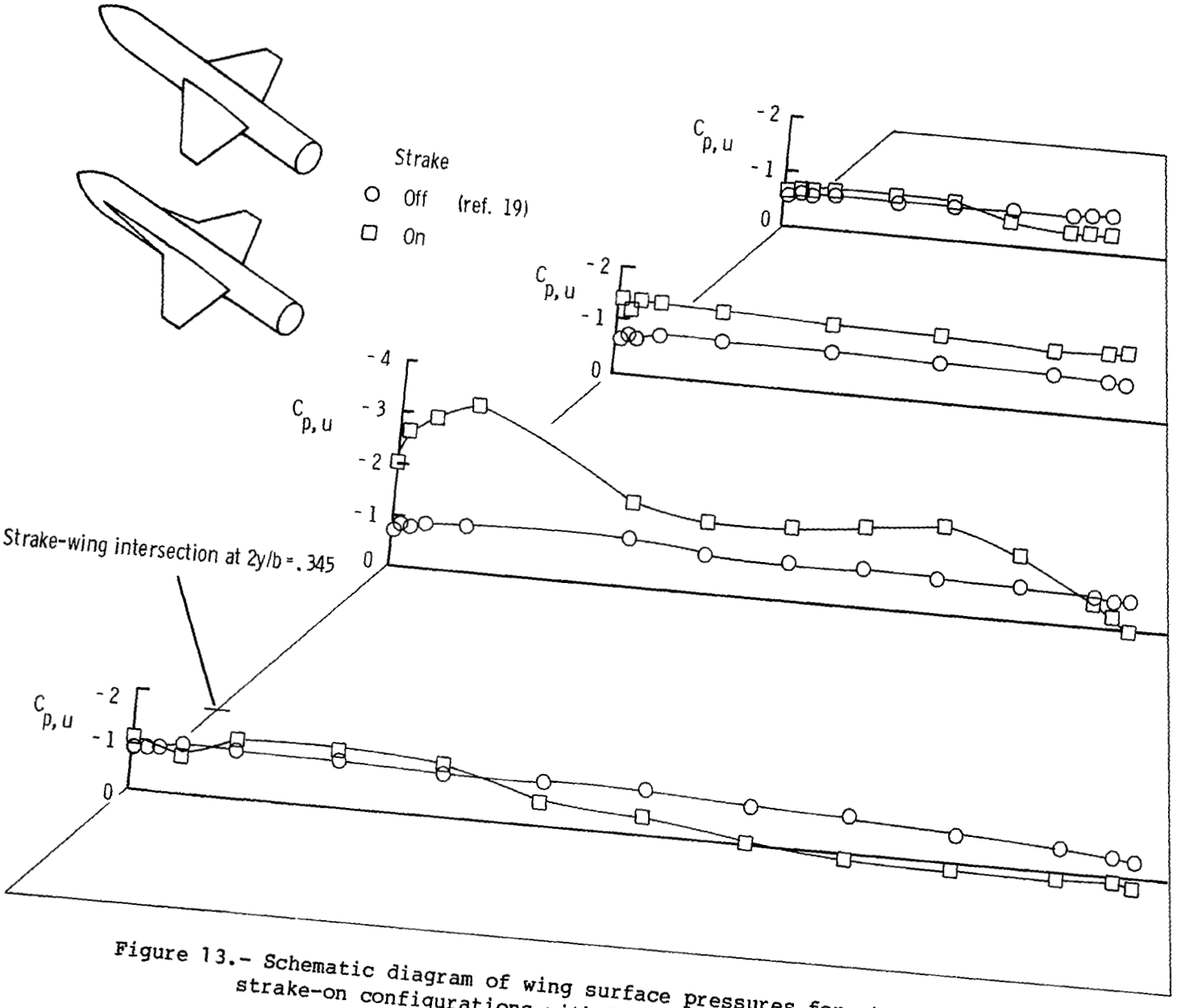

Figure 13.- Schematic diagram of wing surface pressures for strake-off and strake-on configurations with blowing off. $\alpha \approx 20.6^{\circ}$.

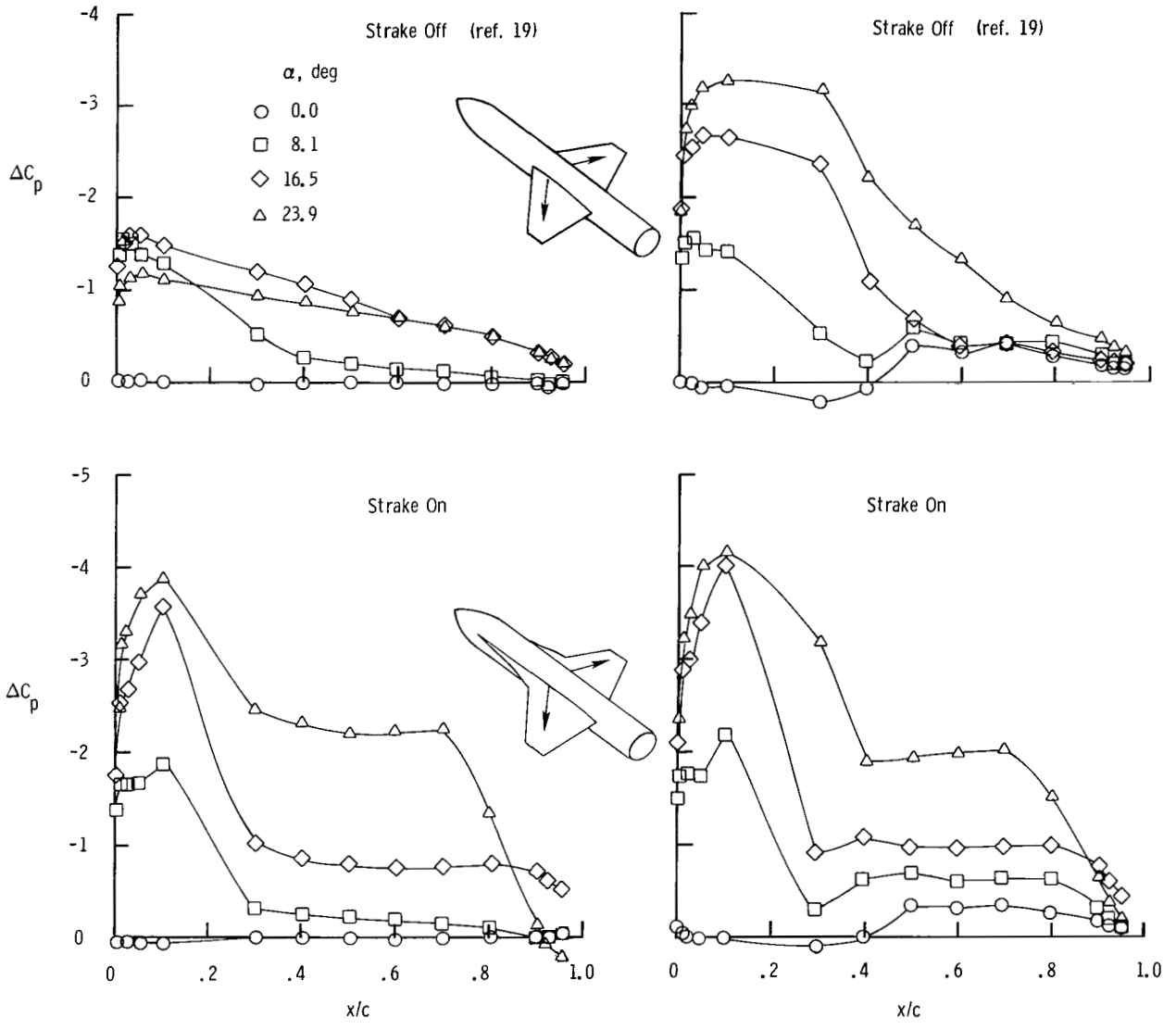

(a) $C_T = 0.$ (b) $C_T = 0.12.$

Figure 14.- Effect of α on chordwise pressure distributions of ΔC_p at $2y/b = 0.501$ for the strake-off and strake-on configurations for two values of C_T. $x_n/c_r = 0.23$.

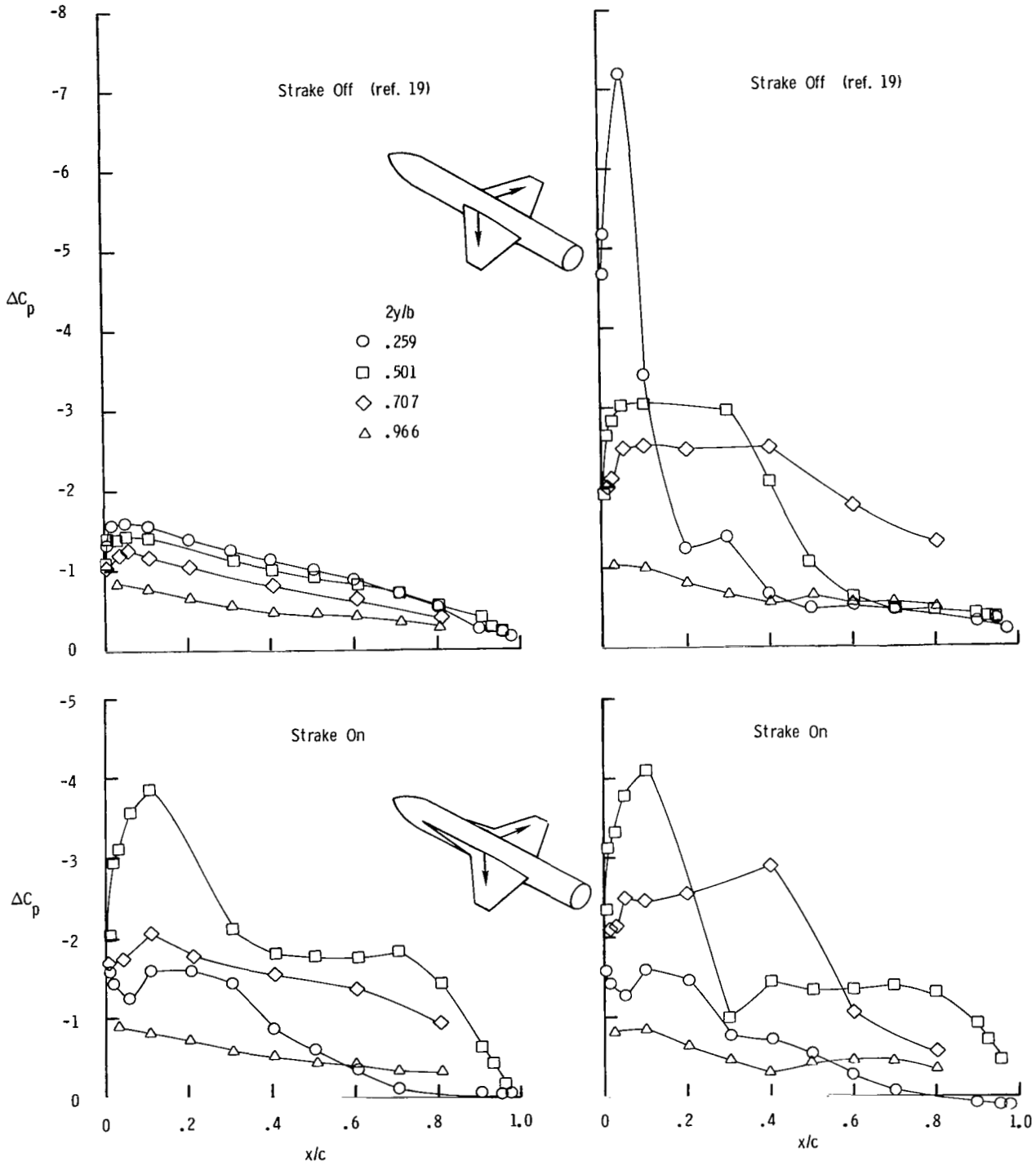

Figure 15.- Effect of span location on chordwise pressure distributions of ΔC_p for the strake-off and strake-on configurations for two values of C_T. $\alpha \approx 20.6^{\circ}$; $x_n/c_r = 0.23$.

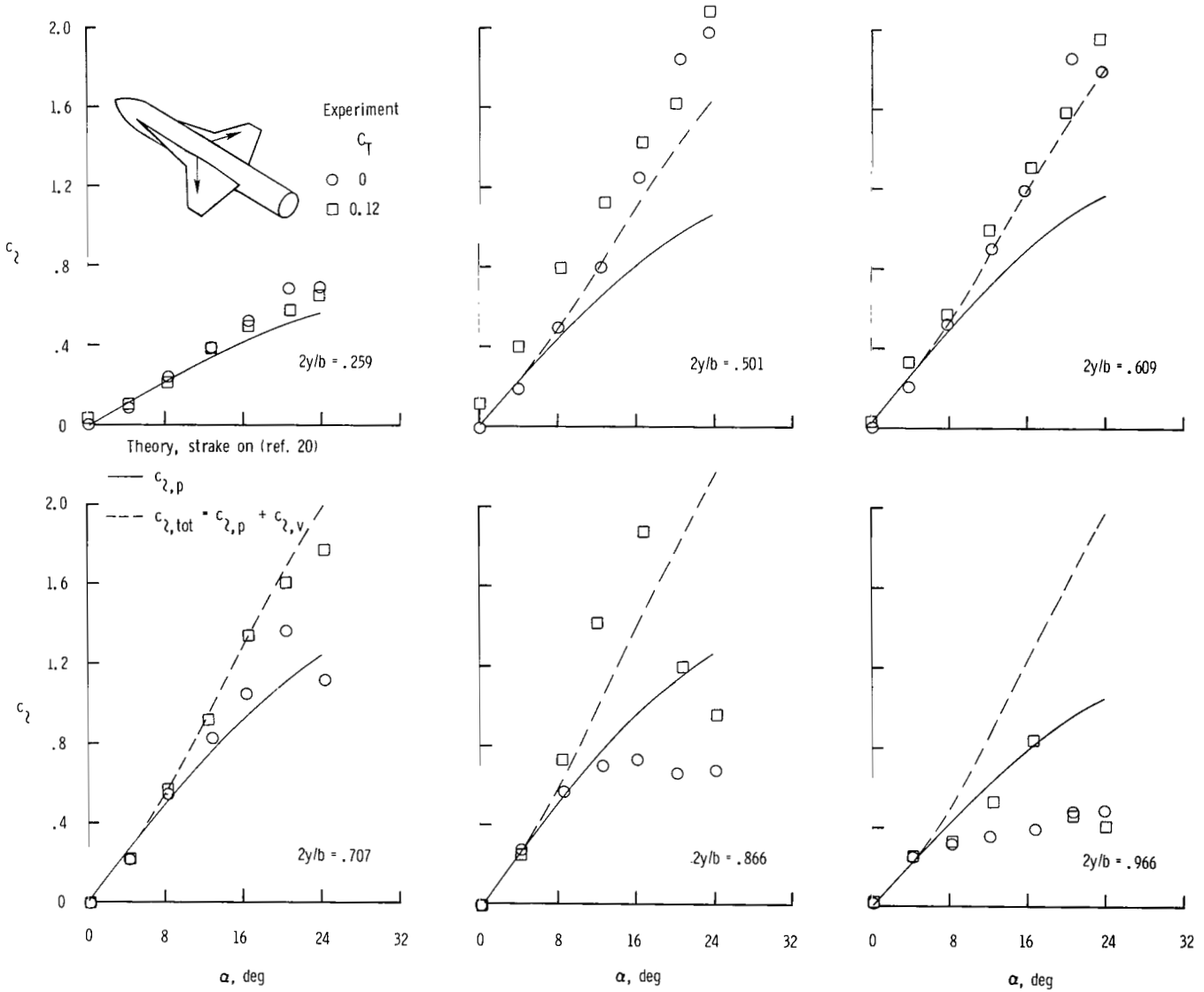

Figure 16.- Effect of spanwise blowing on wing section lift characteristics with strake on. $x_n/c_r = 0.23$.

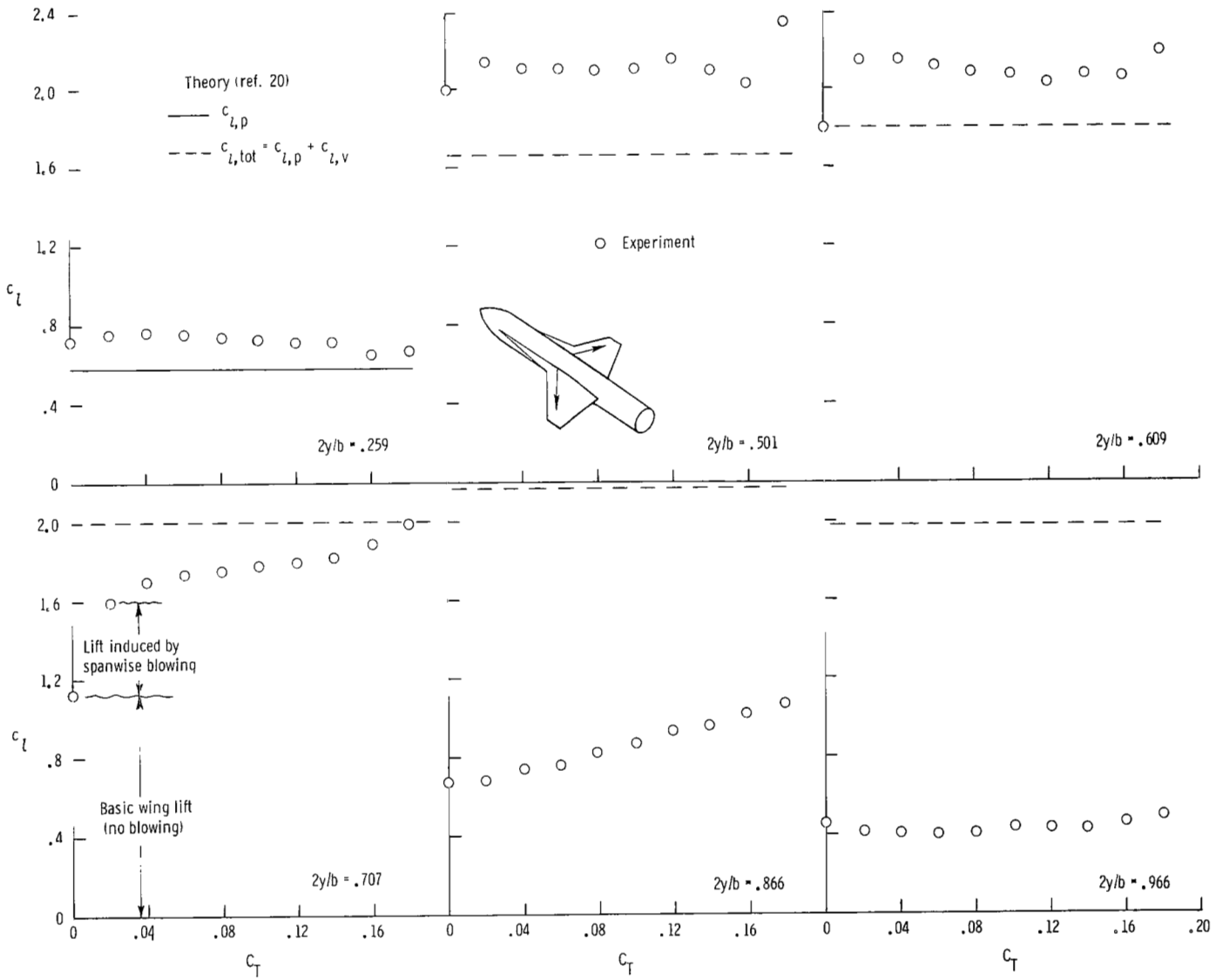

(a) Variation of c_l with C_T.

Figure 17.- Effect of C_T on section lift characteristics with strake on. $\alpha = 23.9^o$; $x_n/c_r = 0.23$.

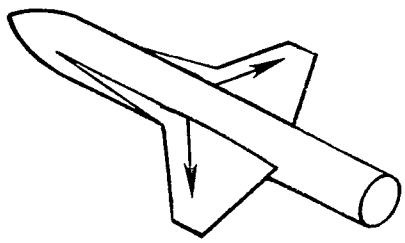

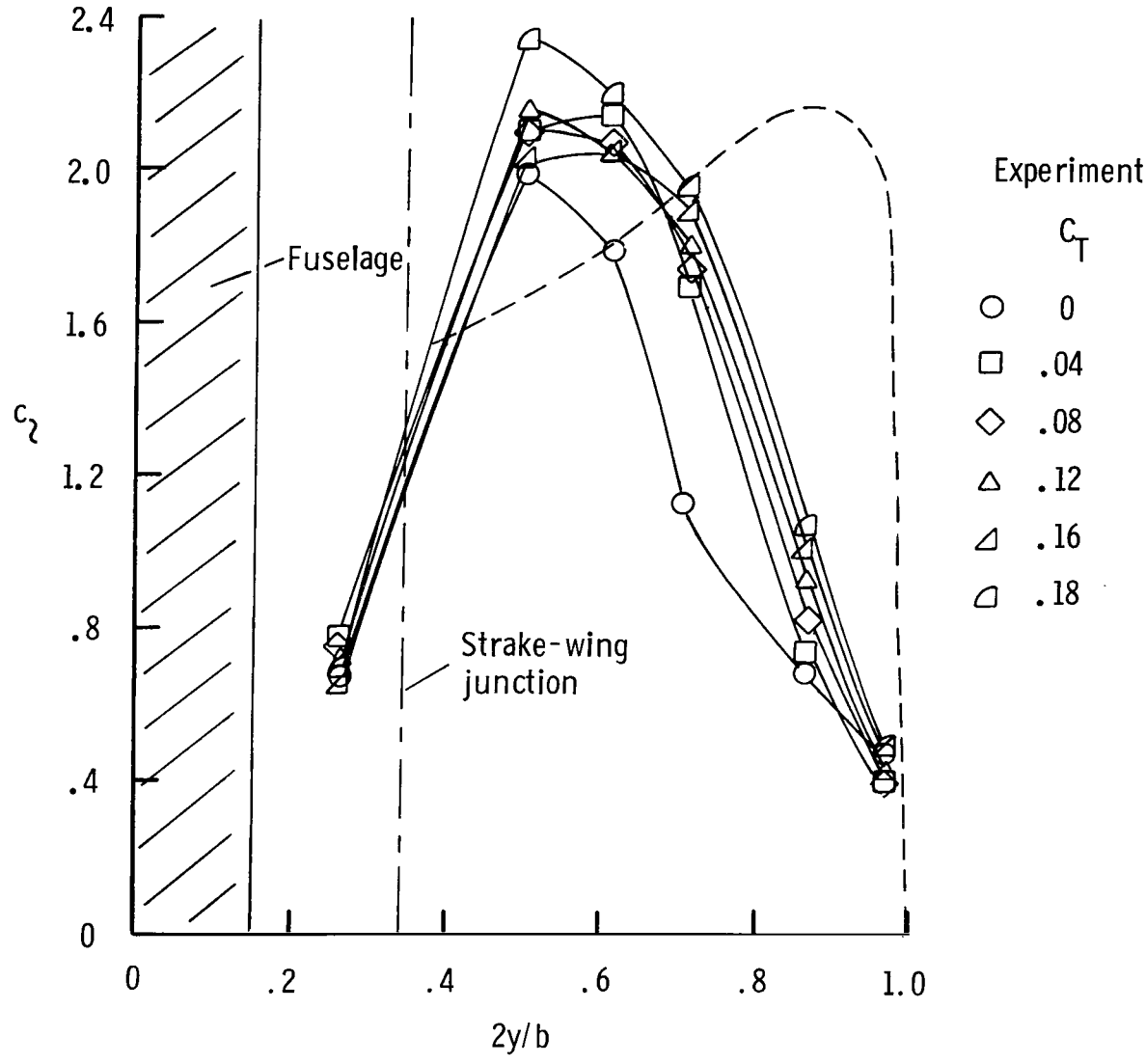

(b) Variation of c_l with 2y/b.

Figure 17.- Concluded.

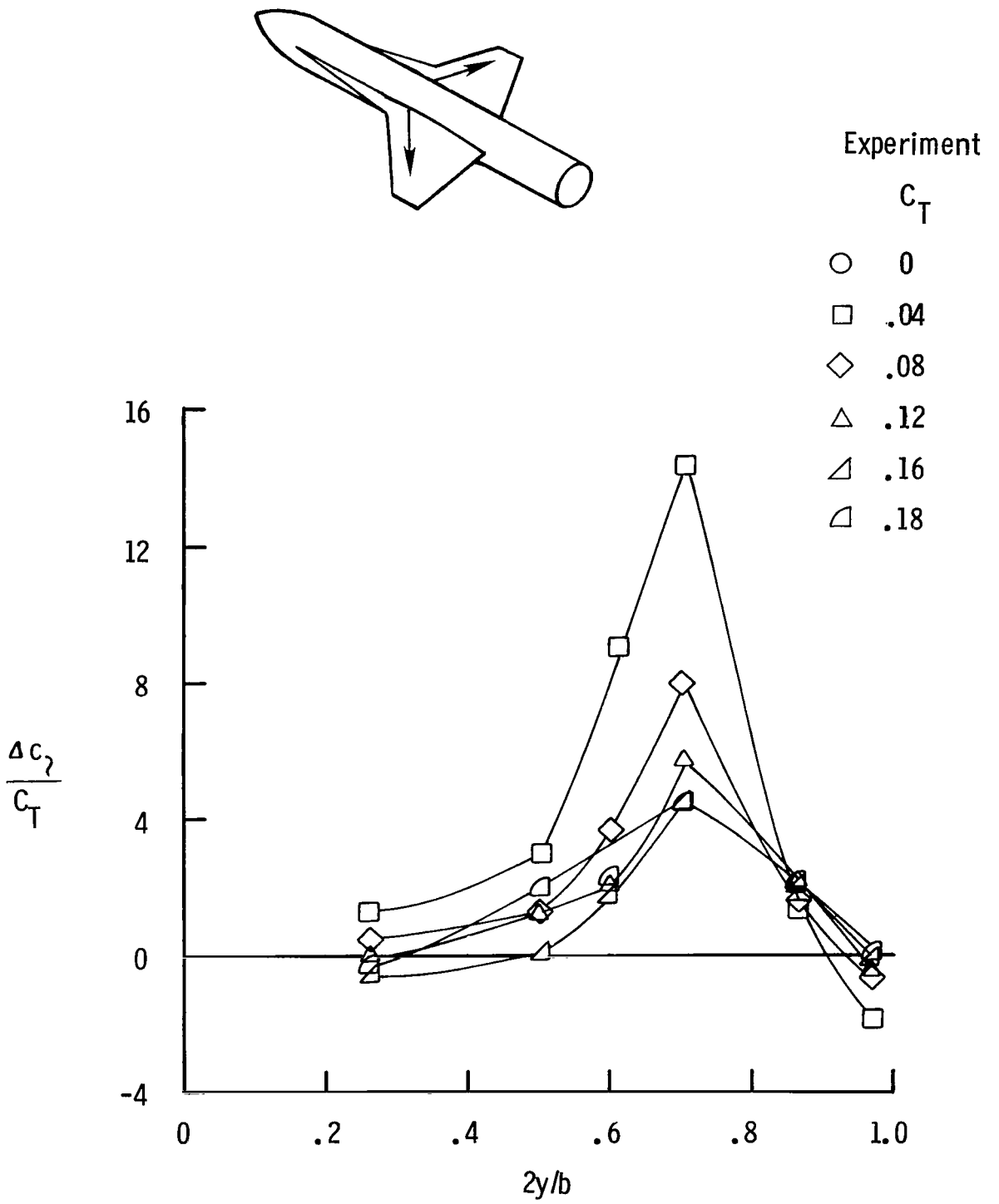

Figure 18.- Variation of section lift coefficient and lift augmentation ratio along the span for a range of C_T with strake on. $\alpha = 23.9^o$; $x_n/c_r = 0.23$.

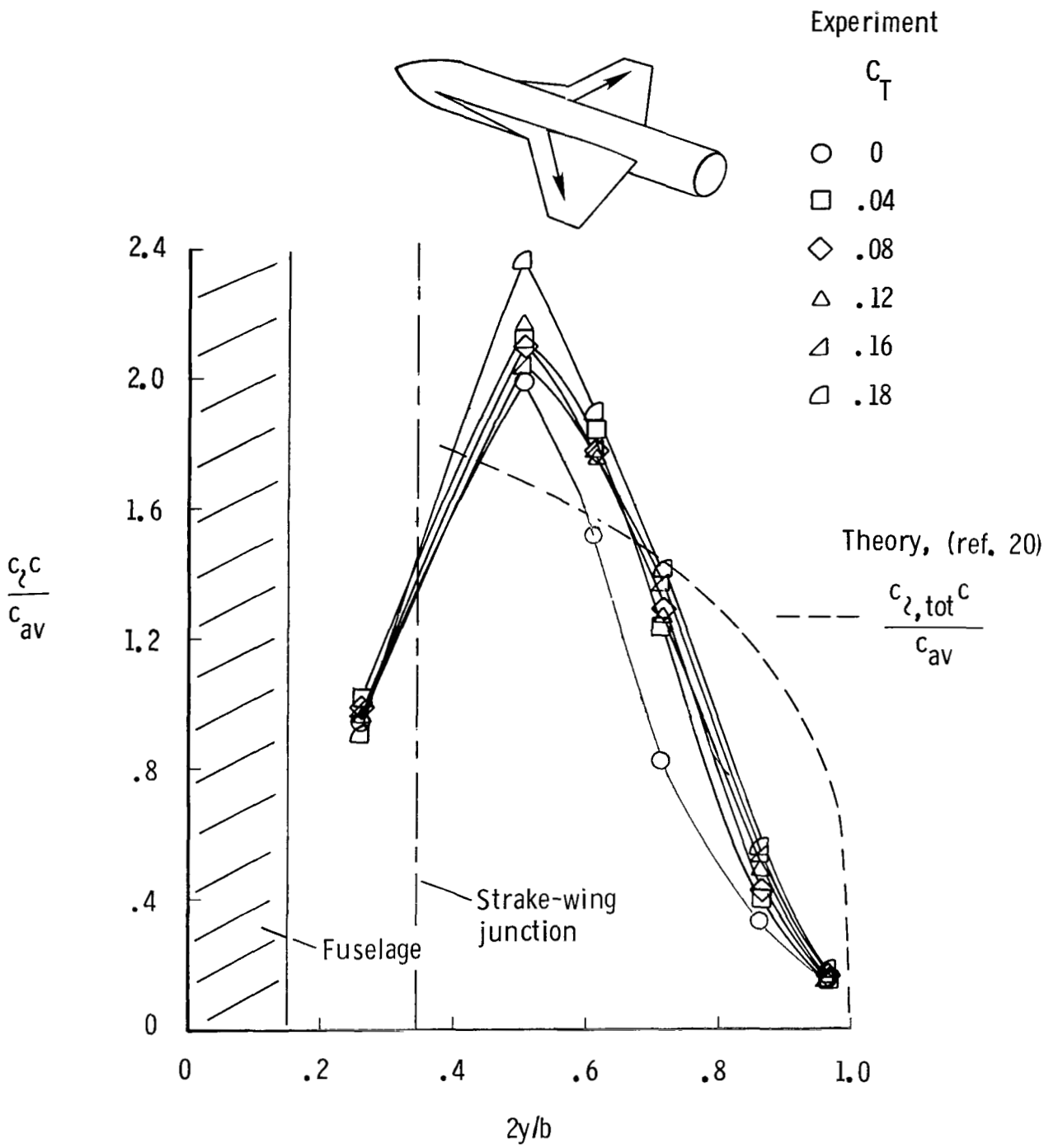

Figure 19.- Effect of spanwise blowing on span loading for the wing with strake on at $\alpha \approx 24^{o}$. $x_n/c_r = 0.23$.

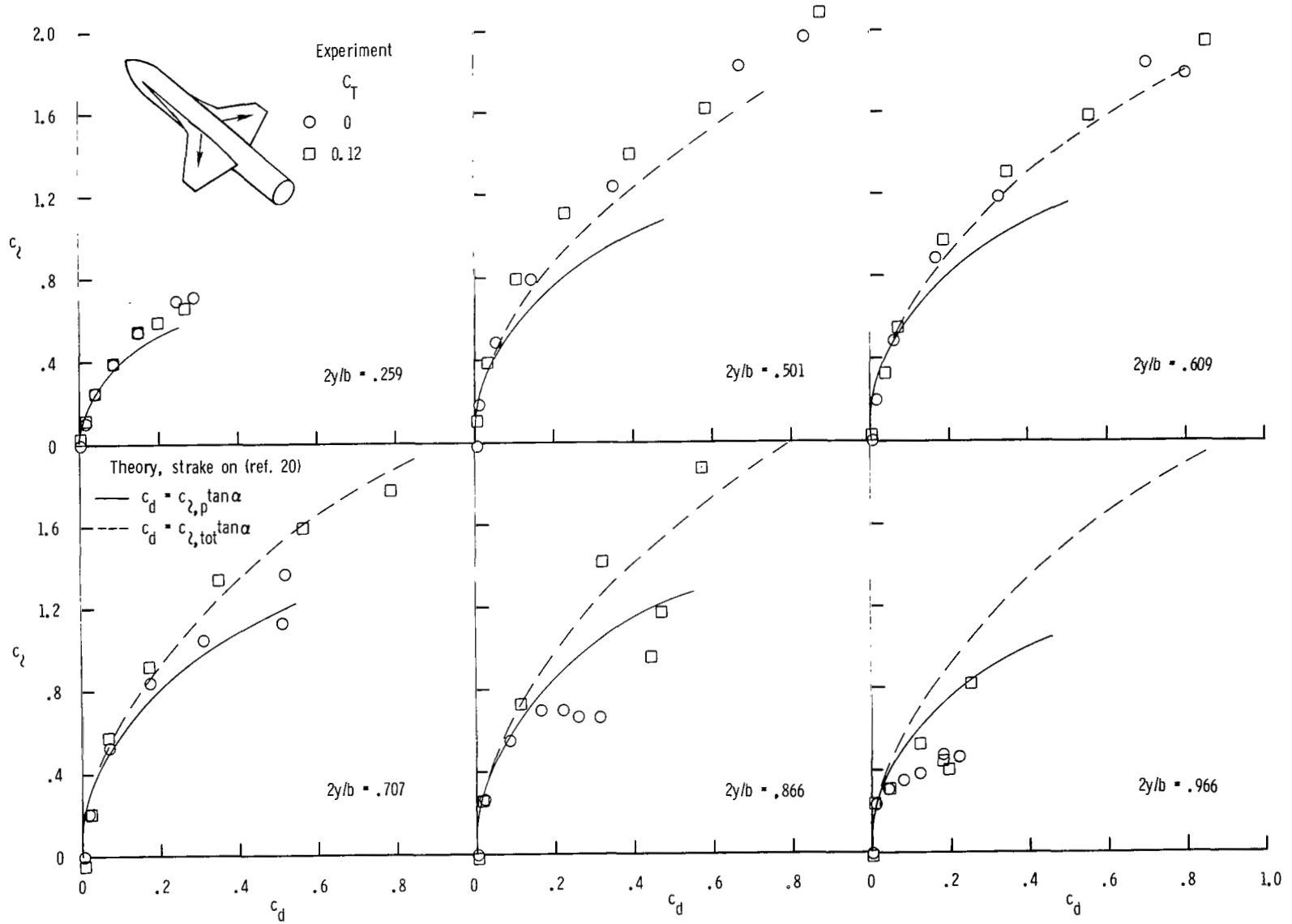

Figure 20.- Effect of spanwise blowing on wing section drag characteristics with strake on. $x_n/c_r = 0.23$.

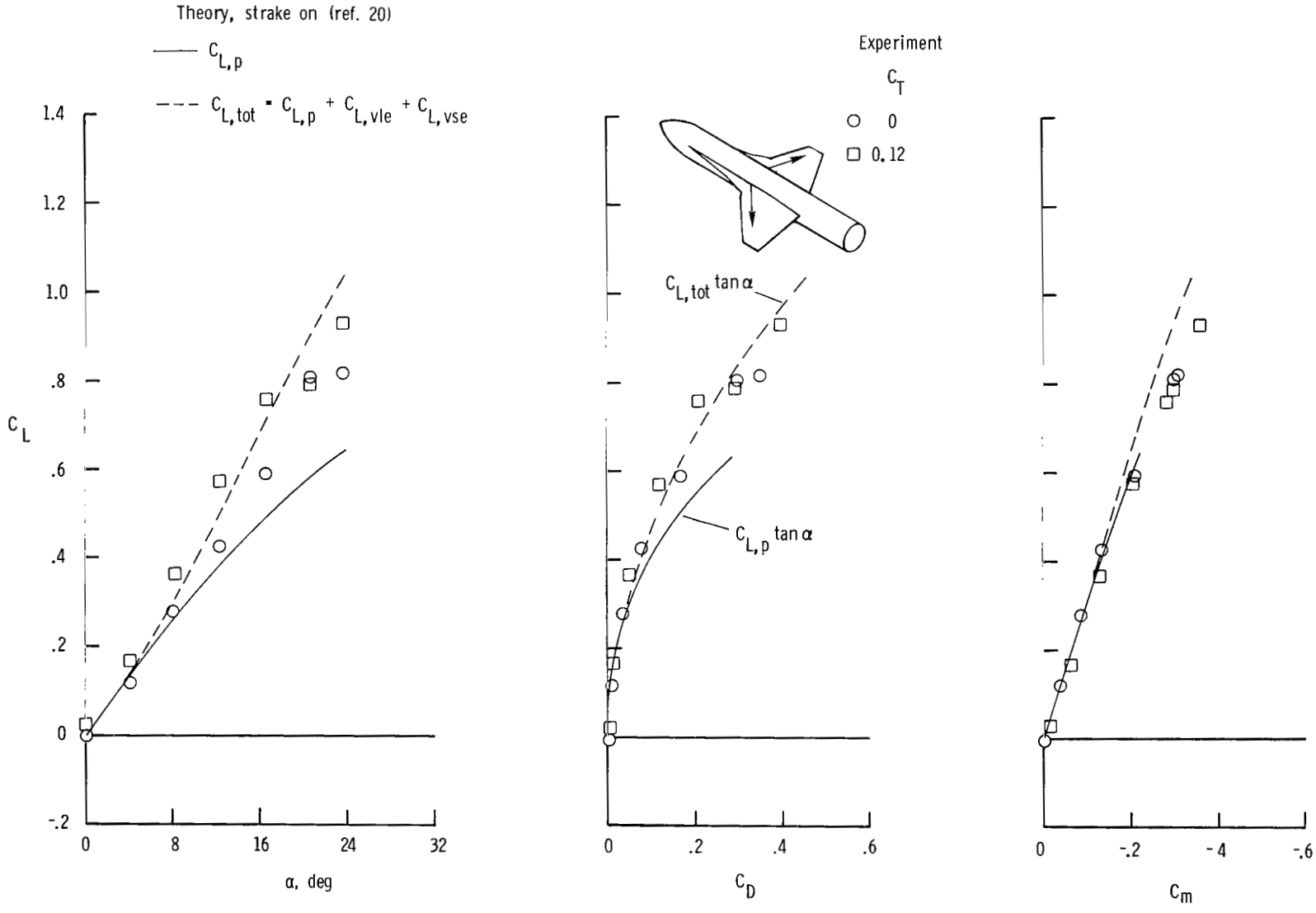

Figure 21.- Effect of spanwise blowing on longitudinal aerodynamic characteristics with strake on. $x_n/c_r = 0.23$.

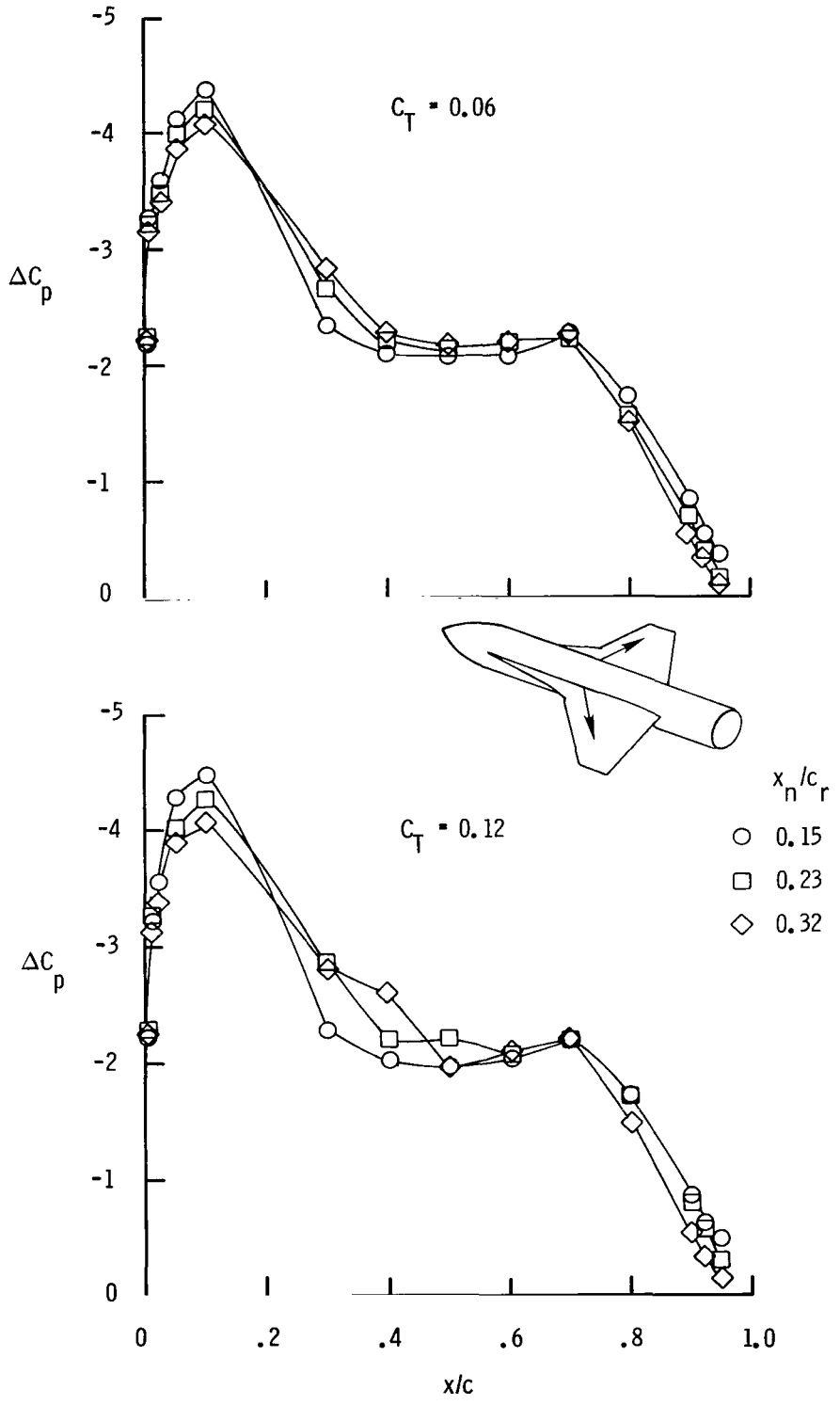

Figure 22.- Effect of x_n/c_r on chordwise pressure distributions of ΔC_p at $2y/b = 0.501$ for two values of C_T with $\alpha \approx 24^o$.

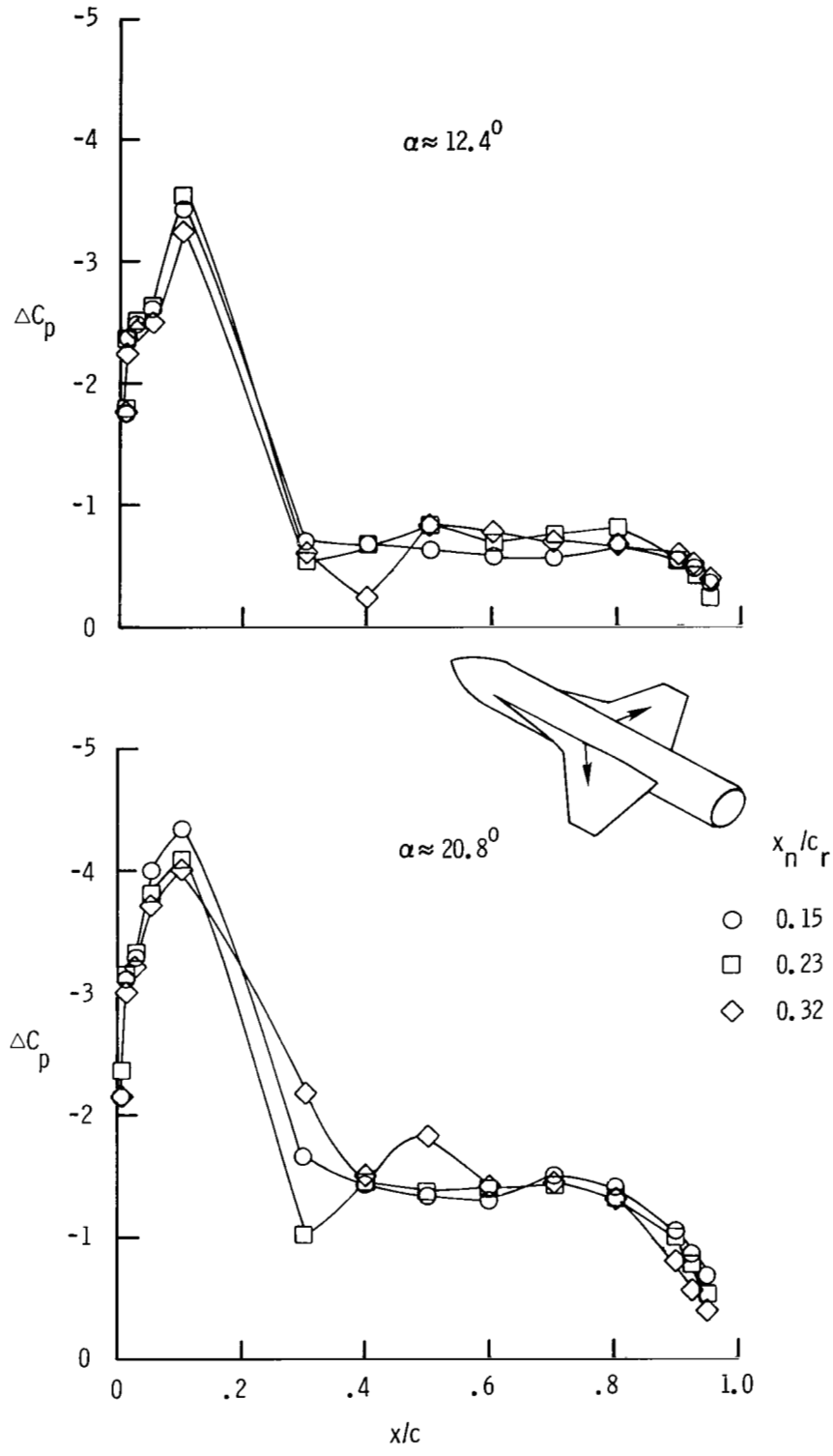

Figure 23.- Effect of x_n/c_r on chordwise pressure distributions of ΔC_p at $2y/b = 0.501$ for two values of α. $C_T = 0.12$.

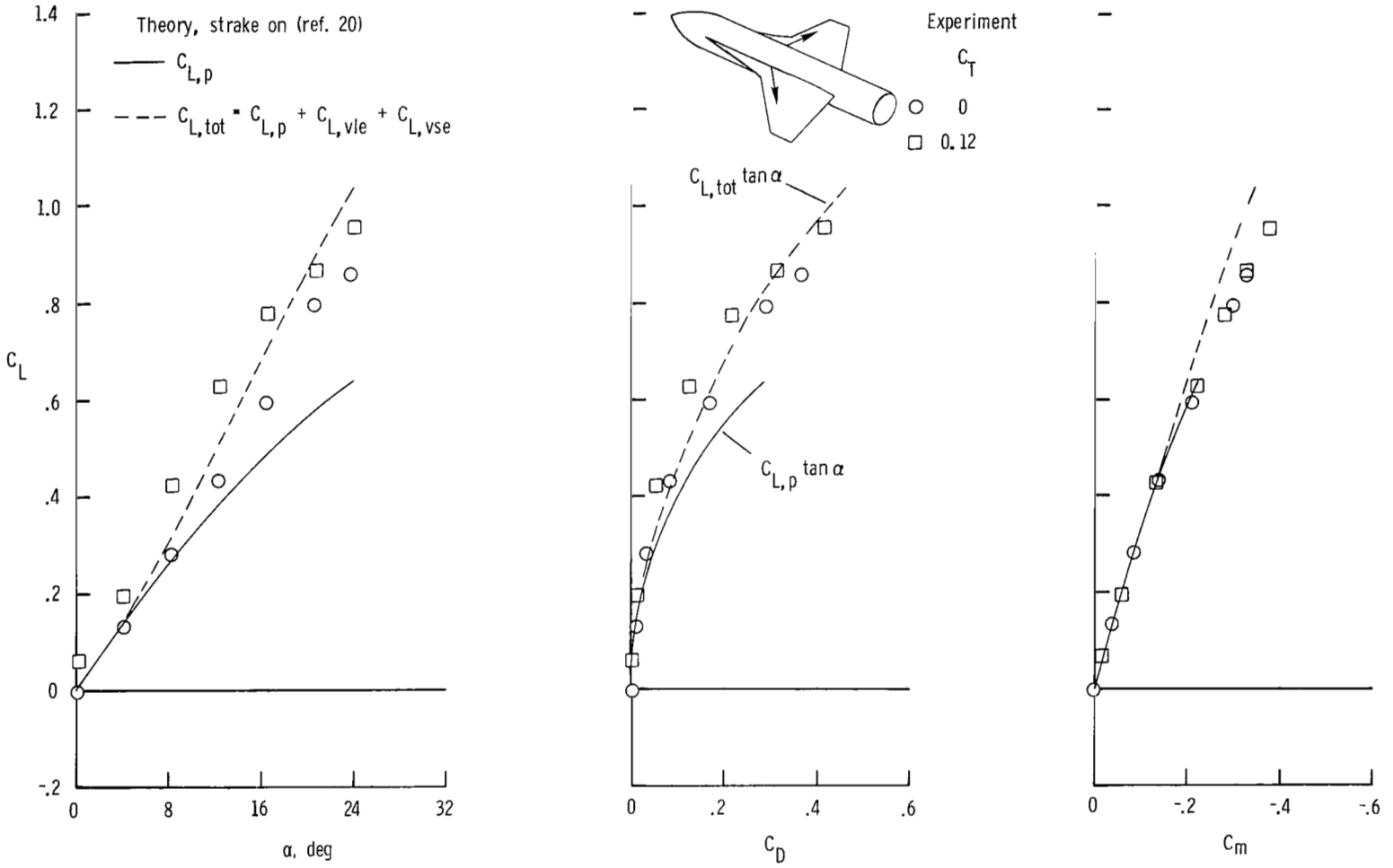

Figure 24.- Effect of spanwise blowing on longitudinal aerodynamic characteristics with strake on. x_n/c_r = 0.15.

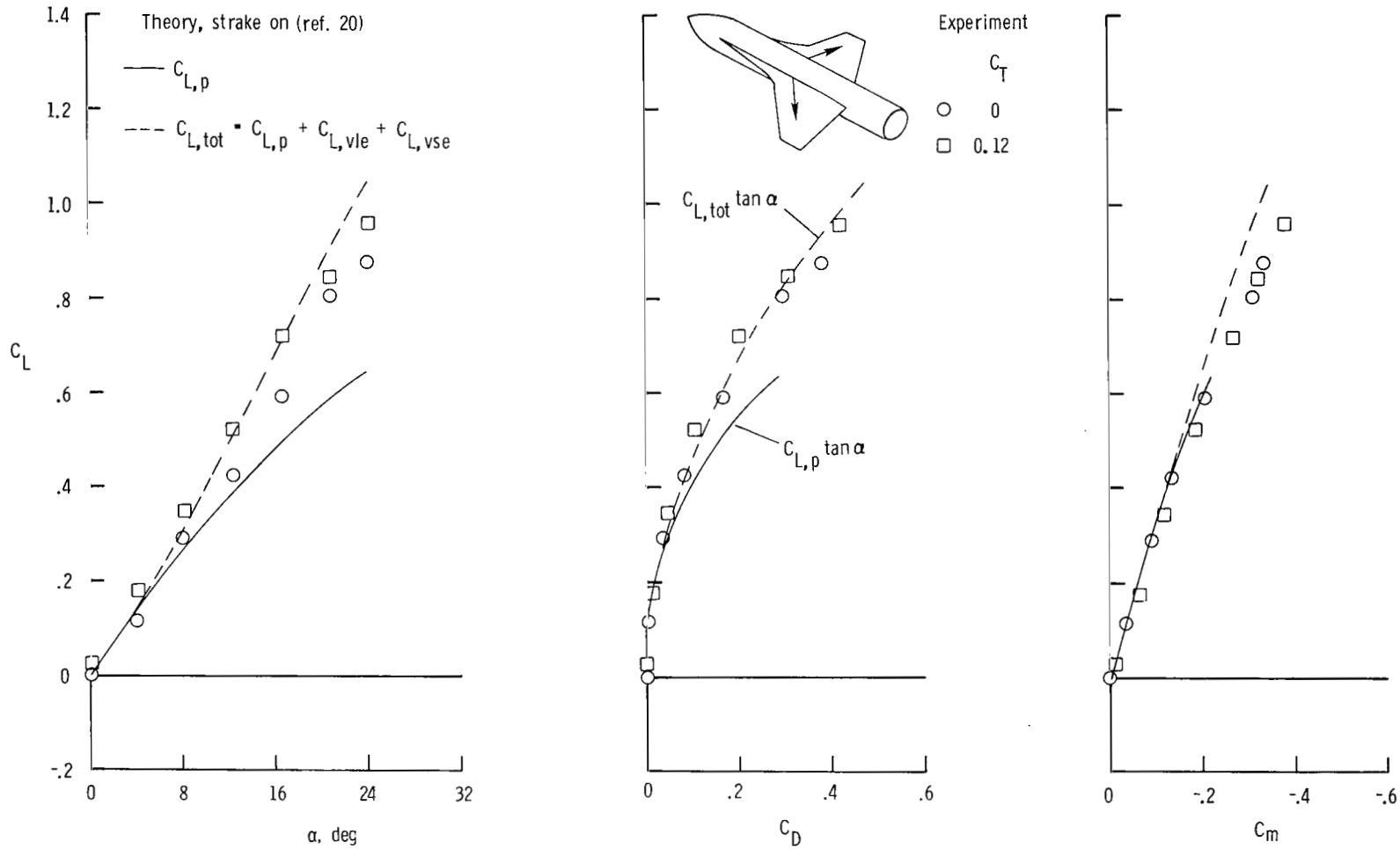

Figure 25.- Effect of spanwise blowing on longitudinal aerodynamic characteristics with strake on. $x_n/c_r = 0.32$.

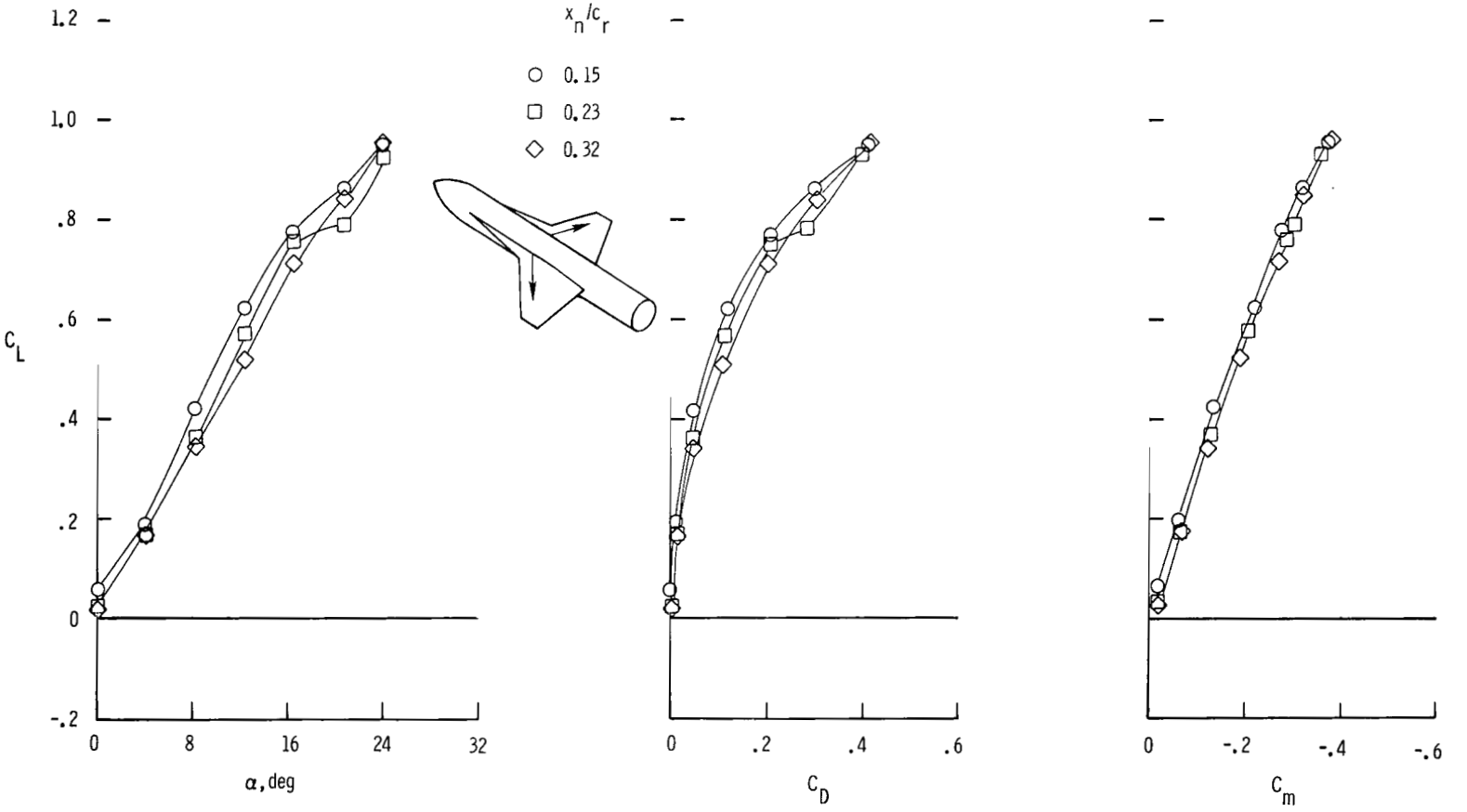

Figure 26.- Effect of x_n/c_r on longitudinal aerodynamic characteristics with strake on. C_T = 0.12.

1. Report No.	2. Government Accession No.	3. Recipient's Catalog No.
NASA TP-1290		

4. Title and Subtitle
EFFECTS OF SPANWISE BLOWING ON THE SURFACE PRESSURE DISTRIBUTIONS AND VORTEX-LIFT CHARACTERISTICS OF A TRAPEZOIDAL WING-STRAKE CONFIGURATION

5. Report Date
February 1979

6. Performing Organization Code

7. Author(s)
James F. Campbell and Gary E. Erickson

8. Performing Organization Report No.
L-11641

10. Work Unit No.
505-11-21-02

9. Performing Organization Name and Address
NASA Langley Research Center
Hampton, VA 23665

11. Contract or Grant No.

13. Type of Report and Period Covered
Technical Paper

12. Sponsoring Agency Name and Address
National Aeronautics and Space Administration
Washington, DC 20546

14. Sponsoring Agency Code

15. Supplementary Notes
James F. Campbell: Langley Research Center
Gary E. Erickson: Northrop Corporation, Hawthorne, California

16. Abstract

The present investigation was conducted to measure the effects of spanwise blowing on the surface pressures of a 44° swept trapezoidal wing-strake configuration. Wind-tunnel data were obtained at a free-stream Mach number of 0.26 for a range of model angle of attack, jet thrust coefficient, and nozzle chordwise location. Results of this study showed that spanwise blowing delayed the leading-edge vortex breakdown to larger span distances and increased the lifting pressures. Vortex lift was achieved at span stations immediately outboard of the strake-wing junction with no blowing, but spanwise blowing was necessary to achieve vortex lift at increased span distances. Blowing on the wing in the presence of the strake was not as effective as blowing on the wing alone. Spanwise blowing increased lift throughout the angle-of-attack range, improved the drag polars, and extended the linear pitching moment to higher values of lift. The leading-edge suction analogy can be used to estimate the effects of spanwise blowing on the aerodynamic characteristics.

17. Key Words (Suggested by Author(s))	18. Distribution Statement
Spanwise blowing Vortex lift Wing-strake configuration Pressure distributions	Unclassified - Unlimited Subject Category 02

19. Security Classif. (of this report)	20. Security Classif. (of this page)	21. No. of Pages	22. Price*
Unclassified	Unclassified	69	$5.25

* For sale by the National Technical Information Service, Springfield, Virginia 22161

NASA-Langley, 1979

1 1 1U,A, 012779 S00903DS
DEPT OF THE AIR FORCE
AF WEAPONS LABORATORY
ATTN: TECHNICAL LIBRARY (SUL)
KIRTLAND AFB NM 87117